Scholars' Mine

Masters Theses                                    Student Theses and Dissertations

Fall 2013

# Numerical modeling of infrared thermography techniques via ANSYS

Hayder Abdulnabi Thajeel

## Recommended Citation

NUMERICAL MODELING OF INFRARED THERMOGRAPHY TECHNIQUES

VIA ANSYS

by

HAYDER ABDULNABI THAJEEL

A THESIS

Presented to the Faculty of the Graduate School of the

MISSOURI UNIVERSITY OF SCIENCE AND TECHNOLOGY

In Partial Fulfillment of the Requirements for the Degree

MASTER OF SCIENCE IN MECHANICAL ENGINEERING

2014

Approved by

Dr. Edward C. Kinzel, Advisor

Dr. Kelly Homan, Committee member

Dr. K. Chandrashekhara, Committee member

# ABSTRACT

Several inspection techniques have been developed over years. Recently, infrared thermography (IRT) technology has become a widely accepted as a nondestructive inspection (NDI) technique for different fields and various applications as well. Infrared thermography stands as one of the most an attractive and a successful NDI technique that has ability to detect the object's surface/subsurface defects remotely based on observing and measuring the surface's emitted infrared heat radiation by using an infrared camera. The finite element modeling FEM ANSYS was successfully used for the modelling of several IRT techniques; such as Pulsed Thermography (PT) and Lock-in Thermography (LT) that can be used to detect the in-plane defects which are parallel to its surface; besides a Laser Spot Thermography (LST) technique that can be used to detect the cracks which are perpendicular to its surface. Furthermore; this thesis describes how LST method can be extended to a new technique, Laser Digital Micromirror Thermography (LDMT), based on using a digital micromirror device (DMD) that has ability to generate multi-hot spots onto the specimen's surface being examined by using single laser source.

In one hand, this thesis aims to show investigations about infrared thermography technology as a non-destructive inspection by using numerical modeling methods via ANSYS. On the other hand, this thesis presents FEM ANSYS as a powerful tool allows doing several inspections, analyses, and evaluations of thermography techniques tests based on numerical modeling simulations and comparing their results to the corresponding experiments in literature experiment tests to validate these simulations and show a reasonable agreement to use ANSYS as a thermography inspection tool for future study and researches.

# ACKNOWLEDGEMENTS

I would like to express my sincerest gratitude to my advisor, Dr. Ed. Kenzil, and I am very thankful to him for guiding me during this research. This work would not have been possible without his advice and support. He gave me lots of freedom to explore the problems that interested me, while providing me with the direction that I needed. This thesis is a dedication to him for encouraging me to push my boundaries to excel. You are not just an advisor to me but someone I look up to and consider a friend.

Special thanks to Dr. K. Chandrashekhara and Dr. Kelly Homan. I am really proud of you to be my committee members. The abundant support of the Mechanical and Aerospace department's faculty and staff at Missouri University of Science and Technology is greatly appreciated. It is an honor for me to get my Master Degree from this great university.

Also, I would like to acknowledge my sponsor HCED-IRAQ, The Higher Committee for Education Development in Iraq, for giving me this opportunity and supporting me emotionally and financially during my MS degree study at Missouri University of Science and Technology.

It is a pleasure to thank those who made this thesis possible everyone who was important to the successful realization of thesis.

# DEDICATION

I would like to dedicate this work to my father's, brother's spirit, mother, and my rest family, without whose boundless support and care this task would have not been accomplished. I always know that you believe in me and want the best for me. Thank you for teaching me that my job in life was to learn, to be happy, and to know and understand myself; only then could I know and understand others.

Words may barely express my gratitude to my friends for supporting me, whose generous attitude has been inspirited to me. It is because all of you that I was able to accomplish this work, to find the joy in life, the ones who always give me advice when needed and keep me focused. Even thru the toughest of times you have stuck with me every step of the long days and nights, and it's something I will always cherish.

As well as expressing my apologies that I could not mention personally one by one.

Hayder A. Thajeel

Oct., 2014

**TABLE OF CONTENTS**

# LIST OF ILLUSTRATIONS

# LIST OF TABLES

# **NOMENCLATURE**

| | |
|---|---|
| $\lambda$ | Wavelength, [mm] |
| $T$ | Temperature, [$^{o}$C, K] |
| $T_o$ | initial change in temperature, [$^{o}$C, K] |
| $T_i$ | initial temperature, [$^{o}$C, K] |
| $Ti\text{-}1$ | temperature rise at the grid point (i-1), [$^{o}$C, K] |
| $TL$ | temperature rise at the left boundary of the crack, [$^{o}$C, K] |
| $TR$ | temperature rise at the right boundary of the crack,[$^{o}$C, K] |
| $Ti{+}1$ | temperature rise at grid point (i+1), [$^{o}$C, K] |
| $T_G$ | temperature rise at the ghost point, [$^{o}$C, K] |
| $k_B$ | Boltzmann constant, [W/m$^2$ K$^4$] |
| $E$ | total radiant emission energy, [watt] |
| $\varepsilon$ | thermal emissivity |
| $\alpha$ | thermal absorptivity, thermal diffusivity [m$^2$/s] |
| $\rho$ | thermal reflectivity, mass density [kg/m$^3$] |
| $\tau$ | thermal transmissivity |
| $E_b$ | thermal radiation energy emitted by a blackbody |
| $G$ | irradiation |
| $k$ | thermal conductivity, [W/m.K] |
| $c_p$ | specific heat capacity, [J/kg.K] |
| $t$ | Time, [s] |

| | |
|---|---|
| $\tau$ | heat pulse duration, observation time [s] |
| $Q$ | Absorbed energy by the object's surface |
| $e$ | the effusivity, [mm] |
| $erfc$ | complementary error function |
| $ierfc$ | integral complementary error function |
| $q$ | heat flux power density, [watts] |
| $q_0$ | power of the halogen lamp, [watts] |
| $q''$ | heat flux per unit arear, [W/m$^2$] |
| $q'''$ | heat flux per unit volume, [W/m$^3$] |
| $Q$ | the total energy of the heat source, [J] |
| $I_{max}$ | maximum power density of the laser pulse, [watts] |
| $\omega$ | modulation (angular) frequency, [rad/sec] |
| $f$ | Frequency, [Hz] |
| $\mu$ | thermal diffusion length, [mm] |
| $j$ | imaginary number |
| Re | real part of Discrete Fourier Transform |
| Im | imaginary part of Discrete Fourier Transform |
| $A_n$ | amplitude |
| $\emptyset_n$ | Phase, [rad] |
| $D$ | diameter of defect, [mm] |
| $L$ | detectable subsurface defect's deepest depth, [mm] |
| $r_a$ | laser beam radius, [mm] |

| | |
|---|---|
| $x$ | Cartesian coordinate, distance from surface, [mm] |
| $y$ | Cartesian coordinate, [mm] |
| $z$ | Cartesian coordinate, Depth [mm] |
| $r$ | radius in a polar coordinate, [mm] |

# <u>GLOSSARY</u>

| | |
|---|---|
| IR | Infrared Radiation |
| IRT | Infrared Radiation Thermography |
| NDI | Non-Destructive Inspection |
| NDE | Non-Destructive Evaluation or Examination |
| NDT | Non-Destructive Testing |
| IRT-NDI | Infrared Thermography Non-Destructive Inspection |
| PT | Pulsed Thermography |
| LT | Lock-in Thermography |
| VT | Vibro-Thermography |
| LST | Laser Spot Thermography |
| LLT | Laser Line Thermography |
| LDMT | Laser Digital Micromirror Thermography |
| DMD | Digital Micromirror Device |
| DLP | Digital Laser Projector |
| FEM | Finite Element Method |
| FDM | Finite Difference Method |
| NMAB | National Materials Advisory Board |
| ASNT | American Society for Nondestructive Testing |
| VT | Visual Testing |
| RT | Radiography Testing |

| | |
|---|---|
| UT | Sonic-Ultrasonic Testing |
| ET | Electromagnetic-electronic Testing |
| MT | Magnetic Particle Testing |
| LPT | Liquid Penetrant Testing |
| AET | Acoustic Emission Testing |
| NIR | Near Infrared Radiation band |
| SWIR | Short Wave Infrared Radiation band |
| MWIR | Mid Wavelength Infrared Radiation band |
| LWIR | Long Wavelength Infrared Radiation band |
| CFRP | carbon-fiber-reinforced polymer |
| FRP | Fiber-reinforced plastic |
| PVC | Polyvinyl-chloride |
| BVID | Barely visible impact damage |
| FLIR | Forward Looking Infra-Red |
| FPAs | Focal Plane Arrays |
| PCD | Photonic Cooled Detectors |
| PTR | Photo-thermal radiometry |
| FT | Fourier Transform |
| FFT | Fast Fourier Transform |
| DFT | Discrete Fourier Transform |
| CFT | Continuous Fourier Transform |

# 1. INTRODUCTION

## 1.1 OVERVIEW

Shigeo Shingo, head of Toyota, once said "Quality can be assured reasonable only when it is built in at the process and when inspection provides immediate and accurate feedback at the source of defects" [1]. In reaching this goal, infrared thermography techniques have ability to provide a high speed inspection for the surface and sub-surface defects (faults) of large areas without damage them and may be useful in determining root cause.

This introductory section introduces the background and motivation for this thesis and will begin with talking about Non-Destructive Inspection (NDI). Non-Destructive Inspection (NDI) represents an attractive tool and a highly valuable technique that can be used to increase the service life of critical structures which can save resources and extend the useful lifetime of the inspected specimen because this technique does not affect the properties of the object being inspected [2]. NDI represents a safe technology that refers to the detection of defects or subsurface defects without causing any damage, harm, or effect on the operation of the equipment and without changing its integrity and properties [2,3,4]. It has been used for over 30 years in a variety of field; such as agriculture, railways, aviation, automotive, power plants, civil structures, transportation, manufacturing, environment, art, and medicine [5].

NDI methods include an extremely wide range of techniques; such as eddy-current testing [6], ultrasound [7], acoustic emission testing [8], radiographic testing [9],

shearography [10], liquid penetrant testing [11], magnetic-particle inspection [12], and infrared thermography (IRT) as well [13].

Among these different NDI evaluating techniques, Infrared Thermography (IRT) is commonly used as a powerful tool for detecting subsurface defects for achieving fast inspection for large surfaces [14,15]. IRT is a remote technique that has the ability to measure an object's temperature distribution from a distance without needing to contact it and this occurs in real time. It represents a fast and an economic inspection method since it allows evaluating and inspecting the components locally without needing to remove and move them to the local inspection laboratory [16-18]. In this thesis will focus on IRT techniques as a powerful nondestructive inspection modality.

Infrared thermography is a technology that commonly uses an infrared thermal camera in order to capture the temperature distribution on a surface being examined and display it as a visible information as a thermal image; i.e. the temperatures on the examined surface can be measured in real time and can be detected from a distance as a remote technique [19]. Infrared thermal cameras (IR camera) play an important role and represent a main part among the other thermography components since it has ability to observe and image the temperature differences (thermal contrasts).

Infrared thermography (IRT) is a technology based on electromagnetic radiation. Based on the black body law, it is well known that any object with a temperature equal/above than absolute zero ($T \geq 0$ K) emits an electromagnetic radiations [18]. Infrared radiation (IR) represents one of these electromagnetic radiations, where the intensity of the infrared radiation emitted by objects represents a function of their

temperature. Therefore, it can be used as a valuable indicator to measure the temperature of an object, in which the higher the body's temperature, the greater the infrared radiation emitted [20]. IR radiations is invisible radiations with a wavelength (0.75 to 14 µm) longer than visible light which the human beings perceive it as heat, and it can display as visible information by using an IR camera. IR represents a thermal energy that can be captured by an infrared camera and transformed into electronic signal (image processing) which expands to the visible image as a two-dimensional (2D) image. This captured 2D image represents the temperature distribution on the test specimen's surface, i.e. infrared thermography can be classified as 2D technique for temperature measurements [21-23].

IRT was a rarely used technique due to some challenges, such as the high prices and the weak performance of the infrared thermal camera. However; over two decades ago, IRT has increased in popularity and became an increasingly common investigation technique with the greater availability and falling prices of infrared thermal cameras. Basically, the current modern infrared thermal cameras have benefited from the military technology purposes which are used to provide the night vision/visualization of humans in complete darkness and sand storms [24, 25]. Thermal infrared cameras has been expanded to be used for non-military applications besides NDI applications; such as aerospace, security, transportation, civil market, industrial applications, law enforcement, firefighting, and many other industries [25].

Basically, there exist several thermography techniques that evaluating the time dependence of temperature distributions. Where the techniques evaluating the steady-state thermography is often called static thermography or passive thermography, while the techniques that evaluating dynamic temperature contrasts are also called dynamic

thermography/active thermography, in which the specimen's surface being examined is actively excited by external excitation source; such as thermographic flashes, halogen lamps, or laser beam etc.

IRT can be performed either in passive or in active approach [16,26,27]. Where the passive approach thermography is used to examine and evaluate materials that are at different temperature than ambient (often higher); such as heat losses in buildings, monitoring of power stations, and in skin temperature mapping (as biology or medicine) [25]. These applications are known as steady-state (stationary) thermography, since there is no external excitation is needed to use [16,24,25]. Whereas in the case of the active approach; an external excitation source is used such as; optical flash lamps, halogen lamps, cold or hot air guns, in order to disturb the material and produce thermal contrasts which can be detected by an infrared camera [23]. Where, the different active methods vary in the way that the thermal energy is sent to the inspected specimen's surface.

There exists several active infrared thermographic inspection techniques have been developed. The two main classical or conventional of these IRT techniques are pulsed thermography (PT) and lock-in thermography (LT). Most of active infrared thermography techniques; such as PT and LT, are based on the principle of delivering a thermal energy into the object being examined, in which the heat propagates by diffusion through the material, and then the thermal response is observed and recorded via IR camera to reveal the defects presence. But they vary in the method that they are practically implemented [16,27]. Where in PT, a heat pulse of a short duration is applied to the specimen's surface being inspected, and then the thermal evolution of the stimulated surface is observed in transient state. While in the LT, the examined

specimen's surface is stimulated by an amplitude modulated heat wave and the surface thermal evolution is observed in steady state [27].

In general, in conventional setups of active thermography techniques, relatively homogeneous uniform heat energy is applied perpendicularly to the specimen's surface being inspected in form of thermal heat pulses as in pulsed thermography (PT) technique, or in form of periodic thermal waves as in lock-in thermography (LT) [13,16]. Consequently, thermal diffusion from the surface changes the temperature near the defect region after a thermal transit time. Then the resulting temperature distribution at the surface is recorded with an infrared thermal camera, then evaluating these data allows estimating the heat flow into the object. In doing so it is possible to resolve and reveal many varieties of any anomaly or defects; such as breaks, disbond, voids, cracks, pores, or delaminations [23].

In particular, pulse thermography (PT) technique, see section 3, represents one of the most popular extensively evaluated active thermography technique because of its easiness of deployment and due to it represents such a fast technique and safe as well [28]. PT technique was developed for the purpose of non-destructive inspection testing (NDI) of materials and structural components, particularly for subsurface of solid bodies. One of the basic thermal physical properties is its ability to propagate by diffusion through the materials, depending on the thermal capacity and the thermal resistance of the materials [28,29].

In pulse thermography (PT), the inspected specimen's surface is warmed up by a (short/long) heat pulse, depending on the thermophysical properties of the inspected specimen materials and the defect as well, by using high power external excitation

sources, then the heat pulse propagates through the inspected specimen starting from the stimulated surface toward the inside one (rear side). Then the time evaluation of the surface temperature is monitored and the temperature on the surface temperatures distribution is observed by using an infrared camera. Any subsurface non-homogeneities, discontinuity (flaws/fault), or buried object of different heat properties, then this discontinuity (defect) acts like a thermal barriers and works as a  thermal resistance that prevent the thermal propagation and will impact the dynamic local heat energy through the sample crossing this non-homogeneities by changing the heat flow rate. These non-homogeneities will appear in the observed image that obtained by IR camera, representing as a defective zone with different temperature (often higher) with respect to the reference zones (non-defective) [33,34]. Reference zone represents the pure/ non-defective area of the test sample which does not has any hidden/subsurface discontinuities. The time evaluation of the surface temperature represents a suitable way that allows observing the subsurface defects and detecting this non-homogeneity; due to it reflects the extent to which this discontinuity is probable existed. Where the imaging time after the pulse corresponds to the information depth as a consequence; due to the thermal pulse front needs some time to propagate the material and reach the depth of the material depending on the material's thermophysical properties, specifically the thermal conductivity ($k$), and the thermal energy power [35].

The most advantage of pulsed thermography is this technique represents such a quick thermography technique; due to in PT technique, the information about variant depths of specimen can be obtained from some thermograms, which is taken within seconds after a single irritation short heat pulse. However; there is a challenge which can

be represented by that the PT technique is affected by some external factors; such as non-uniform heating, and also, the induced temperatures have to exceed the noise level of the camera as well. Therefore, PT technique is not suitable method to detect very weakly temperature signals [36,37].

Another common classical an active thermography technique is a lock-in thermography (LT), see section 4, which is also known as modulated thermography or thermal wave imaging [16,26,28,33,34]. Lock-in thermography (LT) is an active thermography technique that has been developed and employed to improve the detection capability of surface or subsurface flaws in many various materials, especially these with high thermal conductivity ($k$). This technique is based on using a periodic thermal wave as a periodic excitation method to detect subsurface defects or any non-homogeneity. Lock-in Thermography is based on the fact that the periodic thermal wave has the characteristics of the wave such as phase and amplitude that can be applied for flaws detection. Where after applying periodic thermal waves into the specimen's surface being examined then these will propagates by conduction as thermal waves through the object, then the thermal response is recorded at the same time using an IR camera. Then these recorded get some post-process and analyses generating a phase image (phasegram) and amplitude image (ampligram). The most interesting thing that the phase and amplitude of thermal wave will be changed after being in face with any internal flaws or any non-homogeneity can be detectable based on the phase shift (delay) and the change in amplitude of the reflected thermal wave, where the incoming thermal wave and the reflected thermal wave have the same frequency [38,39].

Lock-in is an advanced infrared thermography technique has been used to provide better detection capability than the other conventional active IRT such as PT, based on the phase image which is very informative. The LT, especially phase image, is an insensitive to these external factors that the PT is affected by; such as non-uniform heating, environmental reflections, emissivity variations and non-planar surfaces. Moreover; LT is a technique that does not require high power thermal waves. However, the disadvantage of lock-in thermography compared to pulse thermography is that LT needs a longer observing time, i.e. it is a slow technique, because a permanent regime that has to be reached, and due to for getting much more information about different depths, one has to make number of observations using different LT frequencies in sequence which makes LT is slow thermography technique in comparison with PT [33].

In general, the previous two techniques PT and LT represents a classical NDI thermography IRT techniques that has been very successful in detecting in-plane defects such as coating adhesion failures, delamination or impact damage in carbon fiber composites and cracks parallel to its surface. However; there are specific defects such as near surface cracks in metals representing a challenge for detecting by PT and LT, such as fatigue cracks, especially the perpendicular micrometer cracks that grow predominantly perpendicular to the surface. Where PT and LT methods are not suitable to be used to detect these types of cracks due to these classical techniques do not block the heat flow that applied to the surface. Therefore; to overcome this challenge, advanced active stimulation thermography technique was developed presenting a new technique which is known as Laser Thermography [40-42], or Pulsed Laser Spot Thermography (LST), see section 5. Laser Spot Thermography (LST), is a novel technique which allows

detecting surface breaking micrometer cracks in metals by using a powerful laser beam. It is an active thermography technique that is based on producing a high power focused pulsed laser spot to provide a highly localized heating spot from which allows providing a heat diffuses radially, hence these heat flow can be changed once be in face with these types of cracks. LST technique is based on generating a thermal hot spot on the specimen's surface being examined, where applying hot spot into crack's proximity allows generating heat flow propagates radially, i.e. perpendicularly onto crack block. Then presence any crack perpendicular to its surface (specimen's surface) will delay the lateral heat flow and change the heat flow rate causing a thermal perturbation and providing a thermal contrast that can be observed by an IR camera, hence it will detect the crack; i.e. the thermal image obtained by IR camera will reveal the perturbation caused by the crack and this can be used to detect its presence [40-42]. As other techniques, LST technique has a limitation too which is represented by the thermal spot has to be applied into crack's proximity, due to it is not easy to get the suitable location on the specimen's surface being inspected to apply the thermal spot on. In doing so, so it is required to repeat doing this technique many times and generating hot spots at different location to cover most of the specimen's surface being examined till reaching the crack or its vicinity which will require long time till detect the cracks.

The present thesis introduces a new technique that can overcome the challenge in LST technique. This thesis highlights an alternative approach which can be implemented in a very short time as compared to LST. This alternative approach can be called as a Laser Digital Micromirror Device Thermography (LDMDT), or Digital Micromirror Device Infrared Thermography (LDMT), section 6. LDMT is a technique based on using

a digital mirror device (DMD) technology which can provide multi-hot spots in same time and saving the inspecting observation time in comparison with LST. LDMT stands as an active infrared thermography approach which is based on using a powerful laser beam and a DMD device which very suitable inspection technique to be used for detecting subsurface cracks, especially the micrometer cracks which are perpendicular to its surface, of a large surface. Where LST technique provides one heat spot that excites the specimen's surface to disturb its material, but this single hot spot without being close to the defect or at its proximity, then the observed thermal image will not reveal the defect. Therefore to detect the defect it is required to keep stimulating the specimen's surface at another place providing another hot spot and keep repeating this process until reaching the defect location or its proximity then revealing the defect. Reaching this point it may take a long time by using LST technique especially for a component of large surface; therefore it is required providing multi heat spot on the test specimen's surface to save the observation time. In this case, it needs to have many laser sources to create those hot spot, but this is expensive even though it allows detecting the defects in short time. This thesis presents the solution key to overcome this challenge without needing to use many laser sources by using a digital Micromirror device (DMD) which has ability to provide many spot upon the test specimen's surface at the same time and by using only one laser source, as will see that in section 6.

## 1.2 OUTLINE OF THE THESIS

The Thesis is organized as follows:

- **Section 1**: Introduction and overview and research objectives

- **Section 2:** Literature review, summarizes, infrared thermography (IRT) fundamentals, the non-destructive inspection (NDI) and its existing techniques, recent developments in infrared thermography, infrared thermography as a NDI technique, excitation sources, and thermal imaging infrared camera

- **Section 3**: Pulsed Thermography PT, operation principles, basic concept and theory, pulsed thermal waves, experimental setup and data acquisition for PT, geometry and meshing, thermal propagation evolution, and simulation and experiment's results of PT

- **Section 4**: Lock-in Thermography LT, operation principles, basic concept and theory, lock-in sinusoidal thermal waves, experimental setup and data acquisition for LT, processing with the Fourier transform, routines in lock-in thermography, geometry and meshing, simulation and experiment's results of LT

- **Section 5:** Laser Spot Thermography LST, operation principles, basic concept and theory, experimental setup for LST, geometry and meshing, simulation and experiment's results of LST, analytical and numerical modeling (ANSYS)

- **Section 6**: Laser Digital Micromirror Device LDMT, basic concept and theory in comparison with for LST, digital mirror device (DMD), and LST and LDMT simulations

- **Section 7:** Conclusion

## 1.3 THESIS OBJECTIVE

Based on the finite element modeling FEM ANSYS, this thesis presents several numerical modeling of IRT techniques; such as Pulsed Thermography (PT) and Lock-in

Thermography (LT) that can be used to detect the in-plane defects which are parallel to its surface; besides a Laser Spot Thermography (LST) technique that can be used to detect the cracks which are perpendicular to its surface. Furthermore; this work describes how the LST technique can be extended using a digital micromirror device (DMD) producing a new thermography technique which represents such a quick technique in comparison with LST one. This new technique; which is may be called Laser Digital Micromirror Thermography (LDMT), is based on using a digital micromirror device (DMD) has ability to generate multi-hot spots onto the specimen's surface being examined by using single laser source.

## 1.4 THESIS PLAN

This thesis presents an overview of thermography techniques, including the background and history, physical principles, theories, concepts, and limitations which belong to infrared thermography.  Furthermore, it presents an investigation by presenting several  simulations which are successfully accomplished using the numerical modeling through the commercial finite element program ANSYS Workbench 14.0, to show a reasonably good agreement in comparison to its corresponding laboratory experimental tests to validate these simulations. Finally, this study presents a new active thermography technique, LDMT, which is derived from laser spot technique (LST) and show how it is faster than LST through presenting several simulations. The experimental tests and literature studies have cited as references in the section of the references at last pages of this thesis. Similarities and differences between experimental and simulated data are analyzed and discussed, then successfully proved.

## 2. LITERATURE REVIEW

This section presents briefly literature reviews about several concepts, basic fundamentals, background, and motivation for this thesis which are related to the infrared thermography (IRT) technology and non-destructive inspection (NDI) tests; such as infrared radiation basics, electromagnetic spectrum bands, heat transfer, infrared thermography principles, non-destructive method, thermal excitation sources, temperature measurement, and infrared thermal camera technologies.

## 2.1 BACKGROUND AND HISTORY

Early of 18th century in Bath of United Kingdom, a German-born a British Astronomer William Herschel (1738-1822) regenerated Newton's experience of separating white light into colors by passing sunlight through a prism. Mr. Herschel was able to measure the temperature of each of these colors by using three thermometers and holding them with blackened lambs in order to ameliorate the heat absorption. Then he discovered that the temperature was gradually growing up from the violet end to the red one of the visible spectrum. When he moved the thermometer and placed it just beyond the red end; surprisingly he observed that temperature was growing up further [36,43,44]. This invisible source of heat which represents a portion of the electromagnetic spectrum corresponds to the Infrared Radiation IR (below red).

Simply, infrared radiation (IR) is invisible light that the human being's eyes cannot see it since its wavelengths longer than those of visible light, but can perceive it as a heat. Basically, it is a thermal radiant energy that emitted naturally by any object whose

temperature is equal to or above absolute zero ($T \geq 0$ K) according to the black body radiation law [36,43]. Therefore; the IR emitted radiation is a function of the object's temperature; the higher the temperature, the greater the intensity of the infrared energy emitted, i.e. the emitted infrared radiation of an object represents a good indicator of its temperature and it can be used to measure its temperature [36,43,44].

## 2.2 NONDESTRUCTIVE INSPECTION (NDI)

Non-Destructive Inspection (NDI) is the method of inspecting, evaluating, or examining a test specimen with technology that does not affect/damage the test specimen's future utility and without causing damage; i.e. without affecting the subsequent serviceability of the part [20]. Non-Destructive Inspection (NDI) can also be referred as Non-Destructive Testing (NDT), Non-Destructive Evaluation or Examination (NDE), or Non-Destructive Testing and Evaluation NDT&E [45].

Nondestructive inspection (NDI) is defined by the American Society for Nondestructive Testing (ASNT) as; the determination of the physical condition of an object without affecting that object's ability to fulfill its intended function [46]. So it is a powerful tool used to increase the service life of critical structures [46].

NDI represents a method of testing and examining the components without changing or destroying their usefulness in a safe and reliable mode that can guarantee to keep using it without any damage or harm which can be applied to each stage of a component's construction. Therefore; NDI techniques can be used to monitor the component or structure's integrity throughout its design life or its service life. Various NDI methods are applied for preventive maintenance, for the inspection of raw materials,

half-finished and finished products, or for in-service-inspection; such as in motor vehicles, trains, aircraft, shuttle, buildings, pipelines, bridges, power stations, refineries; and oil platforms which are all inspected using NDI technology [45-48].

NDI is a method that can be classified as an examination and evaluation technique for determining the existence of internal irregularities in materials without effecting on its physical integrity and subsequent service [46,47].

There are many benefits of using nondestructive testing such as [48,49,50]:

1. Many NDI methods are a mobile techniques, where the components can be evaluated and inspected while it is in service; i.e. it can do it locally without needing to remove it and take it to the inspection laboratory

2. Applying NDI does not change or harm the inspected object usefulness, i.e. it is such a safe and reliable technique

3. NDI technology is a technique can be used for detection, location and sizing of surface and subsurface defects (in welds, castings, forging, composite materials, concrete and many more)

4. Nondestructive testing is an economy technology, where NDI was found to save approximately 80 % the cost of destructive testing, not including the initial investment

Basically, NDI technology has a wide group of analysis techniques that used in science and industry to evaluate the properties of a material, component, or system without causing damage. There are many different techniques of NDI tests, and each one has specific fields to be used in. The National Materials Advisory Board (NMAB) Ad Hoc Committee on Nondestructive Evaluation and The American Society for

Nondestructive Testing (ASNT) has adopted a classification system of several major categories [26,46]:

1. Thermal and Infrared (Infrared Thermography) Testing (IRT)

2. Mechanical- Optical Testing (Visual Testing) (VT)

3. Radiography Testing- (Penetrating radiation ) (RT)

4. Sonic-Ultrasonic Testing (UT)

5. Electromagnetic-electronic Testing (Eddy Current Testing, Magnetic Particle Testing); (ET)

6. Magnetic Particle Testing (MT)

7. Chemical-analytical Testing (Liquid Penetrant Testing) (PT)

8. Acoustic Emission Testing (AE)

Abundant information on the several techniques contained in previous categories is available in [16,45,51].

Basically, NDI's techniques can be used and selected based on four main criteria [52]:

- the thickness and nature of the object being inspected

- Defect type

- Defect location

- Defect size

Among all of those variant NDI techniques, the most attractive and powerful tool for non-contact inspections is the Infrared Thermography (IRT) technique, which is based on observing a thermal contrast between the specimen and the object of interest (subsurface defects). However, in case of a thermal equilibrium between the specimen

and the defect, an external excitation energy source may serve to create a thermal difference; which is well known as the active approach in IRT [53]. This thesis focuses on one of the previous techniques which is represented by the infrared thermography (IRT) nondestructive inspection (NDI) method or IRT-NDI.

## 2.3 INFRARED THERMOGRAPHY (IRT)

**2.3.1 Basics and Principles of Infrared Radiation (IR).** The story of infrared imaging was started during World War II [18]. Subsequently, this technique has extended to other fields such as medicine, maintenance agriculture, and environment [21]. Specifically; the story of using the infrared thermography as an effective tool in non-destructive inspection NDI tests has begun on the beginnings of 1960s in different fields and various applications [54].

Infrared thermography (IRT) has a long history, although it has used increasingly with the commercial and industrial applications of the past fifty years. IRT is a proactive troubleshooting and predictive maintenance tool [55]. In fact, it is not a single tool but it is a system or set of some components, which is totally based on using an infrared thermal camera that has ability to make the invisible infrared radiations to be visible. Therefore, thermography has ability to reveal the variations in temperature based on its emitted infrared radiations.

IRT is a science of acquisition, analysis and processing of thermal information from non-contact thermal imaging measurement devices [56]. Terminology, thermography or thermograph is a term consists of two words; the prefix "therm" which

is a Greek word means heat, and the suffix "graph" which means writing or representation, in other words, infrared thermography is a graphical representation of emitted infrared heat. It is a method that shows a thermal image to detect, display and record thermal patterns and temperatures across the inspected object's surface [57].

Basically, Infrared Thermography IRT works in the thermal section of the infrared spectrum based on the principle that any contrast or inhomogeneity in materials or any sub-surface or up-surface fault or defect creates a different thermal map. By the measuring this emitted radiation via IR camera, it can detect and characterize the subsurface or un-surface defects by analyzing any contrast or difference in the surface thermal map [58]. Due to the intensity of the emitted infrared radiation by bodies represents a good function or indicator of their temperature, Eq. (2). Therefore; this feature is used for many purposes in many applications of infrared thermography IRT which covering a wide range of application; such as mechanical, electrical, medical, maintenance, building and military etc. Recent years, it has seen a noteworthy development in infrared sensing and imaging devices for a wide uses, particularly for military, battlefield, airborne and the thermal non-destructive testing and evaluation techniques [20,59].

There are several infrared measuring devices which has the ability to detect the emitted infrared radiation by an object and transform it into an electronic signal [60]. A pyrometer represents one of the most basic infrared devices which can provide a single output by using a single sensor (IR sensor). Most advanced devices include an array of sensors which is known as infrared camera (IR camera) has ability to provide a detailed infrared image of the scene. Indeed, the difference between an invisible infrared image

and a visible image is that the visible image represents the reflected light on the scene; while in case of the invisible infrared image, the scene represents the source and can be observed by an infrared thermal camera without light. These IR cameras are able to convert those invisible acquired images into visible images by assigning a color to each infrared energy level; thus producing a false-color image which is called a thermogram or thermographic image. Thermographic image are corresponding to the mapping images of the thermal IR energy emitted from the stimulated specimen's surface; i.e. thermographic images are actually visual displays of the amount of infrared energy emitted by an object [60-62].

**2.3.2 Black Body Radiation Concept.** In 1860, Gustav Robert Kirchhoff (1824-1887) defined a blackbody as a surface that neither reflects nor transmits incident radiation. Instead, a blackbody absorbs all incident radiation irrespective of direction and wavelength. In addition to be a perfect absorber, a blackbody is also a perfect radiator. Therefore, all radiation leaving a blackbody is emitted by the surface and no surface can emit more energy than a blackbody. In addition, a black surface is a diffuse emitter, i.e. the emitted radiation is a function of the wavelength and temperature but independent of the direction [36,63].

In physics, a black body is a theoretical object which emits infrared radiation (IR) at its contact temperature. If a thermocouple on a black body radiator reads 50 °C, then the radiation of the black body will give up and will also be 50 °C. Therefore a real black body will have an emissivity of 1. The difference in behavior of a real body with respect to the black body is indicated by the parameter spectral emissivity [59].

In 1900, Max Planck found an expression describing the spectral distribution of the radiation intensity from a blackbody, known today as Planck's Law [36,64]:

$$E_{\lambda,b}(\lambda, T) = \frac{C_1 \lambda^{-5}}{exp(C_2/\lambda T - 1)} \tag{1}$$

Where $\lambda$ [m] is the wavelength, $T$ [K] is the temperature, $C_1 = 3.742 * 10^8$ W μm$^4$/m$^2$ is the first radiation constant, and $C_2 = 1.4389 * 10^4$ μm.K is the second radiation constant.

Planck's law Eq. (1) represents a valuable tool to determine spectral distribution for a blackbody, which corresponds to the theoretical maximum possible emission from any real body [36].

In 17th century, physicists Stefan and Boltzmann established first experimentally expression and then theoretically; the resulting expression known as Stefan-Boltzmann Law Eq. (2). In 1879, Josef Stefan (1835-1893) experimentally established a simple relation relating radiant emission from an object's surface to its temperature. Stefan's results were theoretically confirmed in 1884 by one of his former students, Ludwig Boltzmann (1844-1906) [36]. This law states that the total radiant emission energy (E), integrated over all frequencies (wavelengths), is proportional to the fourth power of the absolute temperature (T) and this is called the law of black body emission which is shown in this relation [30,64]:

$$E = k_B \cdot T^4 \tag{2}$$

Where $k_B = 567 \times 10^{-8}$ W/m$^2$ K$^4$; is the Boltzmann constant.

Planck's law Eq. (1) gives the intensity radiated by a blackbody as a function of frequency (wavelength), whilst Stefan-Boltzmann's law Eq. (2) gives the total flux

integrated over all frequencies [36]. As a nondestructive inspection tests (NDI), the thermography techniques are based on the fact that the energy emitted by an object (real object or blackbody) represents a function of its surface temperature. However, the energy observed by an IR detector, depends as well on the thermophysical properties of the real object surface; such as thermal emissivity 'ε', thermal absorptivity 'α', thermal reflectivity 'ρ', and thermal transmissivity 'τ' which are explained in next section [36]. See Figure 2.1.
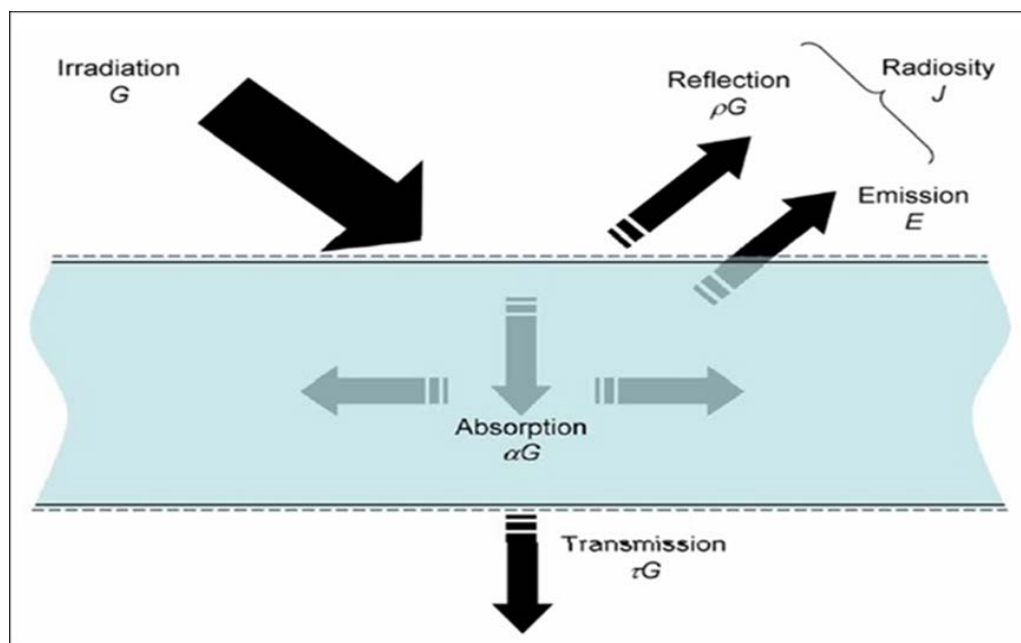
Figure 2.1 Energy balance in a semitransparent medium [36]

**2.3.3 Electromagnetic Spectrum Bands.** Infrared Thermography (IRT) stands as a one of the more promissory techniques for the inspection of materials and structures

which is based on the fact of black body principle, that all the bodies with a temperature equal to or above absolute zero (i.e., $T \geq 0$ K), emit infrared radiation. Since IR radiation is invisible radiation; therefore IR measuring devices; i.e. IR camera are required to be able to acquire and observe this invisible radiation (information) and make it visible [69].

The types of electromagnetic radiation can be classified according to their wavelength in vacuum. Infrared Radiation represents a particular portion of the this electromagnetic spectrum with specific range among these wavelengths, whilst heat represents the whole range of radiant energy, see Figure 2.2 [56,58]. Basically, electromagnetic spectrum consists of different radiations such as; cosmic rays, gamma rays, x-rays, ultra violet, a thin region of visible light, infrared, terahertz waves, microwaves, radar rays, radio waves, and broadcast bands [56]. The Infrared Radiation IR band range corresponds to the band of the electromagnetic spectrum between 0.74 μm to 1000 μm, which is from the end of visible light to microwaves. Therefore, using an IR radiometer is a useful tool to measure the thermal variations; radiometer is a device which using for measuring the radiant flux (power) of electromagnetic radiation [70]. A thermal infrared camera, section 2.8, has ability to detect radiation in range of the mid wave infrared radiation band (MWIR) (3 to 5 μm), or long wave infrared radiation band (LWIR) (7 to 14 μm), which correspond to two of the high transmittance atmospheric zones as shown in Figure 2.2 [16, 26].

Most portion of the infrared range of the electromagnetic spectrum is not a beneficial in IRT technique, because it is blocked by the atmosphere. However; the rest portions represent the useful part of the infrared radiation. In general, there are four IR spectral bands of interest for infrared vision applications [16,26,56]:

1. Near Infrared Radiation band (NIR, from ~0.75 to 1 µm)

2. Short Wave Infrared Radiation band (SWIR, from ~1 to 2.5 µm)

3. Mid Wavelength Infrared Radiation band (MWIR, from ~3 to 5 µm)

4. Long Wavelength Infrared Radiation band (LWIR, from ~7 to 14 µm)

Two of these various bands, which are MWIR and LWIR, represent the most common bands that used in infrared thermography technique, due to two reasons which are represented by the band of peak emissions and atmospheric transmittance [6,20]. The first reason is due to the link between wavelength and temperature. Where for a particular temperature, the most effective measurement is supposed to be carried out for the wavelength at which most intensity is emitted. The second reason is related to the atmospheric transmittance, where IR transfers through air as photons, being absorbed by different air particles, particularly by $CO_2$ and $H_2O$ [20,69]. As it is mentioning before that the absorptivity ($\alpha$) of air for infrared radiation IR depends on the wavelength and is not affected by object's surface temperature. Since there are many wavelengths, it is required to use a high sensitive camera to accomplish identical performance. Due to this absorption is low, for MWIR and LWIR bands; it is allowing more radiation to reach the sensor of the camera as a result. Thus, for most applications, wavelengths longer than SWIR are required [20,61,62].
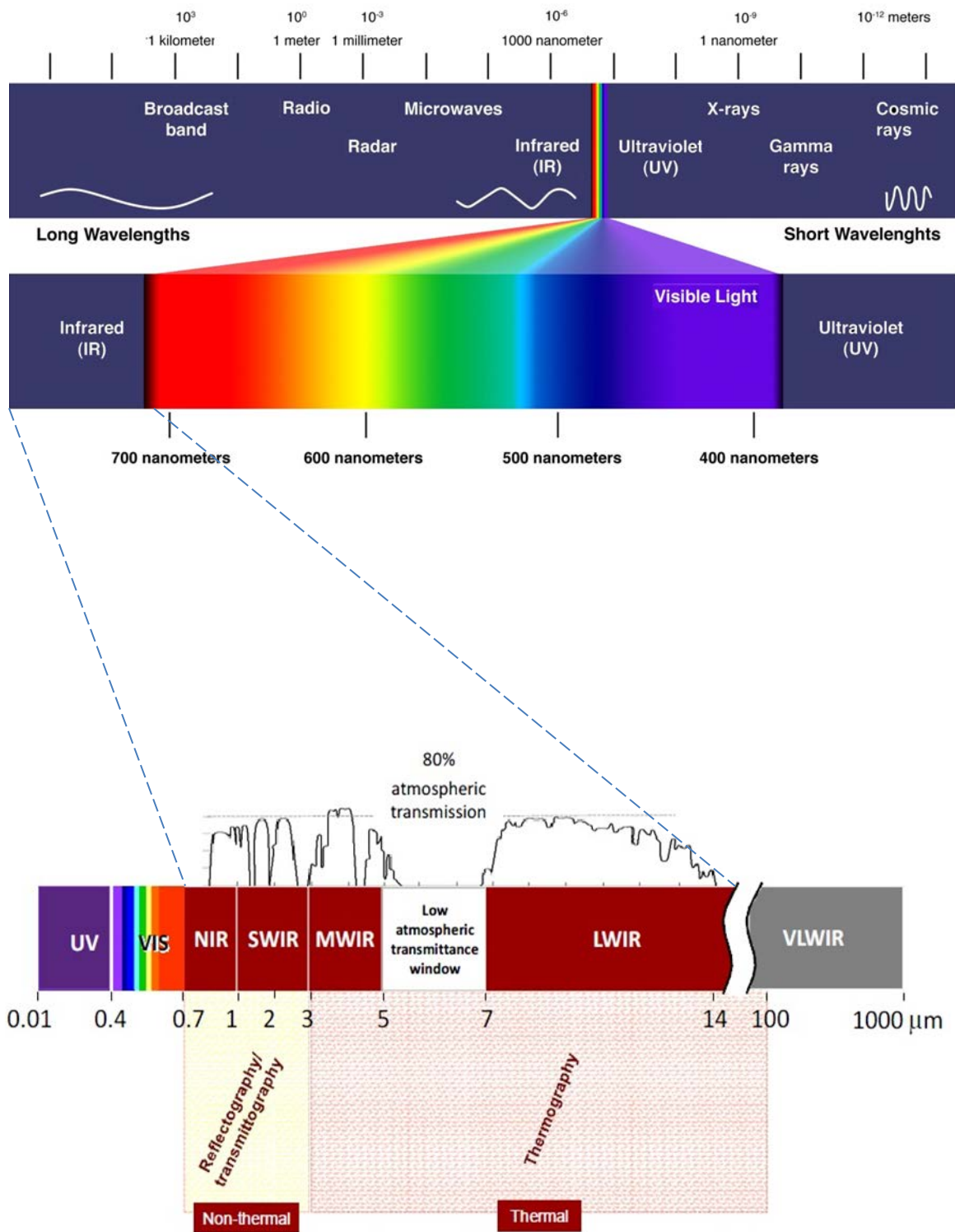
Figure 2.2 Infrared bands in the electromagnetic spectrum [56,71]

## 2.4 INFRARED THERMOGRAPHY APPROACHES

There exist several types of thermography approaches which can be classified based of the methodology for testing the materials, the origin of the source of thermal energy and the measured temperature differences arising from it. In general; the infrared thermography IRT techniques can be classified into two main types as seen in Figure 2.3:

1. Passive, steady state or static thermography; this technique operates in two wavelength ranges, 3-5 µm (SWIR) and 8-12 µm (LWIR).Where IR radiation energy depends on the chosen wavelength range. Passive thermography is essentially based on analysis where no external excitation is used to excite thermal gradients on the test specimen's surface [72]. In this approach, the features of interest are naturally at a higher or lower temperature than the background. Passive thermography has many applications such as surveillance of people on a scene and medical diagnosis; specifically thermology) [26].

2. Active or dynamic thermography; this technique is based on the detection and recording by an infrared camera of thermal IR radiations emitted by object surface. External energy source is required to be used in this approach in order to produce a thermal contrast between the examined specimen and the feature of interest (subsurface defects); where it is required to heat or cool the object being inspected in order to create the required thermal contrast [72]. The active approach is necessary in many cases given that the parts being examined are usually in equilibrium with the surroundings [26].
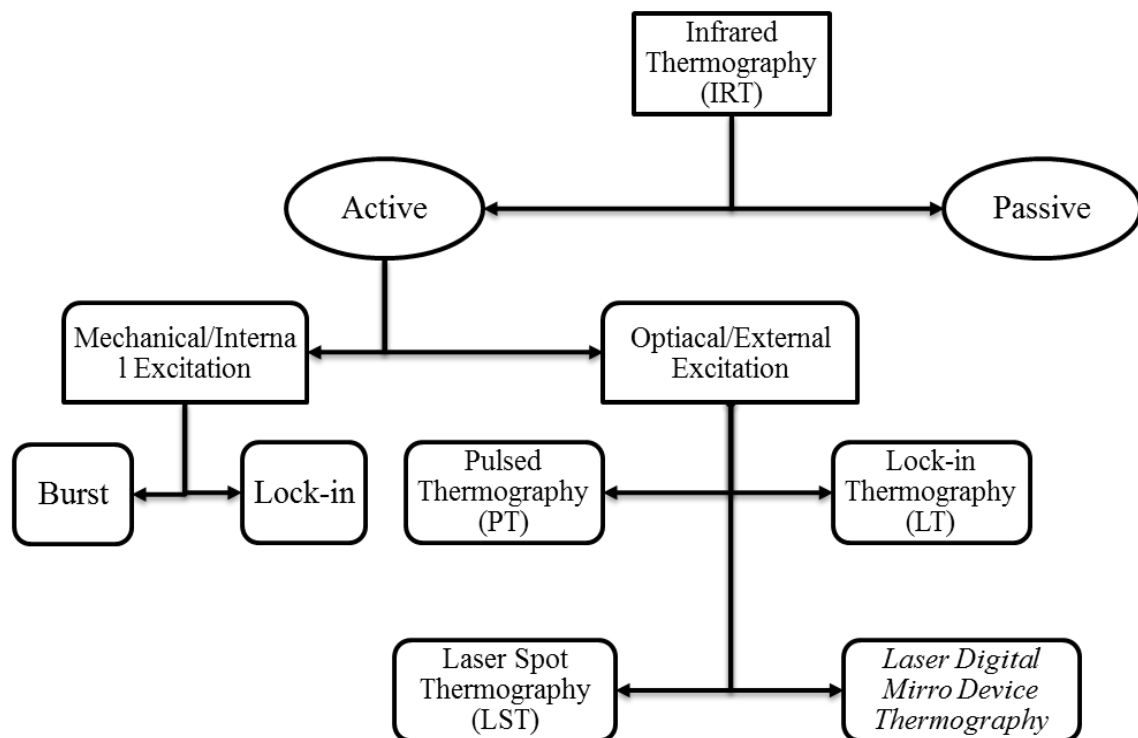
Figure 2.3 Infrared thermography classifications

During a few years ago, both of active and passive infrared thermography (IRT) approaches have become an effective and a robust technology in a wide uses of variant fields and different applications, including architecture, aerospace, industry, NDI tests, science, and in different laboratory researches [20].

In one hand, the passive IRT is the most common approach of these two approaches, which is used to examine and evaluate materials whose at different temperature than ambient (often higher); i.e. the defective areas are naturally observed at a different temperature than the ambient temperature (surroundings), where the emitted thermal radiation from inspected specimen's surface can be observed by using infrared

camera, and obtains information about the temperatures distribution of the inspected specimen's surface in thermal equilibrium state [5,20,74]. The passive infrared thermography has a wide range of applications in different fields such as civil engineering (for evaluation test of thermal insulation of buildings), predictive maintenance such as; inspection test of pumps, electric insulators, bearings and motors), agricultural fields, medicine fields (diagnosis of diseases), and in a different experimental and laboratory researches [5,20,74]. The passive approach is a very successful technique in aerospace fields; such as in the inspection of aircraft structures to detect water inside panels, where the water itself represents a trouble especially it can transform to ice [62].

For instance, in bio-medical imaging fields, in case of passive infrared thermography mode, imaging may not produce enough temperature change for observation of subsurface skin lesion; such as skin cancer. However, to overcome this limitation, advanced stimulation techniques were developed, which is known as active thermography technique or dynamic thermography technique, in which controlled energy is being supplied to the skin. This controlled stimulus not only helps in the detection of deeper subsurface details but also helps in gaining the quantitative information of hidden features. Therefore; infrared thermography is a useful tool that has been widely used for the detection and diagnosis of many problems in various fields and different applications; such as aerospace fields, civil engineering, and bio-medical imaging as well [16,22,26,29].

On the other hand, the active approach is much more popular which represents one of the most common approaches used for nondestructive testing inspections, and it presents a remote (non-contact) detection of defects placing at a short depth under the

surface (subsurface defects). Active thermography approach is based on using an external excitation source; such as optical flash lamps, halogen lamps, cold, or hot air guns, in order to disturb the material and produce thermal contrasts which can be detected by an infrared camera [23]. Where, the different active methods vary in the way that the thermal energy is sent to the inspected specimen's surface. In other words, an external excitation energy source is required to be used in order to excite the inspected sample's surface (non-stationary approach) [16]. The purpose of using an external excitation is to disturb the materials and create a thermal contrast on the inspected object's surface and forces it to be in thermal non-equilibrium state [5]. The thermal contrast on the surface which is resulted from differences in radiation emission due to the presence of a defect, it can be captured and observed by an IR camera. The thermal images provided by infrared thermal camera can lead to information about defects and non-homogeneity inside the inspected specimen and the thermal physical properties of inspected object and defects as well. Basically, it is common to use the active IRT techniques as an effective evaluation tool in a wide range and a variety fields of nondestructive inspection (NDI) tests to detect and reveal the subsurface faults; such as pores, bubbles, cracks, or any abnormality inside the inspected object without changing the integrity and properties of the inspected specimen or without causing any damage [16,26,74].

It is worth to mention that the passive IRT gives a qualitative estimate, i.e. it is used in quality control and process monitoring applications, but not a quantitative estimate of the damage present. On the contrary, active IRT can give a qualitative and quantitative estimate of the damage or fault present; such as the defect type, depth, shape,

or size [5]. Many different stimulation methods can be applied; most of them can be classified as optical, mechanical or inductive [62].

## 2.5 EXCITATION SOURCES

As it has mentioned using infrared thermography as an active IRT technique needs an extra heat (thermal excitation) supply to excite an object and disturb it to provide a controlled change in its temperature with respect to surrounding its surroundings [20]. Thermal contrast can be achieved either by heating or cooling of the examined specimen's surface. However typically thermal excitation by heating is preferred to be used due to it leads to get better parameters; such as the density of the heat flux, noises and process ability. The purpose of using a heat or cool pulse is in order to disturb the material and produce thermal contrasts which can be detected by an infrared camera as an infrared image which represents the temperatures distribution on the inspected specimen's surface, and indicates material subsurface defects in different depths [16,23,34].

There are different active excitation methods in use that vary in the way of energy is sent to the specimen's surface being inspected; where the most common method is the optical techniques [75,76]. The most common IRT optical sources are photographic flashes lamps, as it is shown in Fig. 2.4a, for an optical pulsed heating which are used with Pulsed thermography (PT) technique; and halogen lamps, as it is shown in Fig. 2.4b, for periodic heating that provide a thermal waves which it is the most common affordable stimulation heating source that is used with Lock-in thermography (LT) technique [74].

Both of the flash and halogen lamps can be used to excite any object with a large or small areas by controlling the number of lamps and their distance relative to the inspected specimen's surface, analyzing the warming-up and the cooling-down stages, and creating a high repeatability rate [20].

There exists many energy sources can be used to stimulate an object producing a thermal difference between the defective zones and reference (non-defective) zones; which can be divided into two main types as follow:

1. *Internal excitation*, it is achieved by applying the energy into the object's surface being inspected in order to excite exclusively the flaws. The internal excitation can be implemented by mechanical oscillations, with a sonic or ultrasonic transducer for both burst and lock-in stimulation [34].

2. *External excitation*, it is achieved by applying the energy (illumination) to the specimen's surface being examined. Where this delivered energy will transform to thermal energy and warm the specimen's surface up then the thermal energy will propagate through the specimen until it will be facing the defect and creating a thermal contrast that can be captured by an infrared camera [34].

Basically there are three main classical active thermography techniques, Pulsed Thermography (PT), Lock-in Thermography (LT), and Vibro-Thermography (VT) [16, 26]. Where, both of the PT and LT techniques stand as optical techniques, whilst the VT

technique uses ultrasonic waves (amplitude modulated or passive pulses) to stimulate the internal characteristics then creating a thermal contrast [34].



a. Flash lamp [77]                              b. Halogen lamp [78]

Figure 2.4 Common optical stimulation sources in NDT

In general, these optical stimulation techniques have ability to achieve very useful results. However, there are some challenge to use them with specific defects, such as cracks in metallic parts; such as CFRP (carbon-fiber-reinforced polymer) composite materials plate, and the micrometer crack that are perpendicular to the object's surface, in which using the classical optical stimulation techniques (PT or LT) are unable to produce enough thermal contrast, thus cannot be detected in most cases. To overcome this challenge, more advanced stimulation techniques were developed, such as Laser Spot Thermography (LST), Laser Line Thermography (LLT), and Laser Flying Thermography

[79,80]. Furthermore, the proposal new technique this thesis aims to present, which is called as Laser Digital Micromirror Device Infrared Thermography (LDMT).

Recently, infrared thermography (IRT), specifically the active mode, has proven a useful evaluation tool for thin flat structural components, and is getting a reasonable agreement as a one of the most effective tool as a nondestructive inspection (NDI) technique. IRT is becoming increasingly attractive for the detection of hidden or sub-surface defects especially in a variety of composite structures. Due to the recent enhancements that have happened in the quality of thermal data acquisition system, and the interest in broad area scanning procedures for a truly noncontact NDI system that can manage inspections of complex structures in real time inspection [81].

## 2.6 THERMOGRAPHY NONDESTRUCTIVE INSPECTION

Infrared Thermography (IRT) is one of the most attractive nondestructive inspection NDI methods because it is a non-contact technique, safe, clean, painless, and such a fast inspection method that allows the remote measurement of the surface temperature of a specimen [59,82]. IRT is becoming a widely adopted technique to detect the presence of variety of internal flaws or defects; i.e. discontinuity or non-homogeneity, inside materials [26,34].

Infrared thermography IRT has been used in a wide range of NDI's applications and fields; such as medical applications, maintenance, and building inspections. For instance; structures in civil engineering filed such as bridges and buildings inspections, for example to detect cracks in concrete [83] and defects in concrete structures strengthened with FRP (Fiber-reinforced plastic) composites [84]. It has also been used in

different fields in the aerospace industry for detecting different types of defects; such as voids, disbands and barely visible impact damage (BVID) in composite airframes [85]. The thermal signals, that used for examining defects by thermography, are diffusive in nature therefore there is drop in detectability of subsurface defects which is nonlinear with depth. For this reason thermography is best convenient for NDI of thin structures such as those found widely in the aerospace industry [86].

IRT has many advantages over other technologies [62]. In general, the main advantages of IRT are the following:

1. IRT is a noncontact technique where the used devices are not in touch with the heat source, i.e., they are non-contact thermometers. Therefore, the dangerous products, such as acids and the objects that have a high temperature, can be measured safely and keeping the user out of any danger.

2. IRT creates two-dimensional thermal maps (thermogram), which can reveal the temperature contrast of object, i.e. detect defects.

3. IRT is a direct test in real time and can reduce the maintenance and repair costs

4. IRT is a harmless technology. It has none of the harmful radiation effects of technologies, such as X-ray imaging.

In general, there are two possible observation approaches in which the inspected specimen is heated up from one side while the infrared thermal camera is being either from the same side, i.e. reflection mode; or from the opposite side, i.e. transmission mode [36], as it is shown in Figure 2.5.

In reflection mode; both of the thermal source and infrared thermal camera are located on the same side of the inspected specimen's surface; as it is shown in Figure 2.5. While, in transmission, the heating source is located on the side of the inspected specimen's surface (front), and the infrared thermal camera is located on corresponding side of the inspected specimen's surface (rear) [87]. In general, it is a suitable to use the reflection mode for detecting the defects that located close to the stimulated surface; i.e. shallower defects, whilst using transmission mode is preferred for detecting the defects closer to the non-stimulated surface; i.e. for deep defects, due to the spread/diffusion effect of the energy propagating through the specimen by conduction. Therefore, if the non-heated surface is not accessible, hence using the transmission mode is not applicable, i.e. depth quantification is not possible in transmission mode [87]. In general, resolution is higher in reflection and it is easier to deploy given that both sides of the specimen do not need to be available [36,80,88].
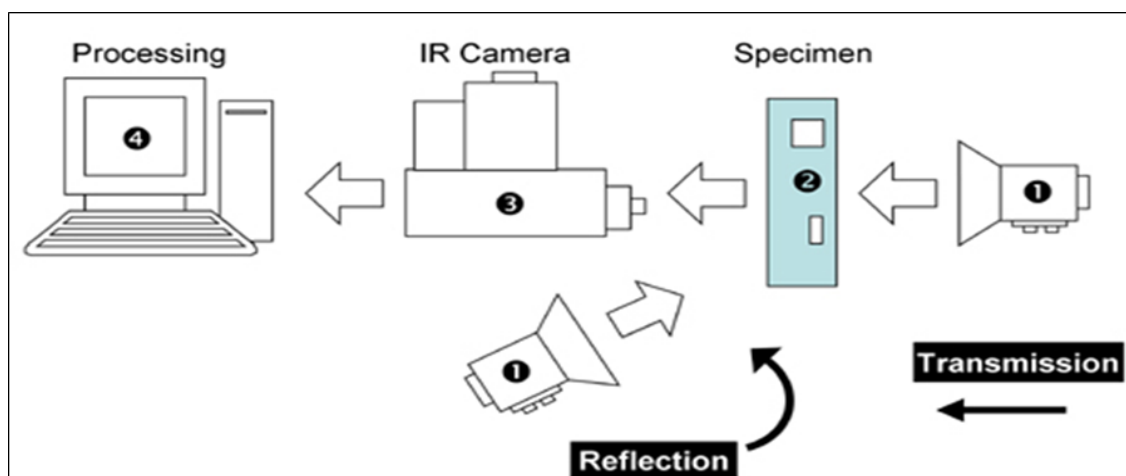


Figure 2.5 Experimental configurations in active thermography in reflection and transmission mode: 1-Heat source, 2-specimen, 3-IR camera, and 4-PC for data display, recording and processing [36]

## 2.7 IR DETECTORS AND SENSORS

In general an infrared detector is an electronic device or sensor that has ability to transform a radiant energy in form of the infrared into a measurable form; i.e. it represents a transducer of radiant energy [36,89]. In other words, an infrared detector is a sensor has ability to respond to IR radiation. The thermal sensors have ability to react to incident IR radiation by increasing its temperature up, and they display high sensitivity at room temperature. Basically, there are two main types of IR detectors which are; thermal detectors and photonic detectors [90].

In one hand a thermal detector is being at equilibrium state whenever there is no thermal conduction due to the detector, in this case, emits radiation energy at the same rate as it absorbs it. On the other hand, when the incident radiation raises it above the equilibrium state then the thermal detector absorbs more energy than it emits; hence increasing the detector's temperature up. Theoretically; a thermal sensor does not react or respond to the wavelengths [15,36]. There are several types of thermal detectors such as liquid crystals, pneumatic detectors, thermocouples, bolometers and pyro-electric detectors. A detailed description of these and other detectors can be found in references [89,90].

On the other hand, a photonic detector; or quantum detector, is another type of IR detectors which made from semiconductor materials. Basically, it operates on the principle that incident radiation stimulates electrons from the valence to the conduction atomic bands [36,90]. Although the photonic detectors are capable to satisfy a high sensitivity and a short response time in comparison with the thermal detectors, but

typically quantum detector needs to be cooled (cryogenic cooling) in order to reduce the thermal noise level and satisfy a superior relative sensitivity [36].

Eventually, thermal sensors offer a modest performance with slower response time speed than photonic sensors, but they are cheaper and do not require a cryogenic cooling as their photonic counterparts [36,75]. Figure 2.6 shows a thermal leak detector which is available on amazon.com for 28.03$.



Figure 2.6 Black & Decker TLD100 Thermal Leak Detector [91]

## 2.8 THERMAL IMAGING INFRARED CAMERA

Thermal imaging infrared camera is also known as thermographic camera, infrared camera, thermal camera, thermo camera, IR camera, or FLIR (Forward Looking Infra-Red). It is a remote non- contact measurement device that has ability to observe,

reveal the infrared radiations energy that emitted from objects from distance, and transform it into an electronic signal then by doing some post-process which lead to produce a visible thermal image similar to these visible images that are formed by a regular camera [30].

Infrared IR camera is a technology that has capability to observe and reveal objects and people in total absence of light and in various weather conditions as well, and to form visible colored images, in which each color corresponds to a specified temperature scale, these images called thermograms which represents the temperature distribution on specimen's surface that can display as a visible information [92]. Since temperature can be measured in real time, modern cameras have ability to provide real-time thermal images accurate to hundredths of a degree which allow the smallest details to be seen [59,82].

In the late 1950s and 1960s, single element detectors were developed by Texas Instruments, Hughes Aircraft, and Honeywell that scanned scenes and produced line images. The military had a lock on the technology because it was expensive and had sensitive military applications. These basic detectors led to the development of modern thermal imaging. The pyroelectric vidicon tube was developed by Philips and EEV in the 1970s and became the core of a new product for firefighting, first used by the Royal Navy for shipboard firefighting [25].

The ordinary visible light cameras operate in wavelengths of (0.45 to 0.75 µm), and do not have ability to observe and detect the infrared radiation. Whilst the thermal cameras have ability to detect radiation in the IR range of the electromagnetic spectrum

(~0.75 to 14 µm), and form visible images of these radiations which called thermal-images or thermograms [93].

Today's IR cameras have been expanded to be used for many non-military applications, such as aerospace, security, transportation, industrial applications, law enforcement. Furthermore, in firefighters to see through smoke, find persons, and localize the locality of hotspots of fires; besides civil applications such as building construction to see, find, and localize the heat leaks and to improve the efficiencies of cooling or heating air-conditioning systems, and in industrial applications such as the pipes networks system to localize the overheating joints and parts and many other industries applications [25,94]. These thermal cameras typically operate with a temperature sensitivity of about 15 mK for cooled and 80 mK for uncooled [95]. In recent years, IR cameras are used in a wide variety of military fields; such as in border security, and watchtowers (night vision).

One of the most interesting features of today's infrared camera based on focal plane arrays (FPAs), that they have the ability to manage and process the observed data by some methods, i.e. FPAs represents one of the most common infrared thermo-cameras configurations [36]. Essentially, Focal Plane Arrays are composed of many columns and rows of individual IR detectors or sensors; such as a matrix of IR thermal detectors of dimensions of (320H x 240V, 640H x 512V, 320H x 240V, or 320H x 256V); H: horizontal and V: vertical. Basically, FPAs are based on two kinds of detector arrays; which are photonic cooled detectors (PCD) and uncooled micro-bolometers [167]. IR Cameras based on uncooled micro-bolometer FPAs are becoming increasingly common and attractive for IRT testing evaluations and other applications as well, due to their low cost [29,87,96].

Basically, thermographic image (thermogram) that obtained via IR camera is a thermal image corresponded to the mapping images of the thermal IR energy that emitted from the stimulated specimen's surface, which can be described as a function as f(x, y). The amplitude value of *f* at spatial coordinates (x,y) is a scalar positive value, which corresponds to the amount of IR energy emitted from a region of a plane. The function f is continuous in space and amplitude. Thus, in order to transform this function to a digital format, it must be sampled in both space and amplitude [20]. Thermal image data can be transferred to PC. Subsequently, the data can be calculated and utilized freely, where the thermal image data is colored up pixel by pixel based on temperature [19]. Where the temperature distribution image data of IR thermography consists of matrix of pixels (number of detector: for example, 320 horizontal x 240 vertical pixels).

Cooled IR cameras are more sensitive IR cameras to any little differences in scene temperature with comparison to uncooled IR cameras. Hence; they can detect the smallest of temperature differences between objects. Where cooled IR camera consists of an array of photonic sensors, while uncooled IR camera is consisted of thermal sensors. Selection of IR camera type also varies widely, from cooled to uncooled, with large format 640 x 480 pixels now available [95]. Uncooled cameras are designed to work in range of LWIR band, while cooled cameras are designed to work in range of MWIR band the spectrum where the thermal contrast is high due to blackbody principle. Based on Planck's law (Eq. 1) and the electromagnetic spectrum bands ranges in section (2.3.2), it can be seen that the high temperature bodies have their peak emission at short wavelengths, while objects emitting at ambient temperature have their maximum emission at longer wavelength bands LWIR. Therefore, the MWIR band is useful when

inspecting high temperature objects; while the LWIR band is preferred when working with near room temperature objects. Also, long wavelengths LWIR are for which signals are less affected by radiation from the Sun [29,87,97].

Therefore; choice an infrared thermal camera is not randomly task, but it is based on an important feature of the operating wavelength band selection. There exist several features which represent the most significant criteria for wavelength band selection; such as operating distance, temperature, emissivity, and indoor-outdoor operation of the bodies of interest, i.e. for IR detection system selection. Where for operating distances that limited to a few meters, with the absence of fog or water droplets, then the atmosphere absorption has little effect on IRT testing [87].

Ultimately, IR camera is a portable device and very easy to handle, and it provides a remote inspection test (non-contact). It is easily understood and self-explanatory so it does not need to have that much of experience and practice. Just first read the manufacturer instructions manual, then target it, observe, record, and inspect as it is shown in Figure 2.7 [98].
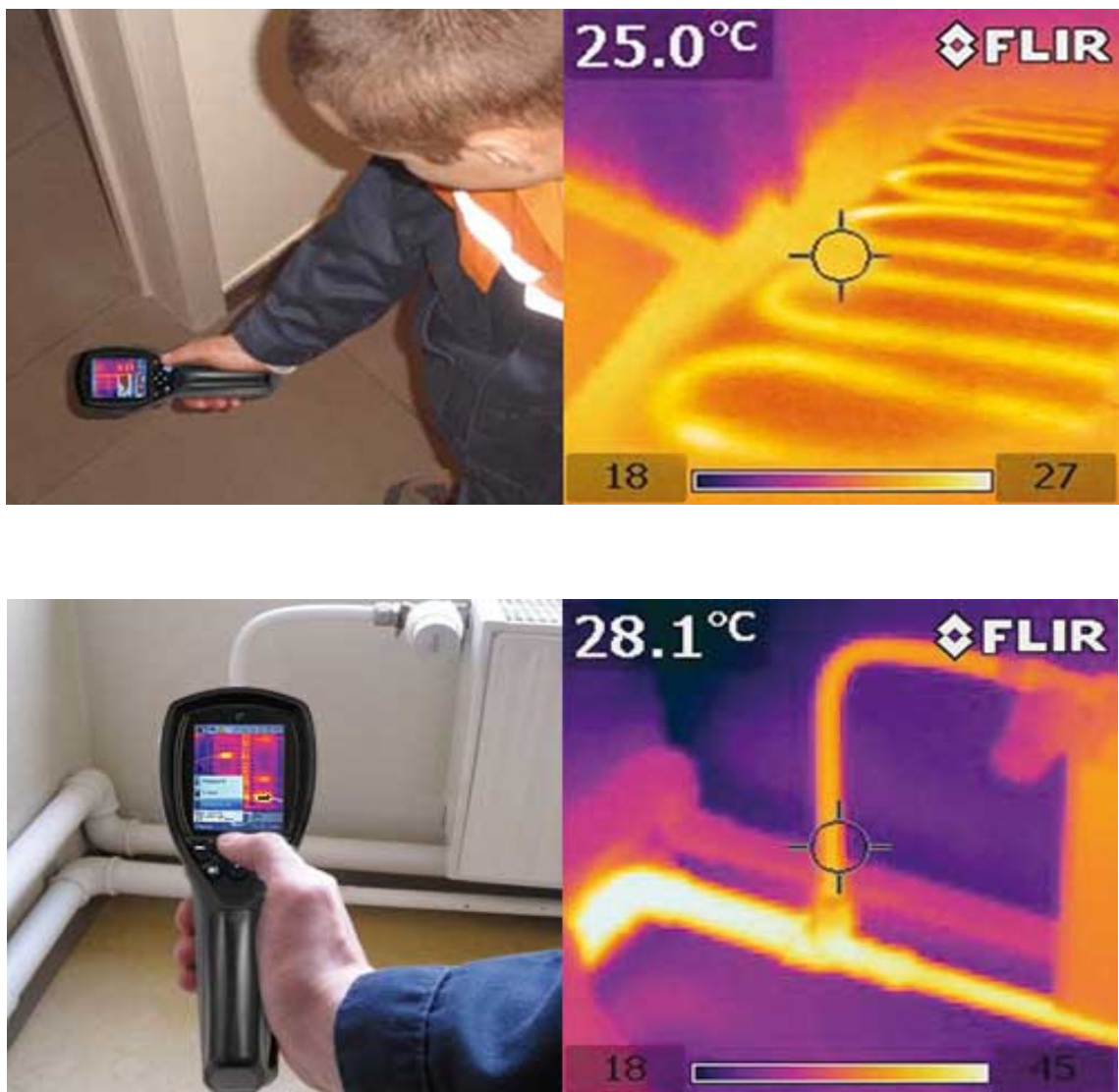
a. Using Infrared camera to inspect which pipes is the hot/cold (Top)

b. Using Infrared camera to inspect underground pipes network (Bottom)

Figure 2.7 IR Camera applications [98]

## 2.9 MODELING AND SIMULATION VIA FEM ANSYS

This study made some numerical modeling simulations based on experimental models which have already inspected in laboratory by others. This thesis introduces a new technology which may call it as LDMT (laser digital micromirror thermography) that has not used ever. These simulations are very important and helpful in research because they represent a way to validate the new technique that the thesis aims to achieve. These modeling and simulations have been done by using ANSYS 14; Appendix A, through a regular computer machine, Windows 7 Enterprise; Intel Core (TM) Duo CPU 3GHz. ANSYS is a finite element analysis method (FEM) software for structural physics that can simulate static (stationary), dynamic (moving) and heat transfer (thermal) problems. ANSYS simulation software enables organizations to confidently predict how their products will operate in the real world. ANSYS is an engineering simulation software (computer-aided engineering, or CAE) developer that its primary purpose was to develop and market finite element analysis software for structural physics that could simulate static (stationary), dynamic (moving) and thermal (heat transfer) problems [99]. ANSYS is one of the most widely used quantitative methods because it is so flexible and can yield so many useful results.

In this thesis, it has picked some models that already have laboratory results by others students or researchers. Then redesigned these models by Auto-CAD, and then exported it to mechanical workbench of ANSYS to run the simulation under the same conditions of the laboratory conditions of these models. Thereafter, the data and information that have obtained from ANSYS stored in a regular computer machine to process and analyses them by some professional software such as MATLAB (matrix

laboratory); Appendix B, and MS-Excel (Microsoft Excel). It can create a thermal image, which represents the surface's temperature distribution by ANSYS which its shape is approximately almost same as this thermal image that is obtained by infrared thermal camera.

The ANSYS program is capable of simulating problems in a wide range of engineering fields. The study in this thesis has focused on the thermal analysis. This analysis type addresses several different thermal problems, especially transient conduction or thermal transient which is a time-dependent problem of the primary heat transfer.

Basically, ANSYS transient thermal model requires the following information:

1. Model generation (Geometry)
2. Material properties, i.e. define materials/material properties
3. Mesh and Type and size of the elements, i.e. generate finite element model
4. Specify boundary and initial conditions (e.g., ambient temperature and time step)
5. Solution and results; obtain the solution, review results, plot/list results, and check for validity.

In geometry stage, the geometric configuration of the model, including the nodes and elements, are defined. Geometry can be either created within the ANSYS program or imported from computer-aided design software (CAD). Direct generation and solid modeling are the two methods used to create the finite element model inside the ANSYS program. In solid modeling, one describes the geometric shape of the model, and then

instructs ANSYS to mesh the geometry with nodes and elements automatically. The size and shape of element can be controlled this way.

In general, a large number of elements provide a better approximation of the solution. However, in some cases, an excessive number of elements may increase the round-off error. Therefore, it is important that the mesh is adequately fine or coarse in the appropriate regions. How fine or coarse the mesh should be in such regions is another important question.

Once the solid model has been completed, element attributes, element type, real constant, material properties, and coordinate system, need to be set and grid controls, the element shape, mid-side node placement, and element size, established. Elements in ANSYS have classifications and are assigned to 7 major subgroups of structural, thermal, electric, magnetic, dynamic, fluids, and coupled categories. ANSYS element library consists of almost 200 element types, among which 40 elements can perform a steady state and transient thermal analysis.

## 2.10 EXPERIMENT AND SIMULATION RESULTS

As a matter of fact, there exist several factors that can make some differences between the experiment's results that obtained laboratory and simulation's results that obtained via ANSYS. These factors can be include each of non-uniform heating, emissivity variations, surface geometry, and environmental reflections which have an extreme impact on thermal data in case of experimental test. Hence; quantitatively the

results obtained via the ANSYS in comparison with those obtained experimentally do not have to be the same values; but qualitatively it is supposed to be reasonable and behave the same way at least to be able to validate the simulation work. Simulation results allow optimization of the active infrared thermographic method, optimal setting of heat pulse parameters and the thermogram observation time. In the active thermography experiment tests special care should be taken if the stimulating of the inspected specimen's surface is non-uniform, the emissivity of the surface is non-uniform, or the surface of the object is non-uniformly irradiated by the IR source. This can lead to some different between the simulation and experimenter's results. One of the most significant different between the ANSYS's results and experiment one that the entire incident energy is absorbed by the stimulated surface to be inspected in case of ANSYS simulation; while a portion of this incident energy it absorbed in case of experimental tests. It is worth to mention it has neglect the all radiation and convection losses and assumed to be minimal in all simulations that have been done in this thesis. And also the simulations have been obtained by assuming adiabatic boundary conditions around the inspected specimens except the front side of the inspected specimen (stimulated surface) and its rear side, i.e., absence of heat losses.

# 3. PULSED THERMOGRAPHY TECHNIQUE (PT)

## 3.1 INTRODUCTION

Pulsed thermography; [16,23,26,28,29,34,36,39,53,54,60,74,80,88,93,110,106], represents one of the most common technique among the other infrared thermography NDI techniques, due to it can be used to perform safe inspection of large structures in a fast manner relying on a thermal stimulation pulse, with a short duration, where this technique allows providing a data acquisition in fast and straightforward

Pulsed thermography (PT) is an active technique in which the specimen being inspected is rapidly heated up from one side with a short heat pulse by using a high power source such as photographic flashes lamps (external excitation), where the light is transformed into heat (thermal energy). Then the thermal pulses propagate by conduction through the specimen until they reach a discontinuity that act as a thermal barrier reflecting the thermal pulses back to the surface, then recording, monitored and evaluating the temperature evolution (heat pulse response) by an infrared thermal camera in transitory regime after a certain time of cooling process [3,16,26,34]. However, it is also possible to use a cool pulse such as; ice, snow, or cold air guns [36,80,88], see Figure 3.1.
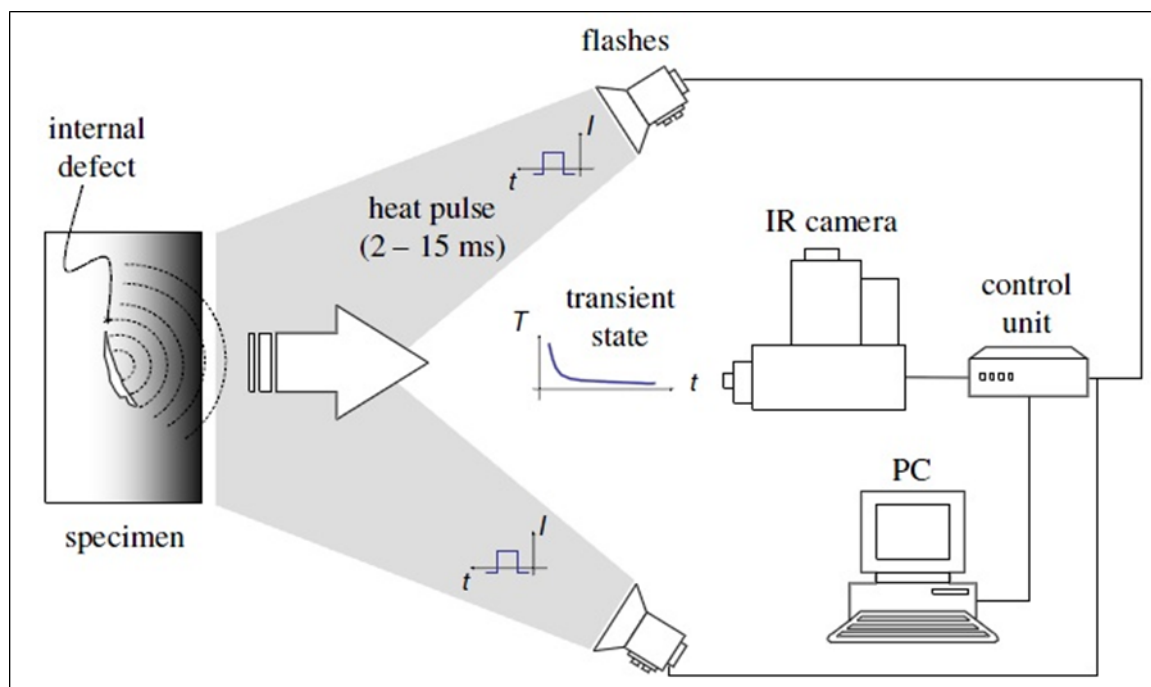
Figure 3.1 Equipment configurations for Pulse Thermography Flash or Transient [34]

The duration of the applied heat pulse may vary from μs, or ms to several seconds depending on the thickness of the specimen and the thermal physical properties of both of the specimen and defect; especially the thermal conductivity ($k$) [26,34,74]. Basically, the duration may be going from a few ms for high thermal conductivity material inspection; such as metal parts; silver, copper, or aluminum, to a few seconds for low thermal conductivity materials; such as plastics, graphite, concrete, epoxy, or polyvinyl-chloride components (PVC) [34,74,100].

## 3.2 BASIC CONCEPT AND THEORY FOR PT

In this method the examined specimen's surface is warmed up by one or more high energy generated photographic flashes lamps, and the temperature evolution on the examined specimen's surface during its self-cooling is recorded via an IR camera then processed and analyzed [16,26,34,36,74,80,88,101].

Pulsed thermography technique consists of a brief heating by applying a heat pulse into the object's surface being examined for a short duration, where the duration of the heat pulse may vary from a few ms (~2-15 ms flash heat using xenon flashes) which is called pulsed flash thermography, to several seconds (transient heat using halogen lamps) which is called pulsed transient thermography, as shown in Fig. 3.2, that is depending on the thermophysical properties of both the inspected specimen and the flaw [95,102-104]. In both cases, the equipment setup is as indicated in Figure 3.1.

In one hand, pulsed flash thermography represents a powerful tool for thin layers with shallow defects; such as corrosion under paint where the other active IRT techniques (such as pulsed transient thermography or lock-in (LT)) would not be workable in this type of situation. Basically, this technique requires a high power xenon lamp and a brief heating (typically 6 kJ power with 2 ms pulses), and it is a suitable for objects of high thermal conductivity materials; such as metal parts; silver, copper, or aluminum. Since this technique takes about (~2-15 ms) then this technique provides a short measuring times, i.e. it represents such a fast active IRT technique.
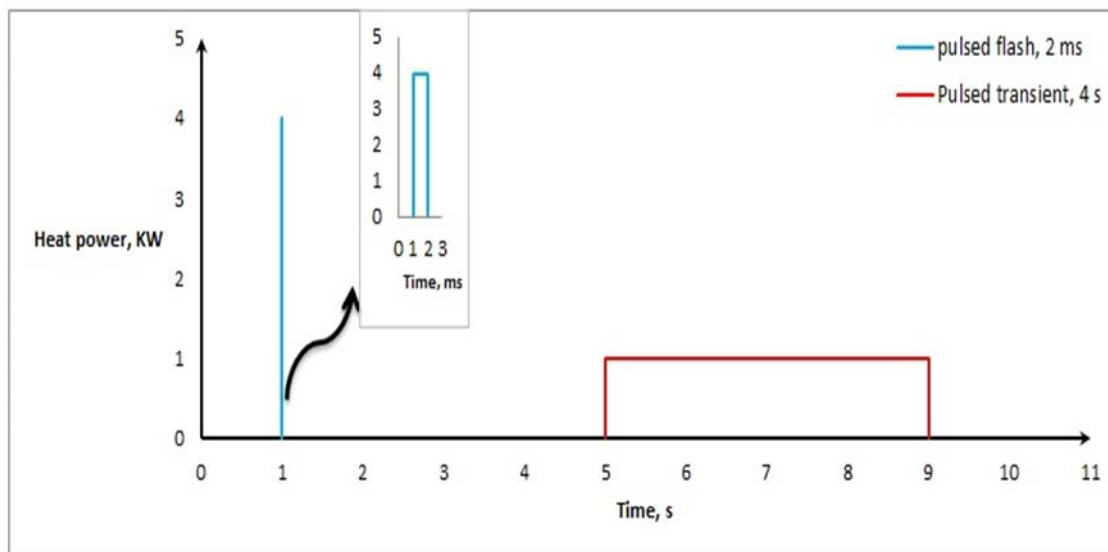
Figure 3.2 Pulse duration, power, and temperature regimes for flash PT, and transient PT

Moreover, it is able to perform depth-resolved inspections and providing high performance for examination of thin samples, with shallow defects. However; this technique includes some limitations; such as this technique is workable with a limited depth range of samples (shallow defects) with limited inspection area, besides it requires high thermal energy stimulating specimen since it uses a brief heating [34,95].

On the other hand, pulsed transient thermography does not need a high power stimulation, but it takes a heating duration longer (several seconds) than in case of pulsed flash thermography, with typically (1- 4) halogen lamps (1 kW each) with a 10 sec heat pulse and a (20~30sec) cool-down depending on the thermal physical properties of inspected object. Therefore, it is a suitable to be used for objects of low thermal conductivity materials; such as plastics, graphite, concrete, epoxy, or polyvinyl-chloride components (PVC). This technique provides a better ability of investigation a large

structure (typically 4 ft. x 6 ft.) which can be evaluated and imaged in a single shot. As the other techniques have limitations then pulsed transient thermography is also, that it is not suited for thick objects being examined. But, as a comparison, then for composite defect examination pulsed flash thermography is able to detect a composite subsurface defect for up to 3 mm depth, while pulsed transient thermography can detect a composite subsurface defect for up to 6 mm [34,95].

In general, the phenomenon is as follows; the heat pulse transfers by radiation from the energy source through the air (medium) until the heat pulse front comes in contact with the specimen's surface being inspected then the object's temperature starting rises up rapidly during the excitation [36].

Based on the emissivity of the inspected specimen's surface then some of the illumination that applied onto the inspected specimen's surface is absorbed and transformed into a thermal energy, which propagates by conduction under the stimulated surface through the object starting towards the inside one [74]. After the pulse and as time elapsed, the thermal energy will decay over time. If the heat pulses, which are travelling through the specimen, reach any discontinuity (defect) then this fault will block the heat diffusion and change the heat flow rate by reducing it, and reflecting the thermal waves back to the surface (stimulated surface). The presence of a discontinuity produces a thermal resistance (thermal barrier) to the thermal pulse front, hence reducing the heat diffusion rate and causing a thermal contrast between the defective area and the reference one. So by observing the temperature of the surface via IR camera then any discontinuities such as; porosity, delaminations, disbonds, fiber breakage, or inclusions, will appear as areas with a different temperatures (often hotter) with respect to the

surrounding non-defective areas; i.e. these discontinuities will be detectable . In fact in such a case the reduced diffusion rate that caused by the subsurface defect presence translates into heat accumulation; i.e. on the observed surface being examined then the area over the defective appears in hotter relative to the reference area. Therefore, deeper discontinuities will be observed later and with a smaller contrast [16,26,34,36,74,100].

## 3.3 PULSED THERMAL WAVES

When a thermal energy is applied into the surface of a solid material, then the object's surface being examined will absorb some of the incident energy and propagate by diffusion through the materials. The thermal energy propagation through a solid can be described by Fourier's partial differential equation which is well known as heat equation [34,105]:

$$\rho \cdot C_p \frac{\partial T}{\partial t} + \nabla \cdot (-k \cdot \nabla T) = Q \tag{9}$$

The heat diffusion through material with isotropic materials is a complex 3D problem that can be expressed in a simplified case by Fourier's law of heat diffusion which can be written as [34,105]:

$$\nabla^2 T - \frac{1}{\alpha} \cdot \frac{\partial T}{\partial t} = 0 \tag{10}$$

Where T [$^o$C] is the temperature, $\alpha = k/\rho.C_p$ [m$^2$/s] is the thermal diffusivity of the material being inspected at constant pressure, $k$ [W/m.K] is the isotropic thermal

conductivity of the material being inspected, $\rho$ [kg/m$^3$] is the mass density of the material being inspected, $c_p$ [J/kg.K] is the specific heat capacity at constant pressure; and $t$ [s] is the time.

Thermal diffusivity ($\alpha$) is a physical property that associated with transient heat flow, which indicates and measures the ability of materials to convey or transfer thermal energy relative to its ability to store thermal energy. Therefore, materials which have a high thermal diffusivity respond speedily to any change in their thermal surroundings and reach the thermal equilibrium in a so brief time and vice versa, i.e. materials which have a low thermal diffusivity respond slowly to any change in their thermal surroundings and require a long time to reach the thermal equilibrium [106].

The 1D solution of the Fourier equation for the propagation of a Dirac heat pulse by conduction through a semi-infinite solid with isotropic materials has this expression [34,106,107]:

$$T(z,t) = T_i + \frac{Q}{\sqrt{k\rho c_p \pi t}} \, exp\left(-\frac{z^2}{4\alpha t}\right) \tag{11}$$

Where $Q$ [J/m$^2$] is the energy absorbed by the object's surface, $T_i$ [$^o$C,K] is the initial temperature; and $z$ [m] is the depth.

A Dirac heat pulse is an ideal instantaneous waveform defined as an intense unit-area pulse of a very short duration that no measuring equipment has ability to distinguish it from even shorter pulses. A Dirac heat pulse is composed of periodic waves at all frequencies and amplitudes. Although it is not possible to reproduce such a waveform in practice; however a heat pulse provided by a powerful source such as a photographic

flash having approximately a square shape can be used. In this case, the signal is composed by periodic waves at several (not all) frequencies, where the shorter the pulse, the wider the range of frequencies [16,26, 34,106].

At the surface (z = 0 mm), the behavior is somehow different starting at a high temperature and decreasing following approximately the square root of time. Where the thermal evolution for shallower defects show higher peak intensities earlier; whilst for deep defects it starts at zero and reaches peak intensity later, i.e. longer time for deeper defects [34]. Thus Eq. (11) can be rewritten as follows:

$$T(0,t) = T_i + \frac{Q}{\sqrt{k\,\rho c_p\,\pi\,t}} \tag{12}$$

Or;

$$T(0,t) = T_i + \frac{Q}{e\,\sqrt{\pi\,t}} \tag{13}$$

Where $e = (k/\rho.Cp)^{1/2}$ [m] is the effusivity, which is a thermophysical property relevant to transient surface heating processes, which is present in all materials (solids, liquids, pastes, powders, and gases). Effusivity refers to measurements of the material ability to exchange heat with its surroundings [106]. Despite the fact that the heat diffusion represents a complex 3D diffusion problem, but Eq. (13) presents the only approximation of the complex 3D diffusion problem that described by Fourier's law Eq. (9), which has been successfully used by many researchers to develop qualitative and quantitative techniques.

Also, for semi-infinite solid one-dimension heat conduction, the temperature profile for a constant surface heat flux can be depicted in Fig. 3.3 and it can be described in this relation [31]:

$$T(x,t) - T_i = \frac{q''}{k}\left[\sqrt{\frac{4\,\alpha\,t}{\pi}}\,exp\left(-\frac{x^2}{4\alpha t}\right) - x\,erfc\left(\frac{x}{2\sqrt{\alpha t}}\right)\right] \tag{14}$$

Eq. (15) is applicable at any time in this range $(0 < t < \tau)$, where $\tau$ is the heat pulse duration. And for $(t > \tau)$, then uses this form:

$$T(x,t) - T_i = \frac{2q''\sqrt{\tau t}}{k}\,ierfc\left(\frac{x}{2\sqrt{\alpha\,t}}\right) - \sqrt{t-\tau}\,ierfc\left(\frac{x}{2\sqrt{\alpha t - \alpha\tau}}\right) \tag{15}$$

Where *erfc* is the complementary error function, *ierfc* is the integral complementary error function, $q''$ [W/m$^2$] is heat flux; and $x$ [m] is distance from surface.

The error functions are a standard mathematical function, just like the sinus and trigonometric function, whose value varies between one and zero. The relation between the complementary error function and the integral complementary error function can be shown in this relation [108]:

$$ierfc(x) = -x\,erfc(x) + \frac{exp(-x^2)}{\sqrt{\pi}} \tag{16}$$

The value of the integral complementary error function (erfc) can be found by MATLAB and in reference [31] as well.
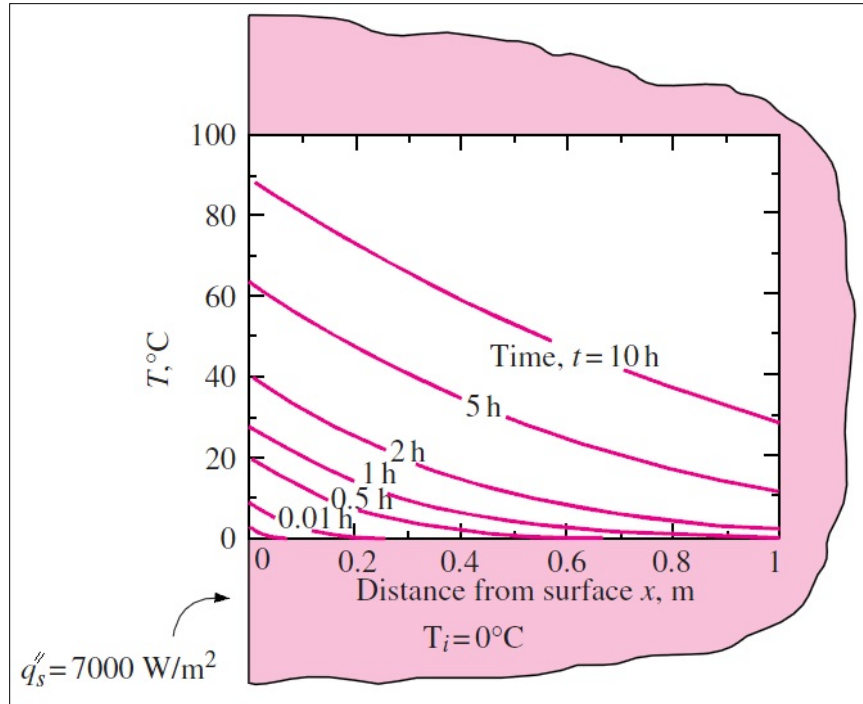
Figure 3.3 Shows temperature profile for a constant surface heat flux, q"=7000 W/m$^2$ [31]

Moreover, such phenomenon occurs in time so that, shallower defects are observed earlier and deeper defects are observed later and with a reduced "diluted" or "spread" thermal contrast. It is apparent that the thermal diffusion is not stationary and therefore exist some lower limit of observation time $\tau$, when the effect (surface temperature contrast) arise after thermal activation of the surface. This time is approximately equal to the time interval of the thermal pulse propagation from the surface to subsurface defect and can be estimated from the Fourier's Eq. (9), in which the observation time $t$ as a function of the square of the subsurface defect depth z ($z^2$) [34, 36]:

$$\tau \approx \frac{z^2}{\alpha} \tag{17}$$

Table 3.1 shows the estimated propagation times $\tau$ for depth of the subsurface defect $z$ =5mm for a different materials of high and low thermal conductivity and other thermal physical properties.

Table 3.1 Estimated times of the heat pulse propagation ($\tau$) to the subsurface defect with a depth 5 mm [36]

| Materials | Thermal Conductivity $k$ [W/m.K] | Specific Heat $C_p$ [J/kg.K] | Density $\rho$ [kg/m$^3$] | Thermal Diffusivity $\alpha$ [m$^2$/s] $\alpha = k/(\rho.C_p)$ | Propagation time for z=5mm $\tau$(s) |
|---|---|---|---|---|---|
| Aluminium | 250 | 870 | 2700 | 1.06E-04 | 0.23 |
| Gypsum | 0.47 | 1090 | 1150 | 3.75E-07 | 67 |
| Concrete | 1.4 | 1050 | 2000 | 6.6E-07 | 38 |
| Epoxy | 0.35 | 970 | 1300 | 2.78E-07 | 90 |

Applying Eq. (17) shows the thermal propagation time in materials of high thermal conductivity is shorter and much faster than in materials of low thermal conductivity. For instance; the thermal propagation time ($\tau$) is about 0.04s (40 ms) for 2 mm of a subsurface defect in aluminum (high thermal diffusivity), and it is about 30s for 2 mm of a subsurface defect in graphite epoxy ( low thermal diffusivity). This means Flash is better for materials of high thermal diffusivity, e.g., metals. Materials with a low

thermal diffusivity, e.g., composites, have a long thermal propagation time, which limits flash thermography to the detection of shallow defects [95].

However, for a polyethylene materials (the material was used in the experimental and this simulation) that were used in this PT simulation, the depth ($z$) is 5 mm and the thermal diffusivity α is 0.1E-06 m$^2$/s, i.e. α=0.1 mm$^2$/s. Then from Eq. (17) the estimated propagation times $\tau$ equals to 5 sec.

## 3.4 EXPERIMENTAL SETUP AND DATA ACQUISTION FOR PT

In general, the experimental setup; as can be seen in Fig. 3.1 consists of one or two photographic flashes are used as excitation sources to stimulate the specimen's surface being inspected. As time elapses, the object's temperature will decrease and cool-down uniformly providing a thermal contrast which can be observed and recorded via IR camera in transitory regime. It is necessary to use a control unit (synchronization unit) to control the time between the launch of the heat pulse and the recording via the infrared camera, see Figure 3.1 Then the obtained data is stored as a 3D matrix, Figure 3.4a, where $x$ and $y$ are the spatial coordinates represent the horizontal and vertical pixel positions respectively, and the z-coordinate corresponds to the time evolution $t$. For the non-defective areas, then the temperature $T$ decays approximately at least at early times as the square root of time, as it is clearly shown in Eq. (13), but for the defective area then the cooling rate is different (red-dotted line), as it is shown in Figure 3.4b. Basically, the thermal evolution for deep defects starts at zero and reaches peak intensity at a given time; i.e. shallower defects show higher peak intensities earlier while deeper defects

reach peak intensity later. Shallower defects show higher peak intensities earlier, then slowly decreases approximately as the square root of time (t $^{1/2}$), as it is clearly shown in Eq. (13) [36,34].

Experimentally, the test specimen's surface was stimulated with halogen lamps, whose power was 15 Watts. The experiment was made in a reflection mode. The specimen's surface was heated up from the side where simulated defects are invisible. The test specimen used in the laboratory test and this simulation as well (37 x 37 mm$^2$) was made of a polyethylene sample with 4 flat bottom holes are shown in Figure 3.5, which is characterized by relatively low thermal conduction $k$ (about 0.28 J/kg.K). The simulated defects are represented by four flat-bottom holes were arranged as illustrated in Figure 3.5. The thickness of the plate is 5 mm.
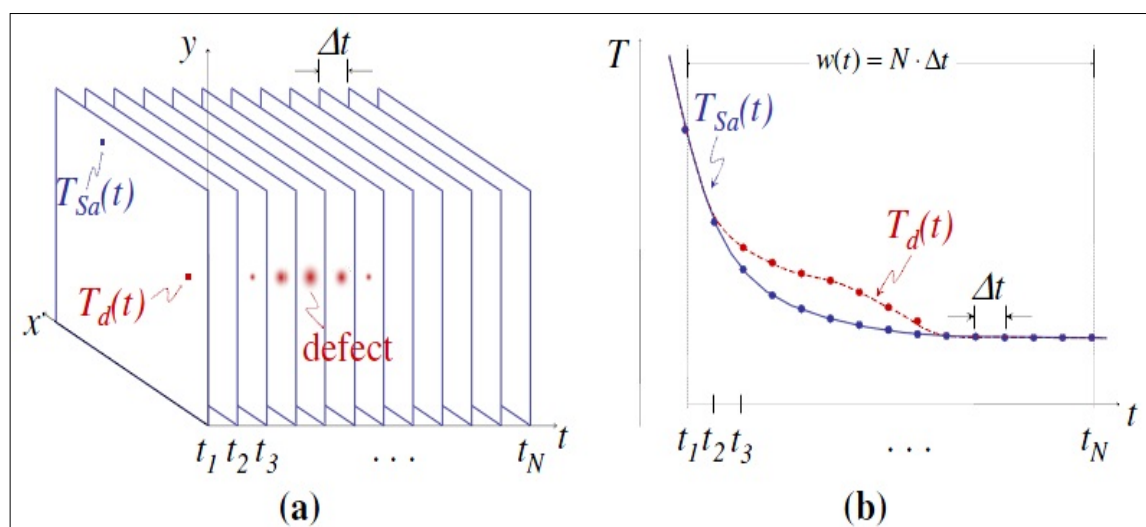


Figure 3.4 Temperature evolution: (a) Temperature data 3D matrix on time domain (x, y, T, t), and (b) temperature profile (t, T) for a defective (Red-dotted line) and non-defective (continuous line) pixels [34]

## 3.5 GEOMETRY AND MESHING

The model geometry was defined to correspond to the inspected specimen. All of the dimensions used in the model were taken from the inspected specimen specifications; such as the defect size and disposition respect the specifications as well. The geometry was studied numerically by using FEM ANSYS tools and run it on a regular computer and without needing a professional computer machine. This work has been done via non-commercial ANSYS 14 through a tansient thermal as an analysis system. The test specimen has designed by Auto-Cad based on the experimental specimen dimensions, then imported it to the design modeler of geometry of ANSYS. For calibrating the analysis procedure, test specimen sized (37 x 37 x 5 mm³ ) made of a polyethylene specimen with 4 subsurface flat bottom holes are shown in Figure 3.5, the thermal physical properties of the inspected object are shown in table 3.2. The unstructured mesh was consisted of tetrahedral elements, with (495393 nodes) and (322874 elements) craeted in a sufficient accuracy features; as it is shown in Figure 3.6. An adjustment of the mesh parameters permitted a different degree of mesh refinement in regions where larger temperature gradients were expected. The element size was not chosen uniformly, but with high smoothing, fast transition, and fine span angle center. The defets have represnted by 4 flat subsurface holes which asssumed they are filled up by air. The heat pulse of 15 Watt has applied uniformly upon whlole the nondefective (zero holes) test specimen's surafce, i.e. up-surface. The pulse duration time was (0.1 seconds); i.e. 100 ms. Hence, the simulation is ready to run via ANSYS on the computer.

Unknown parameters of the experiment modelling; such as power density of the heat source that used in experiment, ambient conditions, and pulse duration long were adjusted during doing the numerical simulation via FEM ANSYS to obtain results as close as possible to those obtained experimentally. Due to they are not avaialable in the experimental paper [109].

Table 3.2 Thermal properties of materials used in PT simulation

| Materials | Thermal Conductivity $k$ [W/m.K] | Specific Heat $C_p$ [J/kg.K] | Density $\rho$ [kg/m$^3$] | Thermal Diffusivity $\alpha$ [m$^2$/s] $\alpha = k/(\rho.C_p)$ |
|---|---|---|---|---|
| Polyethylene | 0.28 | 296 | 950 | 0.01E-05 |
| Air | 0.025 | 1000 | 1.205 | 2 E-05 |
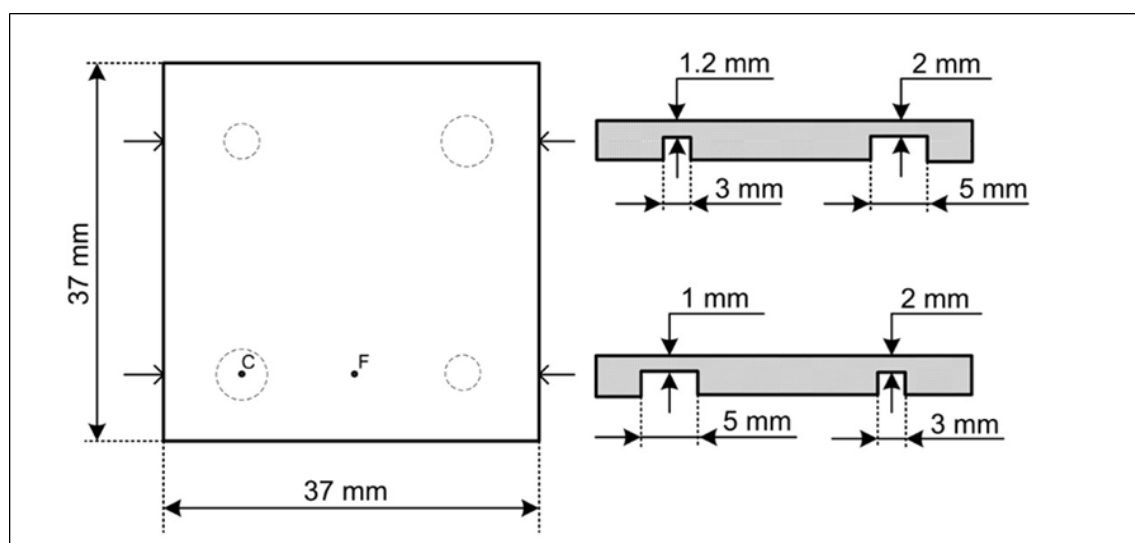


Figure 3.5 Sketch of the inspected sample with 4 flat bottom holes [109]
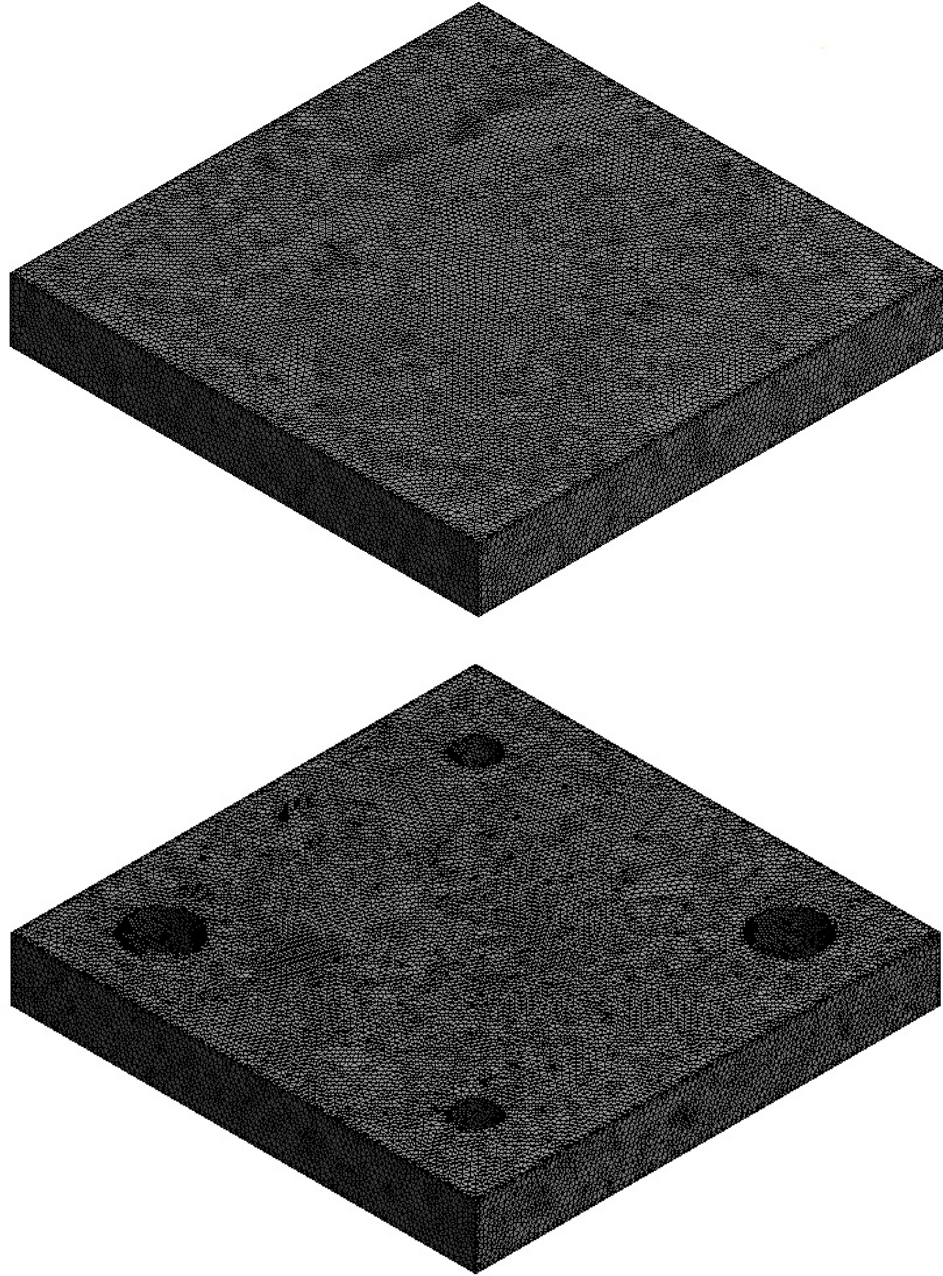
Figure 3.6 Show meshing of test specimen obtained via ANSYS 14

## 3.6 THERMAL PROPOGATION EVOLUTION

Thermal propagation evolution over the whole sample are shown in Figure 3.7. The simulation has been done by ANSYS 14 with the same conditions for both the non-defective sample ( Figure 3.7a ) and the defective sample ( Figure 3.7b ). Figure 3.7a shows a specimen with zero defects (nondefective speciemen), in which it is clearly shown that the heat propogats uniformly from the up surafec inward another one sequentially section by section (layer by layer) through the speciemn. Figure 3.7b shows a specimen with defects (flat bottom holes) appear as hot spots.

The phenomen as follow; the temperatures distribution of the specimen's surface being inspected will change rapidly (increasing) due to the delivered thermal energy that applied onto surface. Then the heat pulses that generated  at the surafce propagates by conduction through specimen by diffusion starting from up surafec (stimulateed one) towards inside one.

After pulse and as time elapses; in one hand, the heat propogats uniformly through the specimen then the surface temperature will decrease uniformly for the examined non-defefctive specimen, as it is shown in Figure 3.7a. On the other hand, subsurface holes will block the the heat flow, due to the presence of these defects change the heat flow rate then producing a non-uniform heat propogation which lead to have abnormal temperature patterns at the surface. In fact in such a case the reduced diffusion rate caused by the subsurface defect presence translates into "heat accumulation" and hence higher surface temperature just over the defect which can be detected with an IR camera, as it is shown in Figure 3.7b.

In other words, subsurface defects (holes) act as a thermal barrier and work as a thermal resistance which changes the thermal diffusion rate; mathematically described by Fourier's Eq.(13), therefore subsurface defects appear as areas of different temperature (often hotter) with respect to surrounding areas.

Figure 3.5 shows two points F and C on the surface of the inspected specimen. Where the cooling rate at point C is much slower than point F, due to there exists a defect directly under point C which act as a thermal resistance. Hence, the zone that exists over the defect will be cooled at a slower rate. Therfore; the defects appear on the observed inspected speciemen's surface as areas of different temperature (hotter) with respect to surrounding areas (non-defective areas), as shown in Figure 3.7.

a. Defective specimen          b. Non-defective specimen
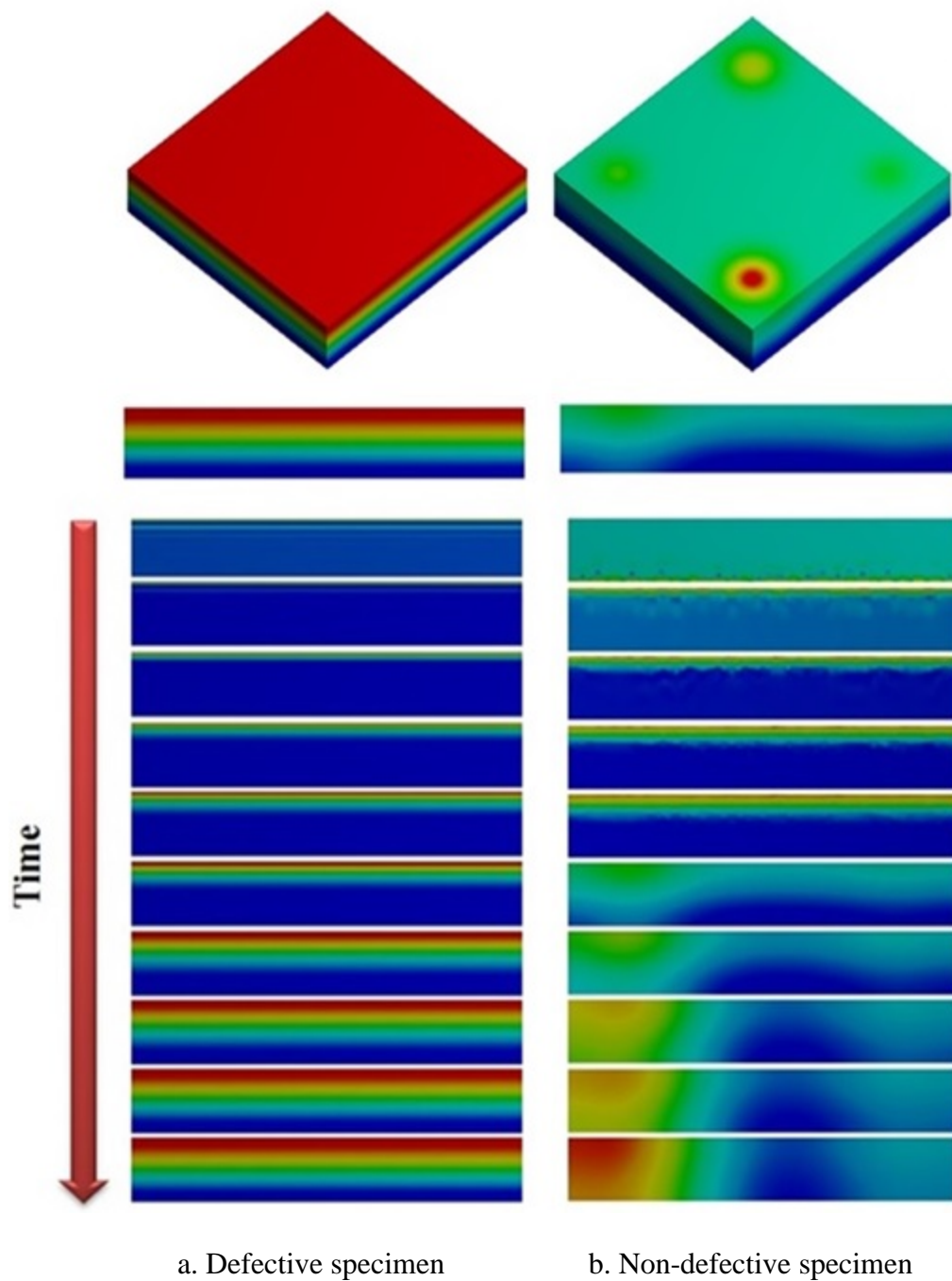
\* Temperature gradient in case of (a) is NOT same as in case of (b).

Figure 3.7 Specimen's IR images obtained via ANSYS results for PT technique, which
show the thermal propogation sequence

### 3.7 SIMULATION AND EXPERMINTAL'S RESULTS OF PT

In this section will introduce a modeling and simulation of pulsed thermography PT. The model has already inspected laboratory [109]. In this simulation, it has applied the same conditions of the corresponding laboratory test to the specimen that has inspected via ANSYS 14.

**3.7.1 Model Parameters.** There are several parameters and factors have an effective control in any thermographic measurement such as; the applied stimulation energy especially its uniformity, total observation time of the cooling process, and the number of thermal images to be taken by IR camera. Where the applied stimulation energy is a variable factor and its power is related to the heat source. The total observation time and the number of thermal images represent control settings of the camera. The observation time has to cover most or the main part of the cooling process, where cooling process continues until the whole sample has reached the surrounding temperature and being in thermal equilibrium. However the most interesting part of the cooling process in pulsed thermography is represented by only the beginning of the cooling. Basically, typical observation time is about 30 seconds. For example, the cooling process in an epoxy, concrete, or a polyvinyl-chloride (PVC) specimen is extremely slow, i.e. it needs a long time to reach the surrounding temperature and being in thermal equilibrium, due to the low thermal conductivity; i.e. the thermal diffusivity is poor. Whilst for materials of high thermal conductivity such as silver, copper, and aluminum specimens, then the cooling process is very quick and needs just a brief heating time in which probably after 1 second is almost over. Thus the total observation time and the

number of images to be taken are set individually according to thermal sample properties and initial tasks [109].

In next two sections will introduce the evolution curves and sequence of thermograms obtained by ANSYS and their corresponding experiments. These evolution curves were used for comparison of the experimental results and results obtained by numerical modeling ANSYS. Furthermore, thermal contrast evolution curves were used to analyze the differences in results that obtained experimentally and through modeling.

**3.7.2 Cooling Curves Evolution.** Figure 3.8 shows the surface temperature development curves over the hole center (C) and away from it (F). The data of these curves has obtained from experimental results [109]. Point (C) is the corssponding point to the subsurace hole (defect) with diamter of 5 mm and depth of 4 mm. Point (F) is the corssponding point to the center of distance between the two subsurafce holes, which is non-defective area. These curves are called cooling curves, decay curves, or temprature profiles. They describe the cooling process inculding the stimultion process as well which is represented by first part, in which the curve is growing up. As the time passes, due to the 3D thermal propagation by diffusion in all directions, then the temperature evolution on the inspected specimen's surface develps and leads to the thermal equilibrium again, where the thermal propagation continues until the whole sample has reached the ambient temperature after about 30 seconds.

On the other hand, Figure 3.9 shows the surface temperature development curves over the holes center (C) and away from it (F). These curves have established based on

data of modeling and simulation that obtained via FEM ANSYS and created by MS-Excel 2010.

Figures 3.8 and 3.9 show that the temperature on point C is higher than point F due to the fact there is a subsurface defect (hole) under point C. Indeed, the temperature on point C is the maximum temperature among entire inspected specimen points, due to the fact that the subsurface defect at point C has deepest depth and largest diameter, i.e. the defect at point C will produce a highest thermal resistance over the entire specimen.
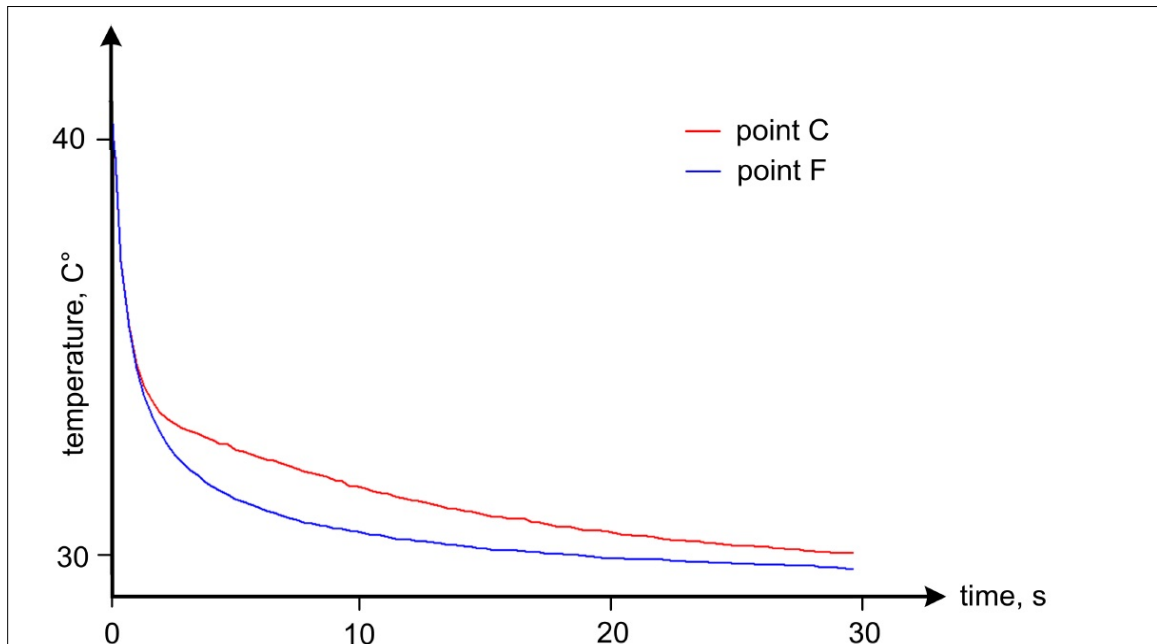


Figure 3.8 Experimental cooling curves at the hole center and apart from it (cooling curves are extracted at the points C and F as it is shown in Figure 3.5) [109]
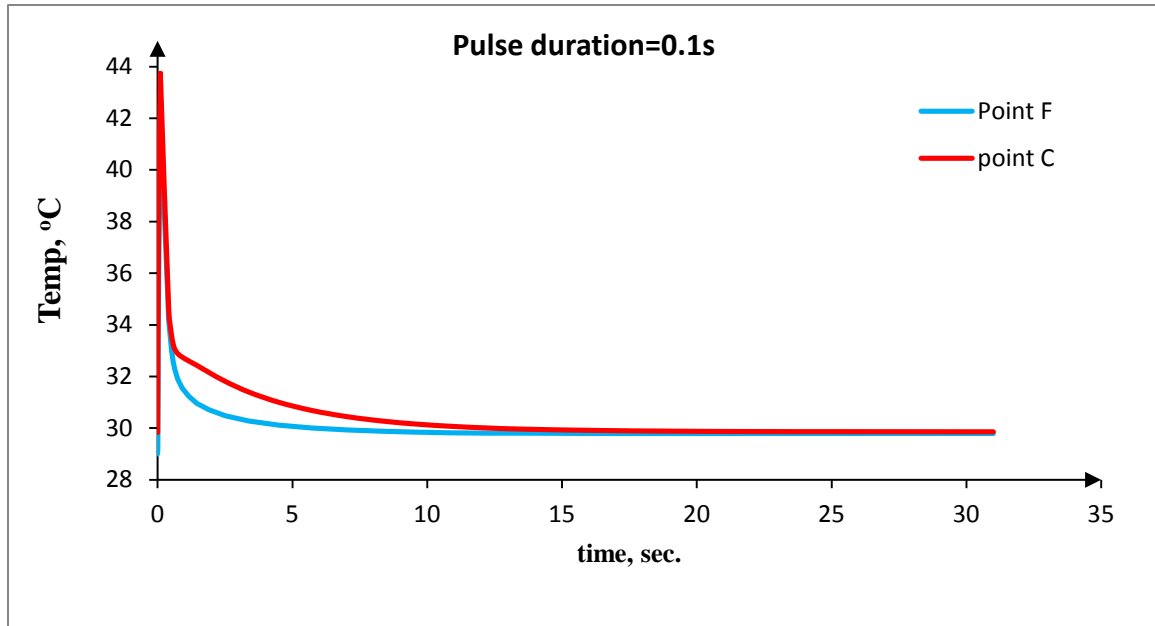
Figure 3.9 Cooling curves at the center of hole and apart from it (cooling curves are extracted at the points C and F as it is shown in Figure 3.5), data has obtained by ANSYS

Also it is clear from both of Fig. 3.10 and Fig. 3.11; there is a little bit difference between them. That is because the laboratory (experimental) test in Fig. 3.10 was done under real condition which is not exactly similar to the ideal condition of the simulation in Figure 3.11. Where, in ANSYS simulation the inspected specimen was perfectly isolated at the four sides around the sample, i.e. zero heat transfer with no convection or radiation; whilst in real (experimental test) it was not totally isolated. Also the initial conditions and assumptions that are considered to build up the transient thermal and mechanical bench of ANSYS can cause this difference between these curves. Moreover, the delivered thermal energy to stimulate the specimen being examined, it may be different in exact amount and its uniformity where it cannot guarantee to stimulate the

object uniformly. However, the temperature profile curves in both figures behave and act almost the same behavior. Hence, this can validate this simulation.

Furthermore both Fig. 3.10 and 3.11 show the difference between applying Eq. (13) and set of Eq. (14) and Eq. (15); it is very clear that both of the temperature decay curves behave the same behavior for using a very short pulse, as it is shown in Fig. 3.10; but there is a difference in case of long pulse especially at the beginning of the cooling process; as it is shown in Fig. 3.11. Therefore, it is very suitable to use Eq. (14) for a short pulse (μs, ms to 1s), i.e. for a pulsed flash thermography; and use set of Eq. (15) and Eq. (16) for a long pulse (1s to several seconds), i.e. pulsed transient thermography.
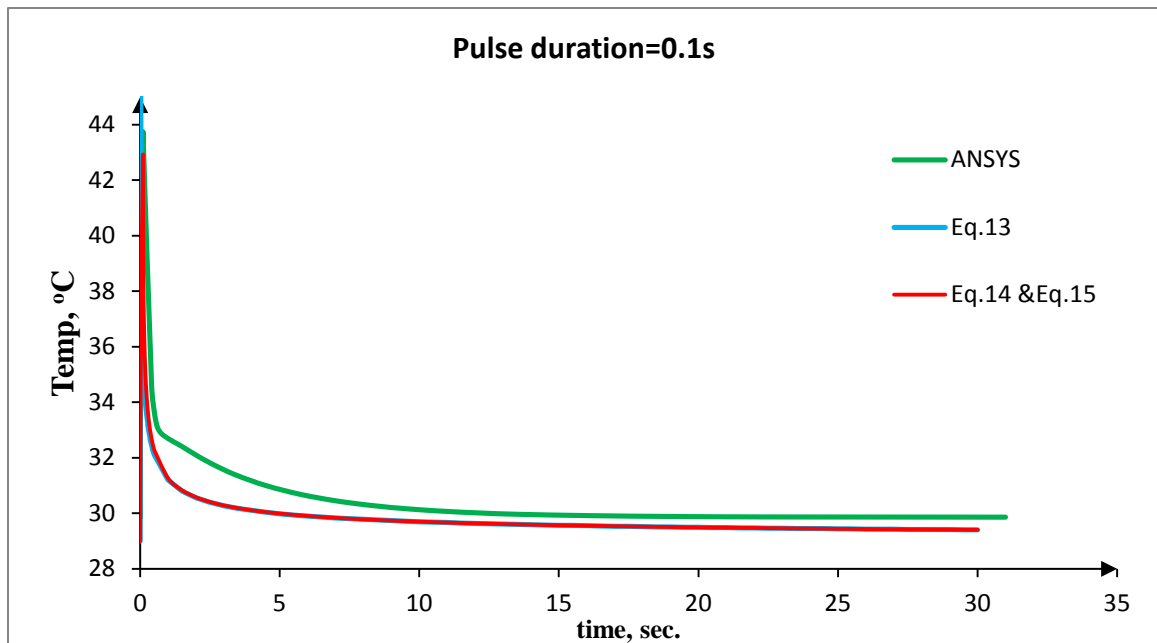


Figure 3.10 Shows temperature decay curves at point C for results obtained by Eq.13, set of Eq.14& Eq.15, and ANSYS for a short heat pulse of 0.1 second
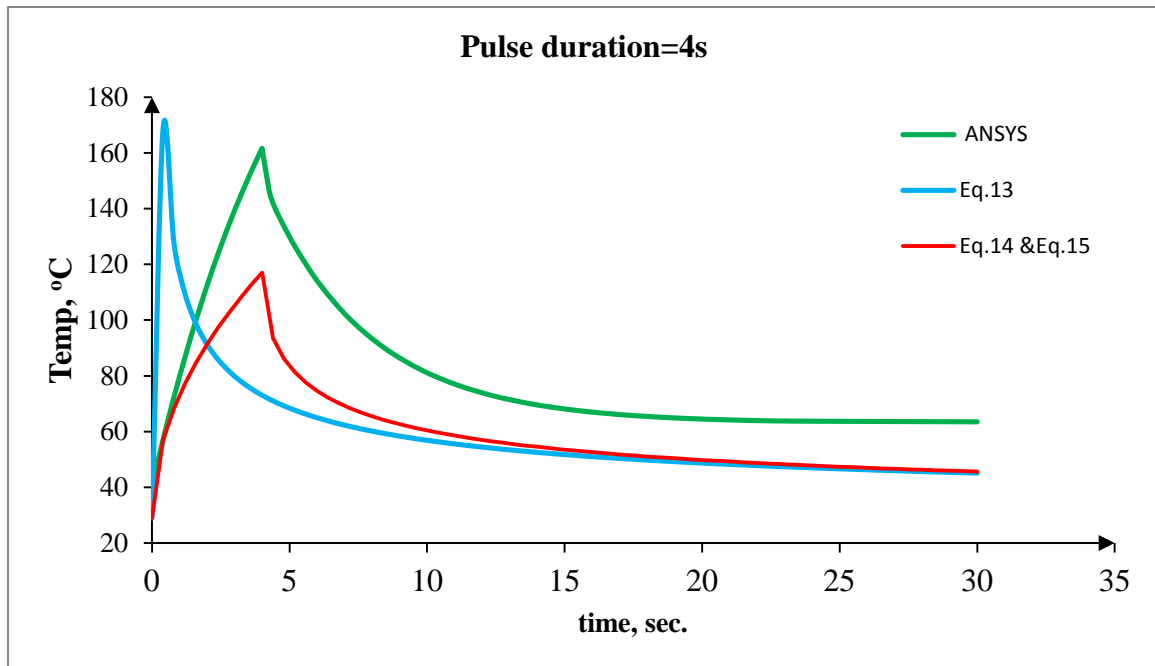
Figure 3.11 Shows temperature decay curves at point C for results obtained by Eq.13, set of Eq.14& Eq.15, and ANSYS for a long heat pulse of 4 seconds

From Fig. 3.12, the overall difference in temperature levels of the experimental, theoretical (Eq.13 and Eq.14 &Eq.15), and numerical ANSYS results is again due to the probability of non-uniform heating, emissivity variations, surface geometry, and environmental reflections which have an extreme impact on thermal data of PT in case of experimental test, but despite certain differences, it can generally be concluded that all these decay curves show almost relatively similar behavior. Hence, the results obtained via the ANSYS show a good reasonably agreement with the experimental data and this validate this simulation.
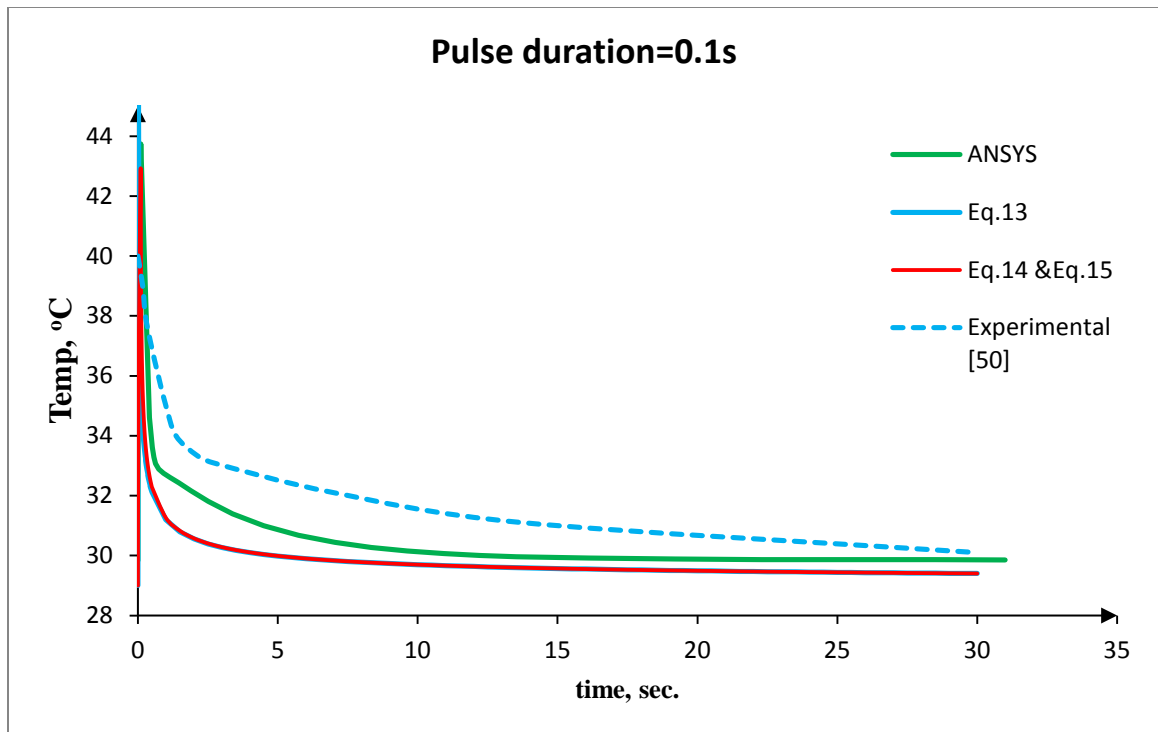
Figure 3.12 Shows temperature decay curves at point C for results obtained by Experiment, Eq.13, set of Eq.14& Eq.15, and ANSYS for a short heat pulse of 0.1 second

**3.7.3 Experimental and ANSYS's IR Images.** Figure 3.13 presents four pairs of corresponding temperature distributions of the inspected specimen's surface (thermal images) in gray scale obtained experimentally [109] and from ANSYS simulation model. Figure 3.13, in one hand, clearly illustrates that the results obtained with the ANSYS show these are subsurface defects (holes) which validate this simulation. On the other hand, the results that obtained by ANSYS show a good reasonably agreement/match in comparison to these results in the corresponding experimental test. Hence, this validates this simulation.

These thermograms represent a useful tool in observations and detections. Where it exists several observations can be made from these thermograms. In which this noticeable thermal contrast refers to existence of a subsurface fault (holes) which helps to reveal the defect and determines its location. These contours represent the non-defective areas, i.e. the defects locate under this contour. Thus, we can conclude that the qualitative evaluation of nondestructive inspection is not a big issue in PT technique. However, the more challenge exists in the quantitative evaluation of the inspection results such as; exact shape, depth and thermal properties. It is worth to mention that the temperature scales are adjusted so that the maximal contrast is obtained for experimental images in order to enhance the visibility of defects. The temperatures range for the corresponding temperatures distribution data of the examined specimen's surface that obtained numerically via FEM ANSYS were adjusted to correspond to the experimental data temperature scale; so that the images can be directly compared. However, any different between the results of the ANSYS model and the corresponding experiment it can be existed due to some changes; where the model has done via ANSYS in ideal conditions while the experiment has done in real condition. These changes are such as the homogeneities of the inspected specimen, heat convection, heat radiation, ambient temperature, the distance between the excitation source and the inspected specimen, and the uniformity of the thermal energy that supplied to the examined specimen's surface which is very important factor that can be effect on the PT experimental results.
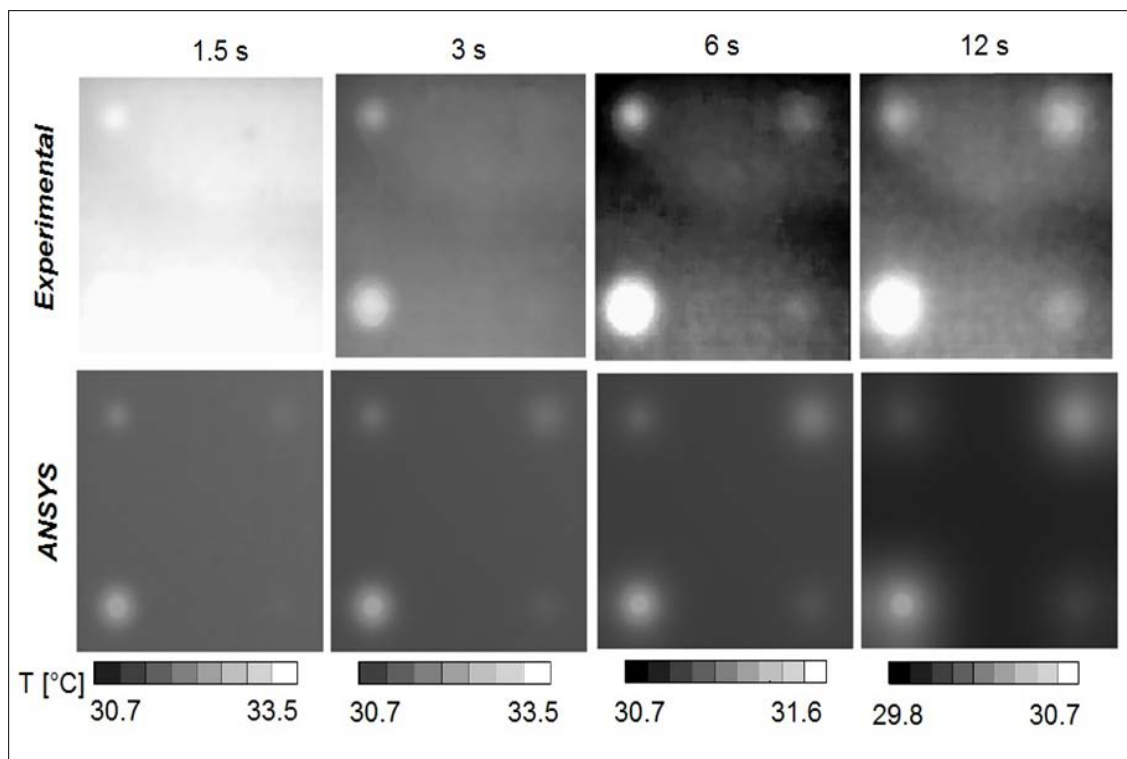
Figure 3.13 Thermograms and surface temperature distribution of the cooling sequence measured by PT that has obtained by ANSYS and experiment [109]

# 4. LOCK-IN THERMOGRAPHY TECHNIQUE (LT)

## 4.1 INTRODUCTION

Lock-in thermography; [6,16,26,28,29,34,36,38,39,53,74,95,100,106,107,110], was invented in 1984 [111] and has been used widely in NDI's testing and evaluating for looking below the surface of solid parts due to it allows detecting subsurface defects, i.e. hidden faults [16,112].

Lock-in Thermography stands as an active thermography NDI technique which is established basing on using a periodic input energy waves (periodic excitation) to send periodic waves (sinusoids) at a given modulation frequency $\omega$; in order to derive information from the observed phase and amplitude of the reflected thermal wave [113], see Fig. 4.1, which it makes visualization of deeper defects with LT is possible better than with PT. The halogen lamps represent the most common affordable stimulation heating source that is used in LT [95].

Lock-in thermography is a technique derived from photo-thermal radiometry (PTR) [114], in which, the thermal waves is delivered into specimen's surface in the form of periodic thermal waves (periodic stimulation), then the thermal response is recorded at the same time by using an IR camera [26,34]. In general in PTR, the examined specimen's surface is stimulated by a plane light beam and its thermal infrared emission is measured and recorded by an infrared IR detector. In one hand, if the infrared IR detector is made of a monolithic IR sensor, then the technique is known as photo-thermal radiometry (PTR), whereas if the detector is made of an array of IR sensors, the

technique is known as lock-in thermography (LT) [113,115]. Using an un-cooled IR-camera in LT is normally sufficient, and then it is an economical technique since the uncooled IR camera is cheaper.
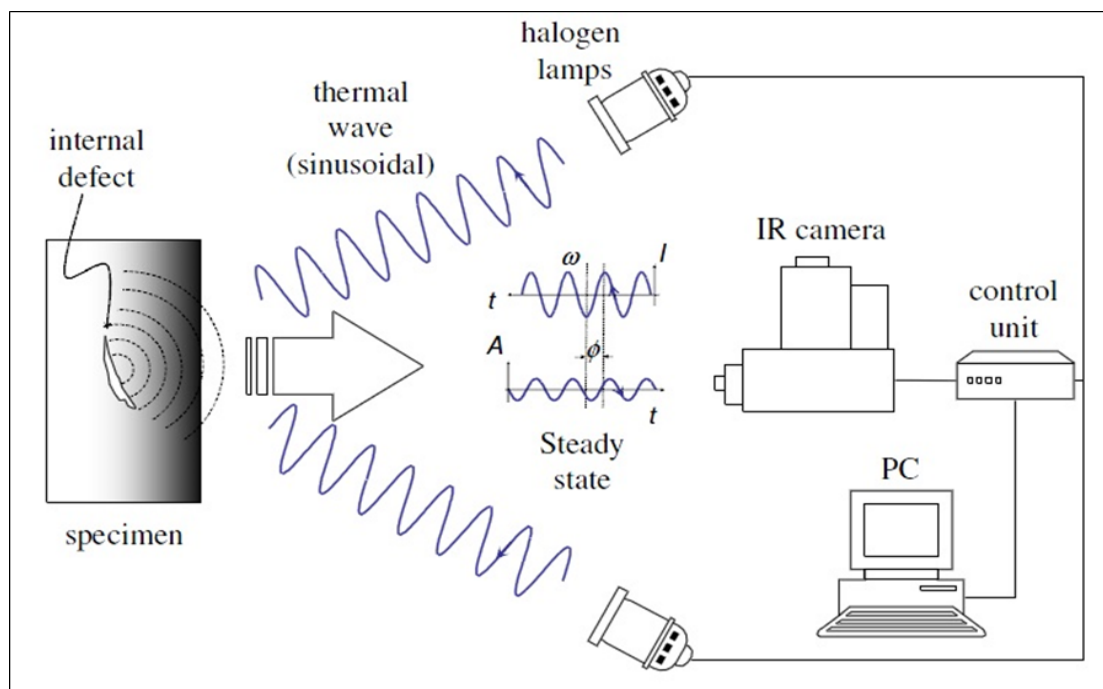


Figure 4.1 Equipment configurations for Lock-in Thermography [34]

The principle of LT operation is based on applying periodic thermal waves into the specimen being inspected. The periodic wave propagates by radiation through the air until it reaches the examined object's surface where heat energy is generated and warm the specimen's surface up then propagates by diffusion through the material as thermal waves. Whenever these thermal waves reach any discontinuity (defect); such as

inclusions, or delaminations, then these defect acts as a thermal barrier (thermal resistance) causing changes in amplitude and phase delay (shifting) of the response signal at the surface. The thermal response is recorded at the same time by using an IR camera [34,54,87].

LT technique has established basing on the fact that the thermal wave is very responded to any slight changes or interfaces between materials, where based on observed thermal images that obtained via IR camera, then any changes in amplitude or phase between defective areas and non-defective areas refers to the defect's presence [54]. In LT technique, it is preferred to use halogen lamps to generate the periodic thermal waves, due to their relatively high efficiency, simplicity in use and possibility of control by amplitude modulation of conventional power units [113].

The most interesting thing as a NDI technique is these periodic thermal waves can be created and detected remotely. In general; lock-in thermography is convenient tool to be used for detecting subsurface defects, measuring thicknesses of coatings and determining material properties [116,117]. Particularly, LT technique stands as one of the common attractive investigation methods that are used in fields of antique art treasures (frescos) [118]. Furthermore, LT technique has increasingly been used for reliable defect detection in composite materials such as carbon-fiber-reinforced polymers (CFRPs) in aircraft structures [116]. Where most CFRP structures have a finite thickness and non-destructive inspection is performed in a natural ambient environment. Hence, LT has been used to detect delaminations in the composite structures of aircraft [117].

## 4.2 BASIC CONCEPT AND THEORY FOR LT

Basically, the lock-in terminology refers to the fact of being required to monitor the exact time dependence between the output signal and the original input signal [87]. Lock-in thermography is a technique based on amplitude modulated thermal waves created inside the inspected specimen. Thermal waves are used as tool to examine objects and reveal the local non-homogeneities; hence it leads to detect hidden faults inside the inspected objects [119]. This is not a new concept since these thermal waves were first created and investigated by Fourier and Angström back in the 19th century [72]. Basically, periodic thermal waves in lock-in thermography represent a repetitive heat, where the source duration in LT technique may be sinusoidal in range of 0.01 Hz to 20 Hz, or rectangular (seconds to hours) [36].

Qualitatively, the phenomenon is as follows; in this technique the examined specimen's surface is periodically stimulated by one or several modulated heating sources, such as halogen lamps, to inject thermal waves perpendicularly into the inspected specimen. Where the periodic thermal waves transfer by radiation through the air (medium) until the sinusoidal heat wave's front being in face with the inspected specimen's surface where the inspected specimen's surface is heating up then the thermal waves propagates by diffusion through the material. The temperature of each point in the inspected specimen will change over time, as it will be affected by the generated waves and those reflected in thermal barriers. Since the subsurface defect or any subsurface discontinuity or non-homogeneity act as barrier for heat propagation, then it will effect on the thermal waves and change its amplitude and phase as a result [16,36].

Simply, wherever these thermal waves being in face with any subsurface discontinuity or non-homogeneity in which there is a change of the thermal physical properties, causing a thermal effect change in terms of reducing the amplitude and its phase delay, then it will be partially reflected. The reflected part of the thermal wave interferes with the incoming input thermal wave creating at the stimulated surface of the examined specimen, causing an interference pattern in the local surface temperature and thus in the surface radiation as a result; which oscillates at the same frequency as the input thermal wave. The thermal response is recorded at the same time by using an IR camera, then evaluating the amplitude and the phase of the local surface temperatures one to earn information about the internal structure of test object. The IR camera can observe the whole or a large part of the inspected specimen's surface typically in a 320 x 256 or 640 x 512 pixel array configurations as example [16,26,28,34,36].

Any phase shift (delay) between the thermal evolution for a defective region and a non-defective region represents an abnormality (defect) which can be observed and revealed. For NDI testing purposes, the phase image (phasegram) is often more informative than the ampligram (amplitude image) one which strongly depends on the local IR emissivity; i.e. the phasegram is independent from the IR emissivity ($\varepsilon$) of the surface. In fact, the phasegram is a measure of the time delay of the surface temperature modulation referred to the power modulation, which is indeed independent of the magnitude of the heat source [112]. Where the amplitude image is related to the thermal diffusivity and the phase image is related to the propagation time [87].

Mathematically, in the lock-in thermography technique the procedure as follow; after observing the inspected specimen's surface via IR camera then the recorded

temperature data is transformed into a frequency domain. In which in each pixel, the measured temporal evolution of the temperature represents a Fourier-transformed for all the recorded images sequence. Each pixel in the thermal image corresponds to a temperature at a given time, so that by using Fourier-Transform method for each pixel per cycle then an advanced new result is obtained. This new result is represented by a phase image and an amplitude image [28,36]. Any fault (discontinuity or non-homogeneity) inside the object will be reflected in these images; hence they can show the internal structure of the inspected object and all possible defects [20].

In LT, the obtained thermal images are not the same as these thermographic images that obtained in case of the pulse thermography in previous section by some characteristics since both amplitude and phase images are available. In one hand, these thermographic images, that obtained by using PT technique, are corresponded to the mapping images of the thermal IR energy emitted from the stimulated specimen's surface; i.e. thermographic images are actually visual displays of the amount of infrared energy emitted by an object. On the other hand, the amplitude image is related to the thermal diffusivity and the phase image is related to the propagation time [16,29,34,87,120]. Therefore; LT thermography technique represents an attractive NDI tool due to it is related to the phase and amplitude delay properties of the reposed thermal waves [36]. Phase image represents a strong characteristic of lock-in as a NDI tool, which is relatively independent of local optical and thermal specimen's surface features [72,87,120].

## 4.3 LOCK-IN PERIODIC THERMAL WAVES

In Paris 1807, the French mathematician Joseph Fourier had made study on the heat diffusion by conduction in solid bodies then was able to complete it in 1807 and submitted its paper to the Académie des Sciences. His study was refused initially because of Lagrange disagreement on the use of the Fourier series. Despite that Joseph Fourier had awarded the Grand Prize in Mathematics of the Academy four years later after he submitted a corrected version of his study, it was not until 1822 that his work Théorie analytique de la chaleur was finally published [121]. His paper was included the concepts that would develop later into what is nowadays known as Fourier analysis which represents the base for FFT (fast Fourier Transfer) [36,122,123]. There exist some benefits of using periodic heating instead of pulses. For example, a relatively low power thermal wave can be used since energy is concentrated at a single frequency [124].

The Fourier's Law 1D solution for a periodic sinusoidal thermal wave propagating through a semi-infinite homogeneous material may be expressed by this relation [80]:

$$T(z,t) = T_o exp\left(-\frac{z}{\mu}\right) cos\left[\frac{2\pi \cdot z}{\lambda} - \omega t\right] \tag{19}$$

Where $T_o$ [°C] is the initial change in temperature produced by the heat source, $\omega=2\pi f$ [rad/s] is the modulation frequency, $f$ [Hz] is the frequency of thermal wave modulation, $\lambda=2\pi\mu$ [m] is the thermal wavelength; and μ [m] is the thermal diffusion length which it determines the rate of decay of the thermal wave as it penetrates through the material and is expressed as [125]:

$$\mu \equiv \sqrt{\frac{2 \cdot \alpha}{\omega}} = \sqrt{\frac{\alpha}{\pi \cdot f}} \qquad (20)$$

Sinusoidal waves are commonly used, although other periodic waveforms are possible. Using sinusoids as input has the benefit that the frequency and shape of the response thermal waves are preserved; see Fig. 4.2, only the amplitude and phase delay of the wave may change with respect to the reference input signal. This property of the sinus and cosines functions is well known as sinusoidal fidelity [126,127].

## 4.4 EXPERIMENTAL SETUP FOR LT

As it is shown in Figure 4.1; the experimental configuration of lock-in thermography technique includes a periodic thermal stimulation source in order to deliver the thermal energy to the inspected specimen's surface in form of periodic thermal. The halogen lamps send periodic thermal waves to the inspected specimen's surface at a given modulation frequency $\omega$, for at least one cycle; ideally until reaching a steady state, which depends on the thermal physical properties of the examined specimen and the defect depth [26,28,34,36]. The thermal response is recorded at the same time using an IR camera that is synchronized with the excitation signal and decomposed by a lock-in amplifier to extract the amplitude and phase of the modulation [126].

## 4.5 DATA ACQUISTION FOR LT

Several researches have showed these are some limitations and challenges in using LT technique with respect to PT technique. Where in LT, the object being examined is periodically excited by using a periodic thermal wave with a single frequency corresponding to a particular depth at which a particular defect can be detectable. However; this procedure (test) has to be repeated with other different frequencies to cover a wide range of depths (each single frequency to detect a defect presence at specific test depth). This makes a lock-in thermography technique to be slow and complex. It is worth to mention that deep depth requires a low frequency and shallow depth needs long frequency [36].

Although the data acquisition in case of PT technique is fast, suitable, straightforward, and easy to implement is fast, and allows the inspection of extended surfaces. However, the data acquisitions in LT technique are more accurate depending on the phasegram of the output signal. Due to the obtained data by PT technique are very sensitive to some external effects which they have an extreme impact on the obtained thermal data of PT technique; such as sunlight, dirt, surface emissivity variations [128], surface geometry, non-uniformities of heating that applied into the specimen's surface being examined [129], and environmental reflections [130], while LT technique is not affected by these effects [131].

On the other hand, lock-in thermography LT, allows the reconstruction of phase images that are less affected by the characteristics mentioned above (non-uniform heating, emissivity variations, surface geometry, and environmental reflections); i.e. LT

represents an insensitive technique to [38,132]. Furthermore; LT technique has ability to detect a wide range of deep subsurface defects better than in case of PT; for instance composite defect inspection then the pulsed thermography can detect a subsurface defects in range up to 6 mm while lock-in thermography is able to detect a deeper subsurface defects in range up to 12 mm [76].

An interesting thing of LT is in the fact that by the use of a periodic excitation detailed examinations can be executed with a relatively low power thermal waves input into the object. This permits the examination of thermally sensitive components and the use of relatively simple heat sources. However; LT technique is a low technique in comparison with PT technique, due to in LT method a permanent regime has to be reached [36].

Investigations on amplitude and phase properties can be tracked back to the early studies of thermal wave imaging [128,133-135]. These and more recent studies [129-131,136] have indicated the fact that the phase image is very interested to be used in NDI evaluation tests, due to the fact that the phase image is less affected and insensitive to these external effects of surface emissivity variations, surface geometry, non-uniformities of applied heating, and environmental reflections [36,132]. Therefore, lock-in thermography has the ability to reconstruct the phase images that are less affected by the problems mentioned above while the PT technique has not. Furthermore, contrary to optical pulsed thermography technique which has a great variety of processing techniques, there is only a limited signal processing methods that commonly used for lock-in thermography data. A four point methodology for sinusoidal stimulation stands as reliable method to retrieve amplitude and phase [36,133,137].

A four point methodology for sinusoidal stimulation is available [34,129,131] and illustrated in Figure 4.2. Figure 4.2 illustrates the sinusoidal input signal (I) on top of it, and the response signal S at the bottom.


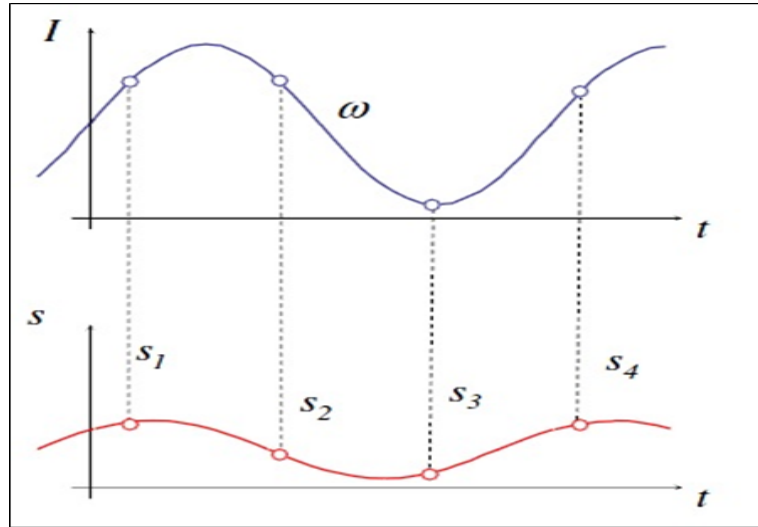
Figure 4.2 Four point methodology for amplitude and phase delay estimation by lock-in thermography [36]

As mentioned in previous sections, input and output signals have the same shape when sinusoids are used; as it is clearly visible in Fig. 3.15, there is only a change in amplitude and phase that can be calculated as follows [34,36,131]:

$$A = \sqrt{(S_1 - S_3)^2 + (S_2 - S_4)^2} \tag{21}$$

$$\emptyset = tan^{-1}\left[\frac{S_1 - S_3}{S_2 - S_4}\right] \qquad (22)$$

The 4-point method is valid only for sinusoidal stimulation. It is a quick method but it is affected by noise. The signal can be de-noised in part by averaging of several points instead of a single one and/or by increasing the number of cycles. Another possibility is to fit the experimental data using least squares regression [36,138], and to use this data to determine the phase and the amplitude. These two alternatives take part to slow down the calculations. The discrete Fourier transform (DFT) can be used as another option to extract phase and amplitude information from lock-in thermography data. The DFT can be written as in Eq. (24) in next section [36,106].

## 4.6 PROCESSING WITH THE FOURIER TRANSFORM

As it has mentioned previously, the thermal response from the inspected specimen's surfaces, is recorded at the same time by using an IR camera and decomposed by a lock-in amplifier to extract the amplitude and phase information. Several methods have been improved to extract the amplitude and phase of the modulation. Fourier Transform analysis is the most common and the preferred processing technique which allows generating images of Ampligram as an amplitude image and phasegram as a phase image [36,139].

**4.6.1 The Continuous Fourier Transform.** The Fourier Transform (FT), or more properly the Continuous Fourier Transform (CFT) can be derived by representing the complex Fourier integral as a sum of exponential functions [34,36,119,140]:

$$F(f) = \int_{-\infty}^{\infty} f(t) \cdot e^{(-j2\pi ft)} dt \tag{23}$$

Where j is the imaginary number; $j^2 = -1$ or $j = \sqrt{-1}$, although the CFT represents an invaluable tool in the analytical formulation of a solution, but the Discrete Fourier Transform (DFT) is usually preferred when working with sampled signals for the actual implementation of the solution [36].

**4.6.2 The Discrete Fourier Transform.** The DFT can be derived by discretizing both time and frequency, that is [34,36,110,119,141,142]:

$$F_n = \Delta t \sum_{k=0}^{N-1} T(k\Delta t) \cdot e^{(-j2\pi nk/N)} = \text{Re}_n + \text{Im}_n \tag{24}$$

Where the subscript *n* designates the frequency increment (n=0, 1…N); $\Delta t$ is the sampling interval; and **Re** and **Im** are the real and the imaginary parts of the transform, respectively [36].

The sampling interval $\Delta t$ is introduced in Eq. (24) as a scale factor in order to produce equivalency between CFT and DFT [141]. For NDI test inspection applications, Eq. (16) is not practical due to lengthy calculations. However by using the Fast Fourier Transform (FFT) algorithm [143], it can extremely reduce the computation timing and is

therefore privileged [36], see Figure 4.3. The Fast Fourier Transform (FFT) algorithm is available on several software packages; such as MATLAB, greatly reduces [36].
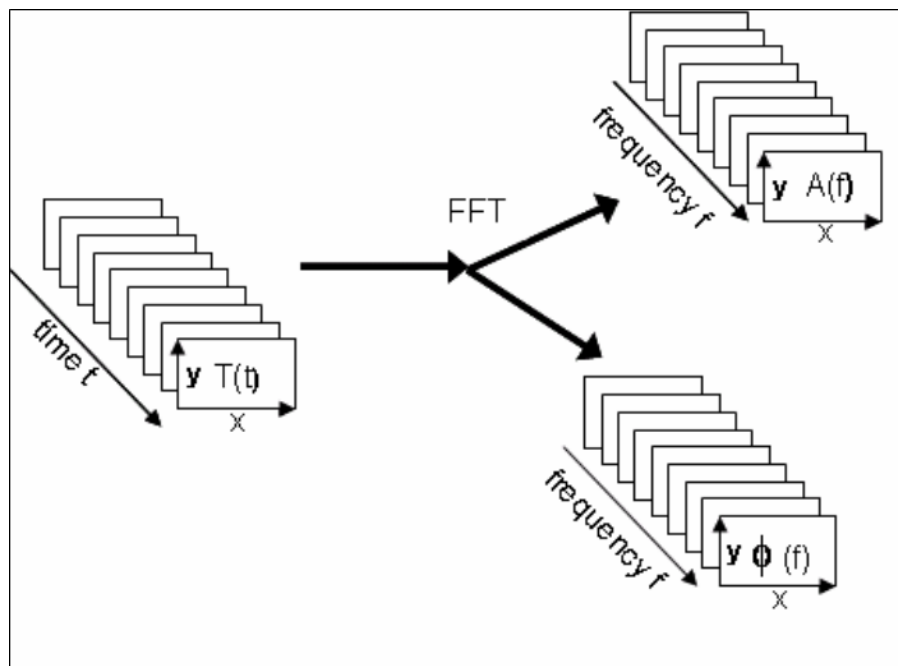


Figure 4.3 FFT representations. [132]

**4.6.3 Amplitude and Phase from LT.** In this case, real (Re) and imaginary (Im) parts of Eq. (24) are used to calculate the amplitude and the phase delay; i.e. the phase angle or simply the phase, of the transform and to reconstruct 3D matrices as depicted in Figure 3.17 [144]:

$$A_n = \sqrt{\mathrm{Re}_n^2 + \mathrm{Im}_n^2} \qquad (25)$$

$$\emptyset_n = \tan^{-1}\left[\frac{\text{Im}_n}{\text{Re}_n}\right] \tag{26}$$

Consequently, matrices shown in Figure 3.16; can be obtained by applying Eq. (25) and Eq. (26) on every pixel of the thermogram sequence in Figure 4.4. Temperature profiles, as the one shown in Figure 3.4b, are real functions that provide a transform with an even, or symmetrical, real part and an odd, or anti-symmetrical, imaginary part. This type of function is referred as Hermite function [142]. As it is shown in Figure 4.4, the symmetry properties of a Hermite function are reflected on the amplitude and phase of the transform, which are even and odd, correspondingly, with respect to $f$=0 Hz, i.e. n=N/2. Therefore, from a sequence of N thermograms, there are N/2 useful frequency components; the other half of the spectra only provides redundant information. Negative frequency data can thus be safely discarded [36,142,144].
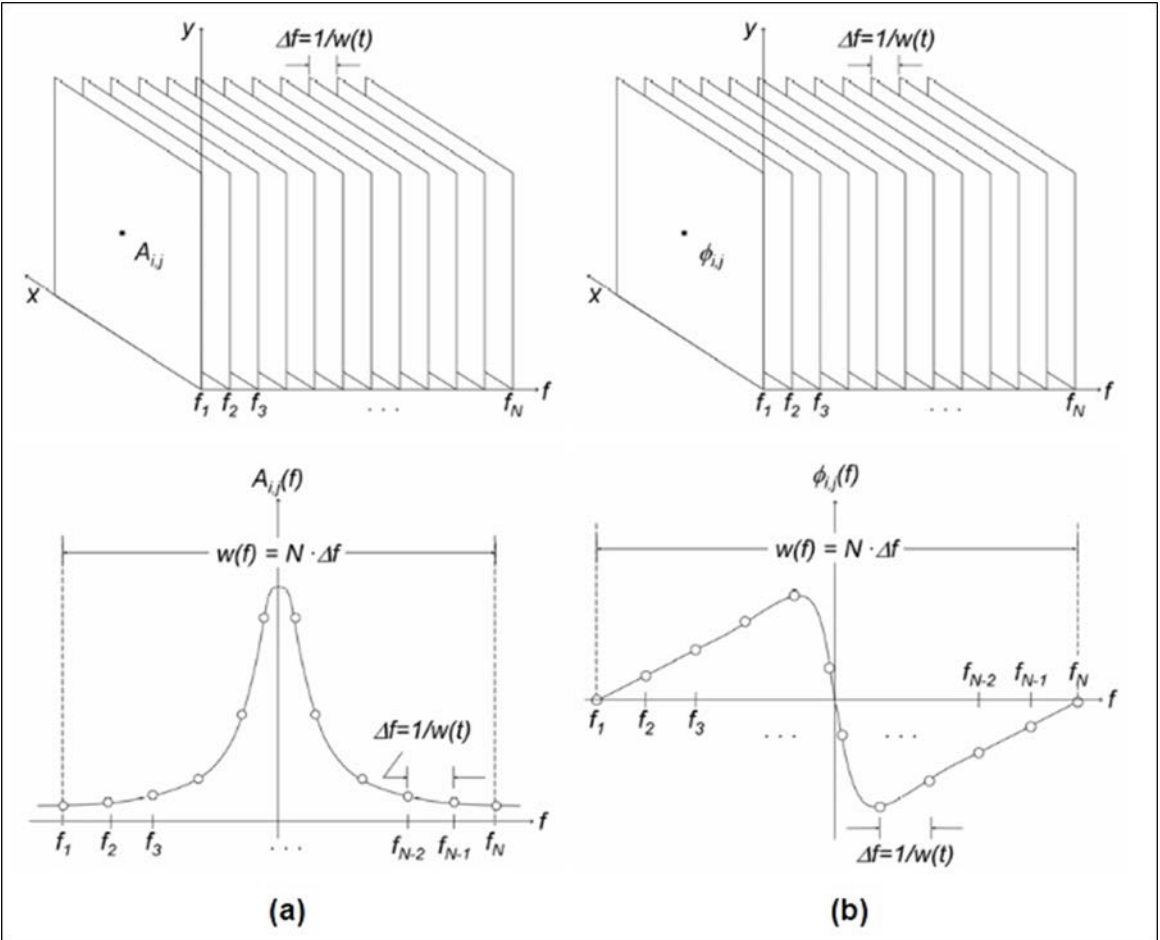
Figure 4.4 (a) Ampligram (Amplitude gram); and (b) phasegram sequences; on top, and their corresponding profiles on the frequency spectra for a non-defective pixel on coordinates (i, j); on bottom [36]

## 4.7 ROUTINES IN LOCK-IN THERMOGRAPHY

After it has illustrated the most theories and concepts in previous sections; in brief this section will present the routines in LT technique. Figure 4.5 shows the main steps in the NDI application of the lock-in thermography and the subsequence routines in the acquisition and data processing.

Initially, the inspected sample's surface is excited periodically by a thermal wave coming from halogen lamps. Also, LT can be applied using two different observation methods; transmission and reflection. As mentioned, in the reflection mode, the heat front produced by the thermal stimulation propagates through the material until it reaches zones (or defective zones) with different thermal properties reflecting back part of the thermal energy applied. In the transmission mode the heat flux is applied by radiation over the surface of the material, so the infrared radiation received by the IR camera is a function of the amount of heat that is transferred by conduction from one side of the material to another [28,36,132].

Once the examined object is thermally stimulated, the thermal response is recorded at the same time by using an IR camera and decomposed by a lock-in amplifier to extract the amplitude and phase information. A thermogram sequence; i.e. thermal map, of the inspected object's surface is collected at a regular time intervals $\Delta t$, composing then a 3D matrix [145], as clearly illustrated in Figure 4.5. In Figure 4.5, the spatial coordinates (x, y) are represented by the horizontal and vertical pixels positions respectively, whereas z represents the evolution time (t); i.e. (x, y, t). The thermal map sequence is then processed and analyzed by applying the Fourier Transform on each pixel of the thermogram sequence by using Eq. (24). Real and imaginary parts of Eq. (24) are used to calculate the amplitude and phase of the transform; from Eq. (25) and Eq. (26) respectively, allowing the reconstruction of the Ampligram and Phasegram maps sequences matrixes, as showed in Figure 3.17 [36,132,144].
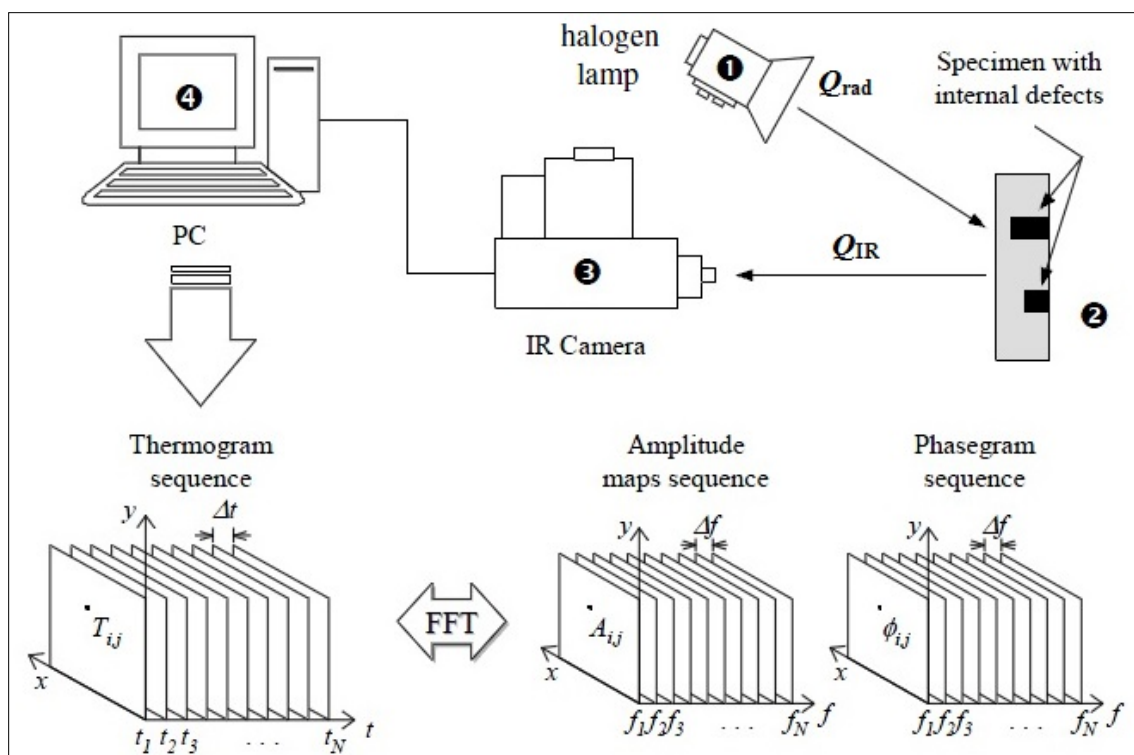
Figure 4.5 Shows routines of data acquisition and processing in Lock-in Thermography
(reflection mode LT) [145]

## 4.8 GEOMETRY AND MESHING

The model geometry was defined to correspond to the inspected speciemn. All of

the dimensions used in the model were taken from the test sample specifications; such as

the defect size and disposition respect the specifications as well. The geometry was

studied numerically by using FEM ANSYS tools and run it on a regular computer and

without needing a professional computer machine. This work has been done via non-

commercial ANSYS 14 through a transient thermal as an analysis system. The test

specimen has designed by Auto-Cad based on the experimental specimen dimensions,

then imported it to the design modeler of geometry of ANSYS. For calibrating the

analysis procedure, test specimen sized (170 x 195 x 3 mm³) made of austenitic steel plate. The simulated defects are represented by flat-bottom holes which are arranged as shown in Figure 4.6. There are 30 defects as subsurface holes. The distances between the defects' centers are equal to 25 mm and 35 mm from the boundary of the sample to the center of the nearest hole. The thickness of the plate is 3 mm. The thermal physical properties of the inspected object are shown in table 4.1. A mesh with (107046 nodes) and (61985 elements) created in a sufficient accuracy features; as it is shown in Figure 4.7. The element size was not chosen uniformly, but with high smoothing, fast transition, and fine span angle center. The defects have represented by 30 flat subsurface holes which assumed they are filled up by air. The test specimen has stimulated uniformly from one side; the nondefective surface, periodically by heat waves of (0.6 and 1 Hz) frequency. The heat wave was a sinusoidal periodic whose power ($q_o$) was changed in a harmonic way by made the heat flow value is changed periodically as a sinusoidal function as shown in Eq.(27). Sinusoidal variation heating condition means the heat flux power density is time-variation:

$$q = \frac{1}{2}[q_o - q_o \cdot \cos(\omega t)] \tag{27}$$

Where $q$ [watts] is the heat flux power density, $q_0$ [watts] is the power of the halogen lamp, $f$ [Hz] is the external heating stimulated frequency, and $t$ [second] is the time.

The halogen lamp power that used in experiment and this simulation was 26 (kW); therefore Eq. (27) can be rewritten as follow;

$$q = 13000[1 - cos(2\pi f t)] \tag{28}$$
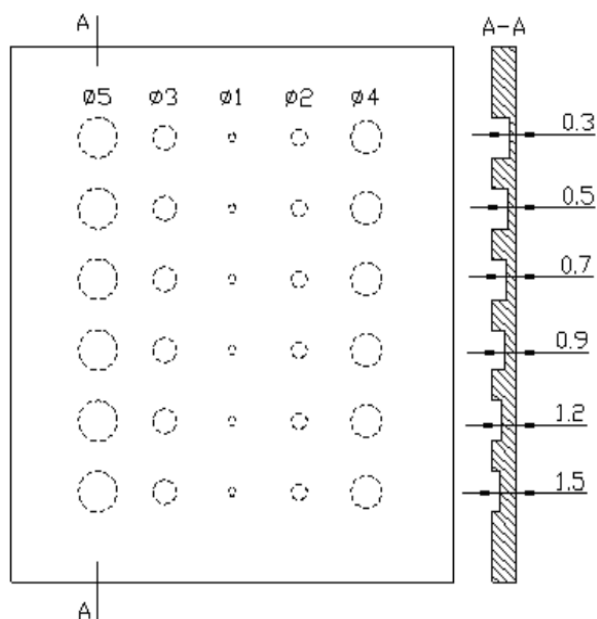
Figure 4.6 Test specimen geometry of LT [146]

Table 4.1 Thermal properties of materials used in LT simulation

| Materials | Thermal Conductivity $k$ [W/m.K] | Specific Heat $C_p$ [J/kg.K] | Density $\rho$ [kg/m$^3$] | Thermal Diffusivity $\alpha$ [m$^2$/s] $\alpha = k/(\rho.C_p)$ |
|---|---|---|---|---|
| Austenitic steel | 15.1 | 480 | 7750 | 0.4 E-05 |
| Air | 0.025 | 1000 | 1.205 | 2 E-05 |
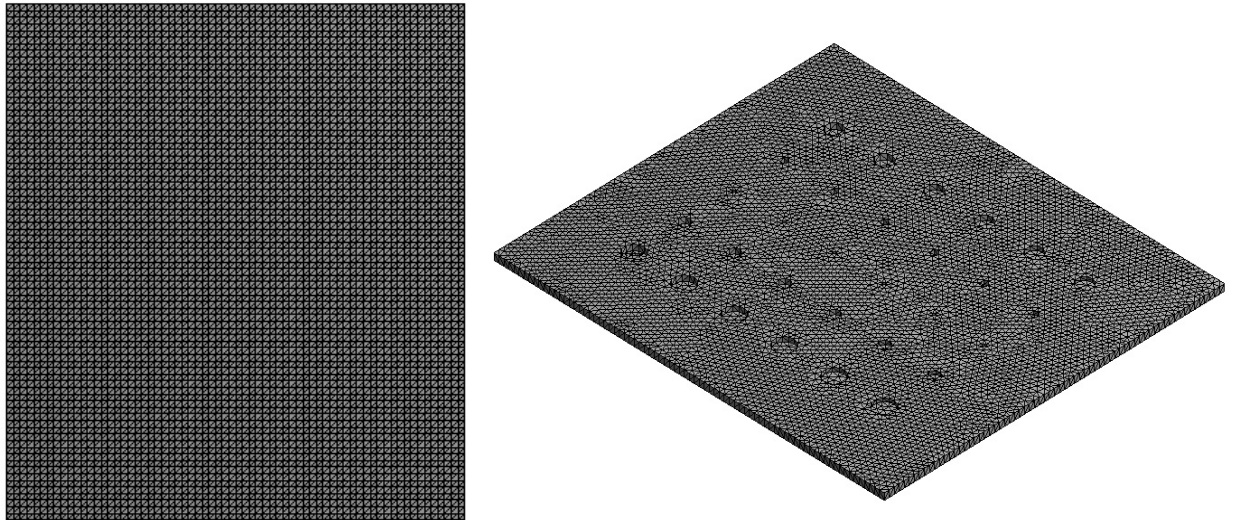
a. Front side                    b. Rear side

Figure 4.7 Show meshing of inspected specimen obtained via ANSYS 14

## 4.9 SIMULATION AND EXPERMINTAL'S RESULTS OF LT

In each of Fig. 4.8b, Fig. 4.9, and Fig. 4.10, in one hand, it is clearly illustrated that the results obtained with the ANSYS show these are subsurface defects (holes) which validate this simulation. On the other hand, the results that obtained by ANSYS show a good reasonably agreement/match in comparison to these results in the corresponding experimental test as it is shown in Fig. 4.8 and Fig. 4.11. Hence, this validates this simulation.

Figures 4.8a and 4.8b illustrate the surface temperature distributions that obtained by experiment tests [146] and ANSYS respectively, for 0.6 Hz stimulating signal. It is clearly evident that the similarity between the both images of the surface temperatures

distributions of Fig. 4.8, show a reasonably validation and good agreement with the. Figure 4.9; show the thermal colored images that obtained directly via ANSYS which represents the test specimen's surface temperatures distribution. Where Fig. 4.9a illustrates thermal image with thermal gradual smooth contours and no wire frame, and Fig. 4.9b illustrates thermal image with thermal gradual smooth contours with showing elements which has created to make it looks like this one obtained by MATLAB in Figure 4.11a. In such, to provide a clear comparison with respect to the 2D phasegram image as shown in Figure 4.11. As it has mentioned in previous section (4.7); after completed the modelling via ANSYS then collected the time history of the temperature distribution of the test specimen's surface which exported later into MS Excel file. The exporting data then processed and analyzed to format a 3D matrix as ($x$, $y$, $z$, $t$, $T$). This 3D matrix is then processed and analyzed applying the Fourier Transform on each pixel of the thermogram sequence by using MATLAB (Appendix B.1) based on the relations of Eq. (25) and Eq. (26) for Amplitude and phase respectively, which allowing the reconstruction of the amplitude map and phasegram one; as it is shown as a 3D image in Fig. 4.10, or as a 2D image in Figure 4.11.

It is very clear from the amplitude-gram and phase-gram to conclude there are subsurface defect and estimate their places based on the thermal contrasts which apparent on the surface. Presence of defects (holes) that apparent in both ampligram and phasegram in Fig. 4.11a and Fig. 4.11c validate this simulation. In addition, it is visibly clear how the phasegram that obtained in this simulation via ANSYS (Fig. 4.11c) is similar to this one that obtained experimentally (Fig. 4.11b).

.
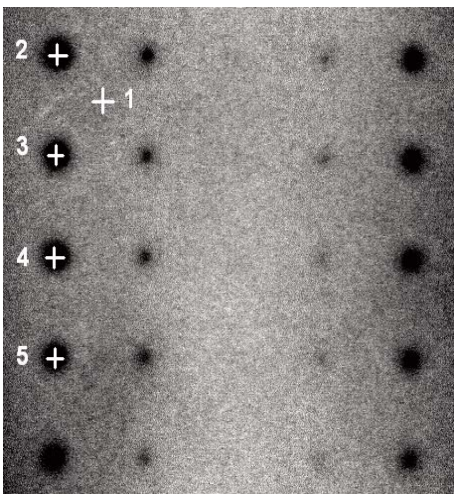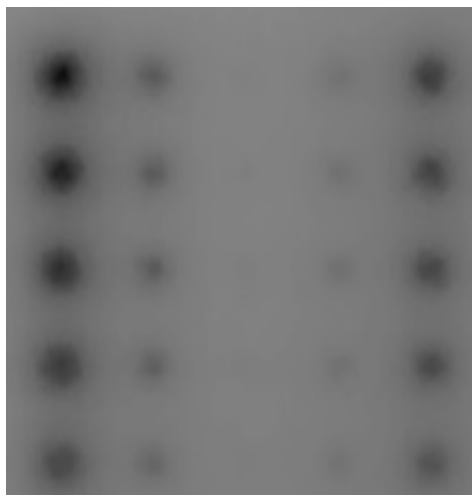
a. Experimental [146]                                    b. ANSYS*

*Image (b) has cropped to be fit with the experimental cropped image (a)

Figure 4.8 Surface temperature distributions for 0.6 Hz stimulating signal
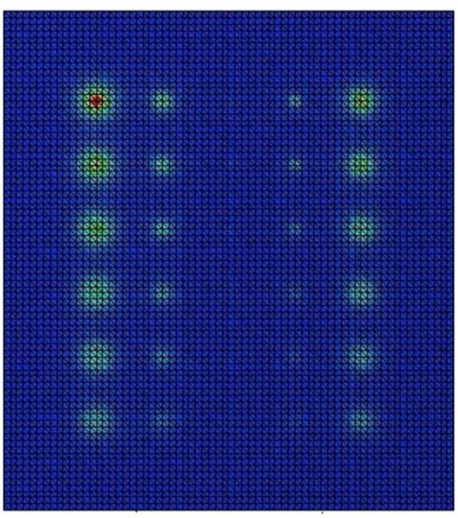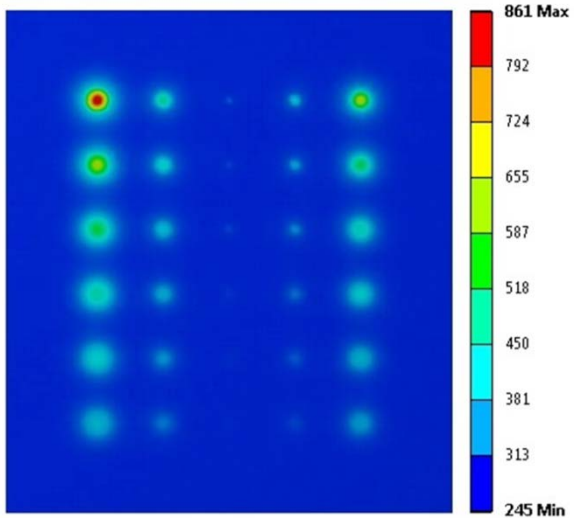


a. showing elements                                    b. No Wire Frame

Figure 4.9 Shows thermal images of test specimen obtained via ANSYS 14 [$^{o}$C], (Surface temperature distributions for 1 Hz stimulating signal)
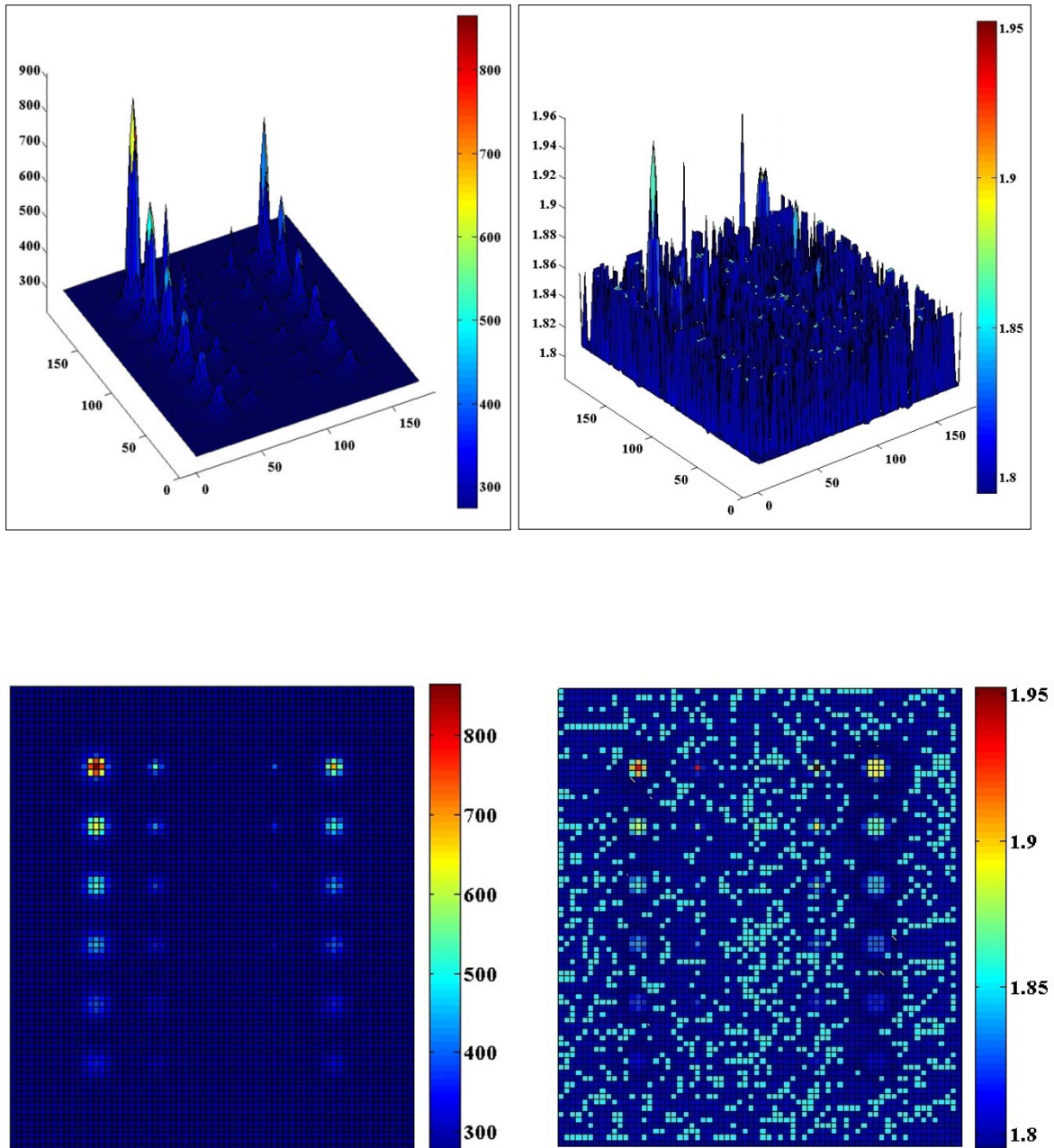
Figure 4.10 Ampligram [$^{o}$C] on left and Phasegram [rad] on right as 3D on top and 2D on bottom repectively, generated by MATLAB (Appendix B.1)
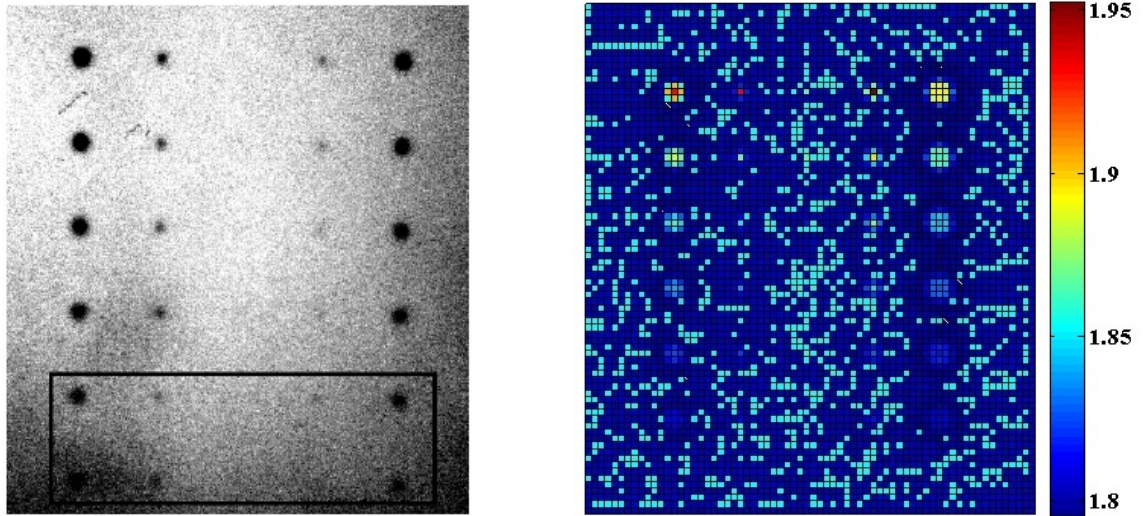
Figure 4.11 Two dimensions Phase images [rad] (on left: experimental [125], on right: FEM ANSYS)

## 4.10 ESTIMATING THE DEFECT'S SHAPE BY USING LT

It is well know that each defect has its specific shape. Infrared thermography has ability to estimate the defect's shape, especifically the simple shpaes such as the subsurafce flat-holwa that are shown in previous sections by using pulsed thermography or lock-in thermography. In this section will examine this advantage by using LT technique with a model which has a complex defect's shape. The defect represents the logo of Missouri University of Science and Technology, as it is cearly shown in Figure 4.12.

The geometry was studied numerically by using FEM ANSYS tools.This work has been done via non-commercial ANSYS 14 through a transient thermal as an analysis system. The test specimen has designed by Auto-Cad based on the experimental specimen dimensions, then imported it to the design modeler of geometry of ANSYS

with size of (52 x 52x 5 mm³) made of structural steel plate. The thickness of the plate is 3 mm.

The thermal physical properties of the inspected object are shown in table 4.2. A mesh with (315344 nodes) and (180426 elements) created in a sufficient accuracy features; as it is shown in Figure 4.13. The element size was not chosen uniformly, but with high smoothing, fast transition, and fine span angle center. The defects has assumed they are filled up by air. The test specimen has stimulated uniformly from one side (front surface); i.e. the nondefective surface, periodically by heat waves of (1 Hz) frequency. The heat wave was a sinusoidal periodic whose power (20 KW) was changed in a harmonic way by made the heat flow value is changed periodically as a sinusoidal function as shown in Eq.(27), which has the same expresion that shown in Eq. (29).



Figure 4.12 Specimen model

a. Front side                                    b. Rear side
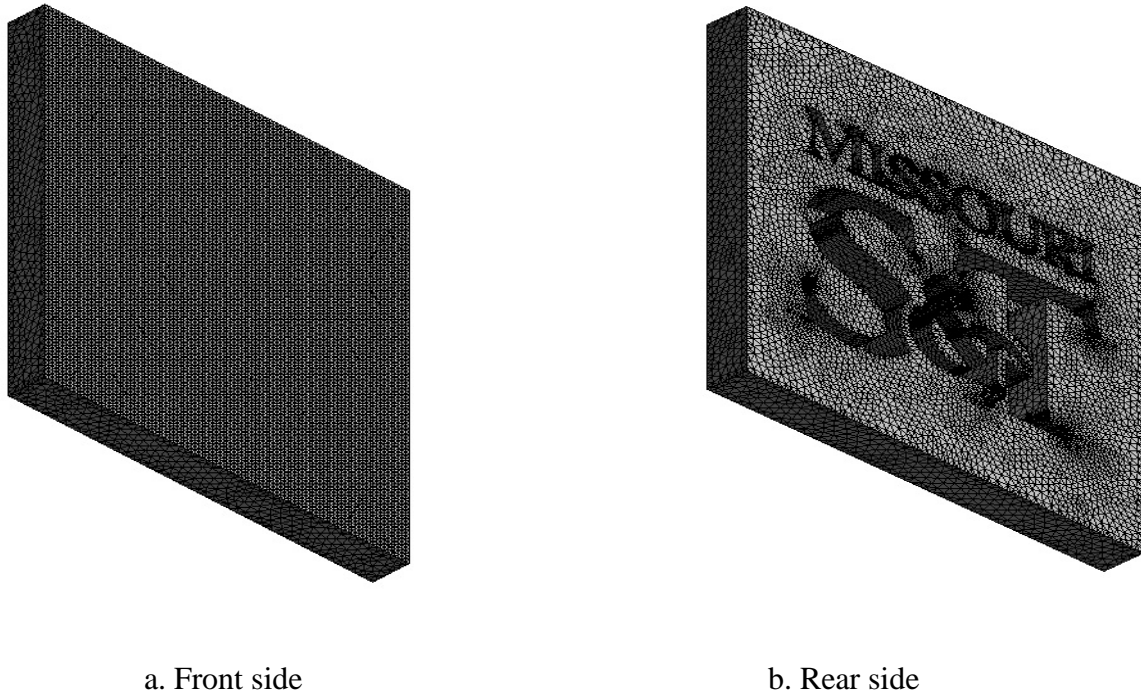
Figure 4.13 Specimen mesh

Figure 4.14 shows; on the top, the 3D Ampligram on the left and 3D Phasegram on the right respectivly, whilst it shows; on the bottom, the 2D Ampligram on the left and 2D Phasegram on the right respectivly which generated by MATLAB (Appendix B.2). As it is clearly illustarted form both of 2D Ampligram and 2D Phasegram that the detcted defect image represent the logo of Missouri University of Science and Technology. Hence, amplitude and phase images can be used not just for inspecting objects and detect their defects, but also to estimate the defect's shape. Defect's shape is an important feature to be estimated especially with maintenance operations in NDI apllications. Whears the defect's shape can tell when it is the suitable/critical time that the maintenance is required to be doing.

Table 4.2 Thermal properties of materials used in LT simulation of MST logo

| Materials | Thermal Conductivity $k$ [W/m.K] | Specific Heat $C_p$ [J/kg.K] | Density $\rho$ [kg/m³] | Thermal Diffusivity $\alpha$ [m²/s] $\alpha = k/(\rho.C_p)$ |
|---|---|---|---|---|
| Structural steel | 60.5 | 434 | 7850 | 1.7 E-05 |
| Air | 0.025 | 1000 | 1.205 | 2 E-05 |

Figure 4.14 Ampligram [$^o$C] on left and Phasegram [rad] on right; as 3D on top and 2D on bottom repectively, generated by MATLAB (Appendix B.1)

# 5. LASER SPOT THERMOGRAPHY TECHNIQUE (LST)

## 5.1 INTRODUCTION

In general, the previous two techniques PT and LT, [14,18,34,36,40,74,80,147,148], represent the most conventional NDI active thermography techniques that has been successfully used in detecting in-plane defects such as coating adhesion failures, delamination, or impact damage in carbon fiber composites, and cracks parallel to its surface as well. But; there are specific defects, such as near surface breaking cracks in metal parts that caused by fatigue or creep that grow predominantly perpendicular to its surface, hence a conventional method (PT or LT) is not suitable way to be used for detecting these type of cracks which are perpendicular to its surface; due to the fact that these type of cracks do not block the heat flow flux that applied perpendicularly to the surface. Therefore, these types of cracks/micro-cracks that which grow predominantly perpendicular to the inspected object's surface represent a challenge for detection by using PT or LT techniques. It has been reported that surface's cracks with openings (widths) of below 0.5 mm on a concrete surface could not be detected by using PT technique [83]. However; this type of cracks can be detected if the heating stimulation operation is localized into a spot or a line on a surface, especially at the crack's vicinity [42]. Therefore; to overcome this challenge, advanced active thermography stimulation techniques were developed a new technique which is known as Pulsed Laser Thermography or Laser Spot Thermography (LST) [149-153]. Moreover, thermal microscope measurements showed that thermally obtained lengths of vertical

crack in silicon nitride were at least 34% longer than those that were optically measured [154].
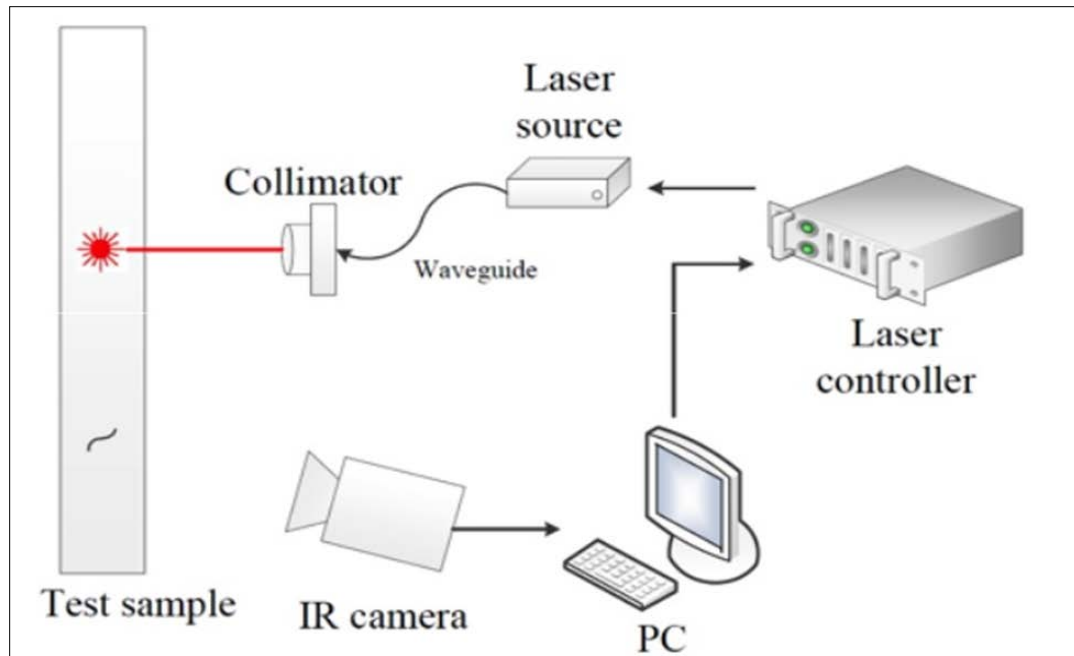


Figure 5.1 Laser spot thermography test setup [149]

## 5.2 BASIC CONCEPT AND THEORY FOR LST

Laser spot thermography stands as an active non-destructive and non-contact inspection infrared thermographic approach. LST technology is a technique based on using an external thermal excitation source supplied by a high powerful laser source. A laser is used for heating at a fixed position in proximity to the crack generating a thermal spot [40].

Laser Spot Thermography is a novel method for detecting surface breaking micro-cracks in metals by using a powerful laser beam. In which the laser beam is focused on the examined specimen's surface to generate a heated spot on the sample being inspected, specifically near to a surface breaking crack, to create a highly focused thermal spot from which heat spreads and diffuses radially as a result. Therefore, any crack that is developed perpendicularly to its surface, which locates at close zone to the heated spot; it will affect the heat flow propagation and delay the lateral heat flow producing a perturbation then creating a thermal contrast that can be easily observed by an IR camera, which will reveal the state or fact of crack's presence; i.e. differences in the thermal diffusivity lead to produce differences in the thermal footprint; hence it can simply be detected [26,42,44,49,65,69,150].

This technique introduces a detection method of open surface cracks; especially the perpendicular cracks with openings in the micrometer range, which represents an important task to prevent structural failure and save them; especially the high performance steel in lightweight construction which is a subject of increasing interest. The observation and measurement is based on the analysis of thermal contrasts on the examined specimen's surface temperature distribution in close area or neighborhood of the stimulating laser spot [152,153].

Figure 5.2 shows the comparison between using the flash pulsed thermography PT and the laser spot thermography LST. For in-plane defects which are parallel to its surface; such as such as voids, pores, or delaminations. Then they can be detectable by stimulating the test specimen's surface by using the conventional thermography techniques (PT or LT) in which a relatively homogenous thermal energy is applied

perpendicular to the surface. Then observing the temperature distribution at the surface with an IR camera, which leads to estimate the heat flow in the object and reveal the defect's presence; as it is illustrated in Figure 5.2a. It is very clear that the pulsed thermography is unable to detect the cracks or especially the micrometer cracks which are perpendicular to its surface, as it is clear in Figure 5.2b. As it has mentioned in previous sections, the defect/crack stands as a barrier and works as a thermal resistance to block the heat diffusion which propagates perpendicularly in relative to this defect, then changes the thermal diffusion rate as a result. The affectivity of this thermal resistance relates to the heat flow power relative to the defect direction. Therefore, it is convenient to detect the cracks, or especially micrometer cracks, which are perpendicular to its surface by applying a localized heat spot such as LST technique at the proximity of the crack, due to this technique (LST) allows generating a radial heat diffusion which propagates perpendicularly relative to this crack, as it is shown in Figure 5.2c.
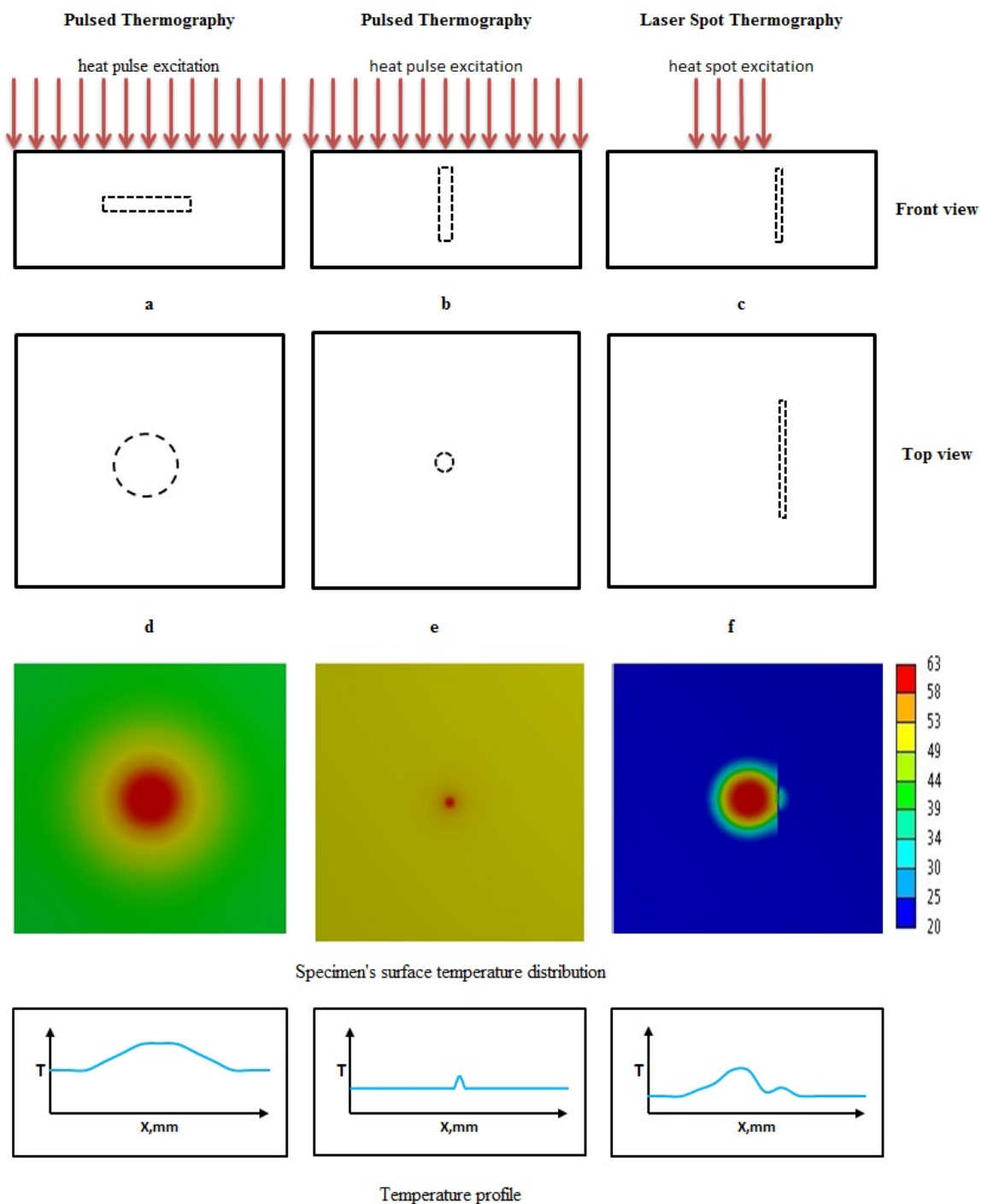
Figure 5.2 Shows the difference between PT and LT for two subsurface defects of test

specimen; parallel to surface (1$^{st}$ and 2$^{nd}$ column), perpendicular to surface (3$^{rd}$)

The phenomenon as follow; in conventional setups (PT or LT), a relatively homogenous heat flow is applied perpendicular to the specimen's surface being inspected by using flash or halogen lamps [34]. After the inspected sample's surface has stimulated by using PT technique and the heat pulse front being in face with the front surface as it is shown in Fig. 5.3, and Fig. 5.4, then it will warm up the surface and producing a subsurface thermal pulse. This subsurface heat pulse propagates by diffusion through the specimen's materials due to there is a thermal gradient and then the thermal pulse will keep diffusing through the materials starting from the front surface to the rear surface.

During this travel, if there is any discontinuity (defect), which is parallel to the inspected specimen's surface, being in face with these thermal pulses, it will change the thermal physical properties at this location and change the heat diffusion flow rate as a result, as it is clearly shown in both of Fig. 5.2a and Fig. 5.3.

Basically, these discontinuities; such as delamination, corrosion, voids, pores, or inclusion, act as a thermal barrier which works as a thermal resistance that block the heat diffusion flow and creating a thermal contrast with respect to surrounding area which have not any discontinuity. Physically, that is due to the fact that these discontinuities have thermal properties different than the inspected specimen's thermal properties. To be more accurate, whenever the thermal pulses energy reaching the defect then some portion of this thermal energy transmits through the defect and another portion will reflect and back to the front surface side. Therefore; when observing the stimulated specimen's surface by using an IR camera, it can simply recognize the defect presence due to the perpendicular heat flux it can resolve the thermal properties changes, which are caused due to the parallel defects, in its direction. In fact in such a case the reduced diffusion rate

that caused by the subsurface defect presence translates into heat accumulation; i.e. on the observed surface being examined then the area over the defective appears in hotter relative to the reference area, as it is shown in Fig. 5.2a and Fig. 5.3.

On the other hand, if the discontinuity is perpendicular to its surface; such as the micro-cracks, then this perpendicular crack will have a very weak impact on the perpendicular thermal flow diffusion, i.e. almost will not change the heat flow rate. Moreover; the reflected thermal pulses that are may generate due to the perpendicular micro-crack will be a slight and cannot be observed and detected in  most cases, as it is shown in Fig. 5.2b and Fig. 5.4.

Therefore, to make these types of micro perpendicular cracks to be detectable it needs to make the heat pulses to propagate radially to generate a thermal contrast. LST technique can provide this feature by generating a high power focused pulsed laser spot to create a highly localized heating spot from which heat diffuses radially. A laser is used for heating at a fixed position in proximity to the crack. Then the crack will interrupt the lateral heat flow and delay the lateral heat flow and this perturbation will lead to an unsymmetrical thermal footprint which can be observed by an IR camera. Hence; will be able to detect the crack, i.e. the thermal image that obtained by IR camera will reveal the perturbation caused by the crack and this can be used to detect its presence, as it is shown in Fig. 5.2c and Fig. 5.5.
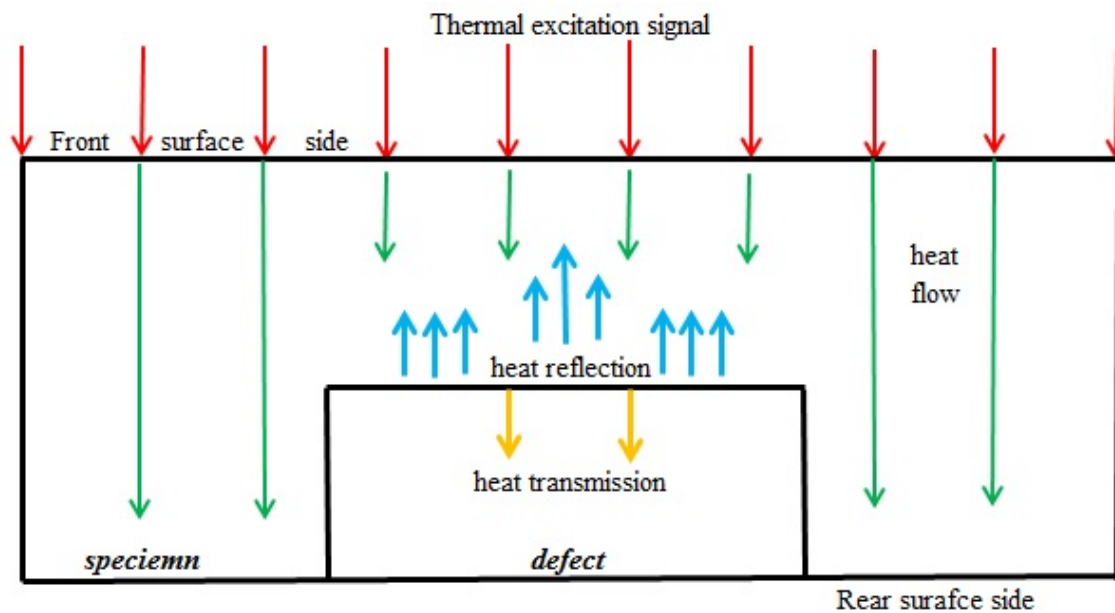
Figure 5.3 Heat transfer with parallel defect by using PT technique
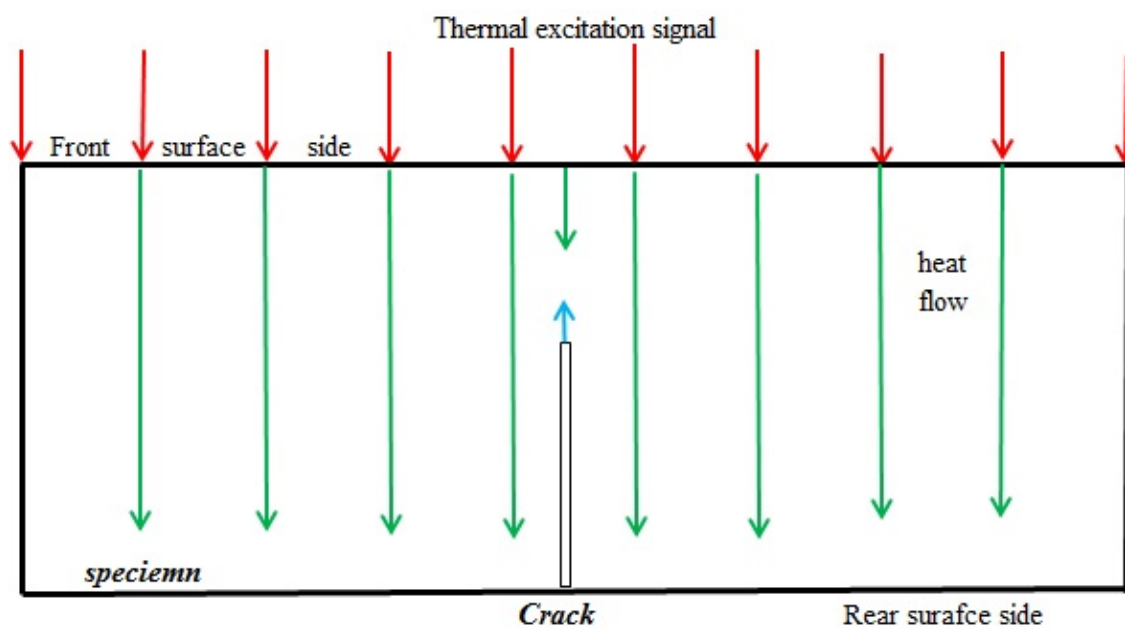


Figure 5.4 Heat transfer with perpendicular crack by using PT technique
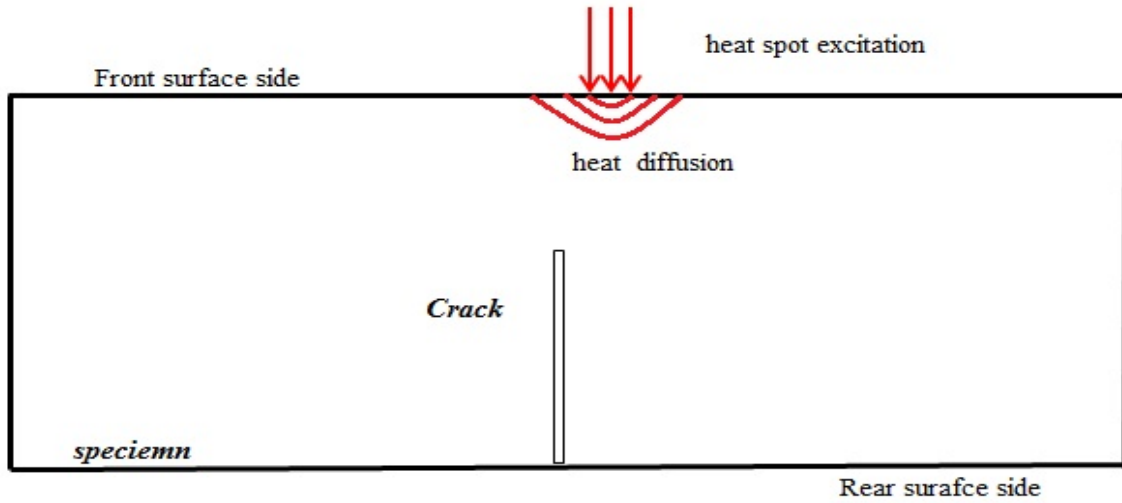
**a.** Front view of inspected sample
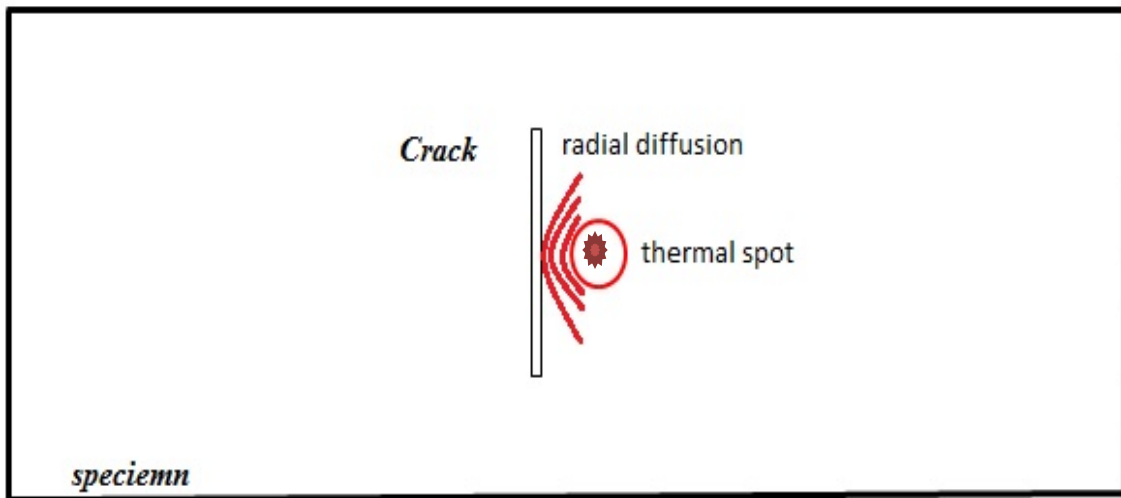


**b.** Top view of inspected sample

Figure 5.5 Heat transfer with perpendicular crack by using LST technique

## 5.3 EXPERIMENTAL SETUP FOR LST

There is several literature studies have reported on laser spot thermography technique. Some of these studies have used a low power of laser of less or about 1 W, whilst in this study a 21W Laservall industrial fibred diode laser has been used. The laser beam wavelength is 808 nm and its focal spot diameter is about 1.8 mm. The laser is operated in a pulse mode. The pulse duration can be set from 1 millisecond to 10 seconds. Figure 5.1 shows the experimental setup of laser spot thermography testing system. This configuration consists of five major components, namely: a laser source, a laser controller, collimator, an infrared camera, and a computer for data acquisition and storage. A collimator is a device that allows producing a parallel beam of rays or radiation. The computer is used to control the laser output power and pulse duration long (width), and for a post- processing as well. Experimentally, the thermal response has recorded by a Raytheon InSb IR infrared camera with a frame rate of 60 Hz [40,151].

## 5.4 GEOMETRY AND MESHING

The model geometry was defined to be corresponded to the sample tested. All of the dimensions used in the model were taken from the test sample specifications; such as the defect size and disposition respect the specifications as well. The geometry was studied numerically by using FEM ANSYS and run it on a regular computer machine and without needing a professional computer machine. This work has been done via non-commercial ANSYS 14 through a transient thermal as an analysis system. The test specimen has designed by Auto-Cad based on the experimental specimen dimensions,

then imported it to the design modeler of geometry of ANSYS. For calibrating the

analysis procedure, test specimen sized (10 x 10 x 5 mm³) made of mild steel plate with a

fatigue crack has developed perpendicularly to the surface. The defect represents a gap

filled within air. The width of crack (opening) is set to 50 µm. The thickness of the plate

is 5 mm. The physics thermal properties of the inspected object are shown in table 5.1. A

mesh with (402,367) nodes and (288,883) elements created in a sufficient accuracy

features; as it is shown in Figure 5.6. The element size was not chosen uniformly, but

with high smoothing, fast transition, and fine span angle center. The test specimen has

stimulated from one side; the non-defective surface side, by a laser spot with 1.8 mm

diameter.

Table 5.1 Thermal properties of materials used in LST simulation

| Materials | Thermal Conductivity $k$ [W/m.K] | Specific Heat $C_p$ [J/kg.K] | Density $\rho$ [kg/m³] | Thermal Diffusivity $\alpha$ $\alpha=k/(\rho.C_p)$ |
|---|---|---|---|---|
| Mild steel | 40 | 500 | 7850 | $1.0191\times10^{-5}$ |
| Air | 0.025 | 1000 | 1.205 | $2.0747\times10^{-5}$ |
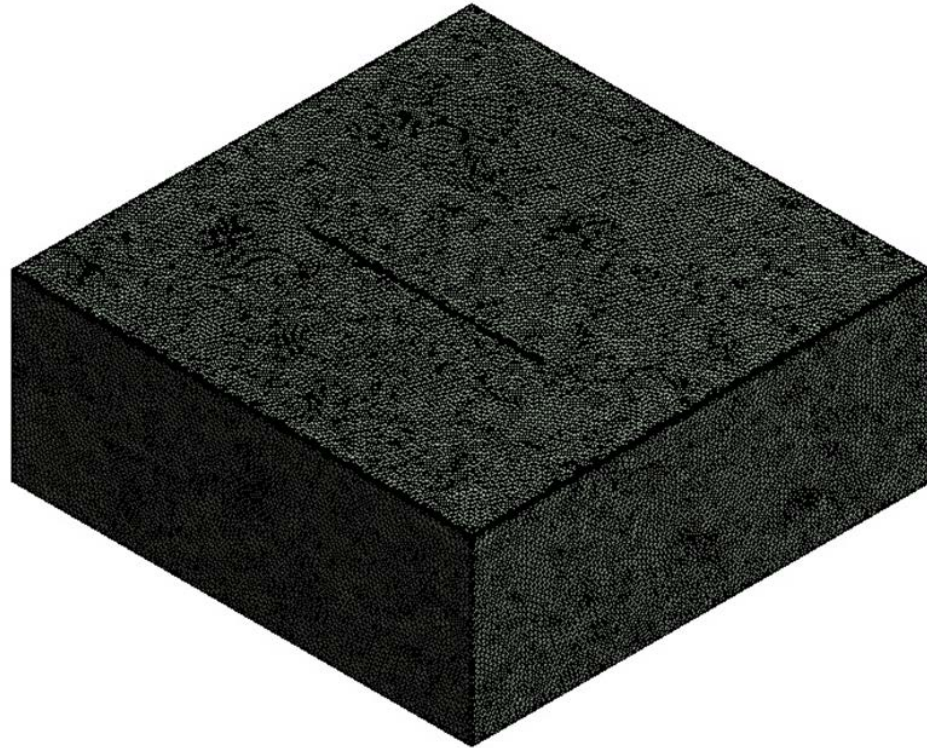
Figure 5.6 Shows meshing of test specimen obtained via ANSYS 14

## 5.5 SIMULATION AND EXPERMINTAL'S RESULTS OF LST

This study presents FEM ANSYS simulation as a tool to model the thermal flow from a laser heated spot in the vicinity or nearness of a crack. The study also presents the results of an image processing method for extracting images of cracks after laser spot is irradiated.

Several studies are found there exists some parameters that can affect the thermal images; such as host material, crack opening, length depth and geometry; laser power and pulse duration; spot imaging time and spot distance from the crack. A pulsed laser spot has chosen to excite the thermal transient because a high temperature difference will be

provided with respect to the neighbourhood. If the pulse is long, heat will start to dissipate in the sample whilst the laser is still on. This phenomenon is more obvious in metal samples.

It is clearly obvious in the both images that shown in Fig. 5.7a (non-defective specimen) and Fig. 5.7b (defective specimen), the crack leads to form a 'D' shape; as shown in Fig. 5.7b, rather than a round shape in test specimen without crack as it is clearly shown in Fig. 5.7a because of the heat blockage by the crack. The effect of thermal resistance of the air-filled crack is to create thermal flows. Due to the fact that this crack acts as a thermal barrier which changes the thermal diffusion rate. Hence; this leads to validate using LST technique to detect these type of defects (crack) and validate using ANSYS as well since this test has been made via ANSYS.

Figure 5.8 shows the modeled surface temperature images of a laser beam incident on a mild steel metal block obtained from this model. These thermal counters image has obtained when the test object was excited by a laser pulse. The laser excitation is applied with power of 13 Watt spot heating of 1 mm radius at the right hand side of a crack. The pulse width duration is 50 ms . The width of crack (opening) is set to 50 $\mu$m, the length is 5mm, and the depth is about 4 mm.The laser spot center was 1 mm away from the crack.

Figure 5.8 shows the temperature distribution on the specimen's surface; i.e. the thermograms. First three images (frames), Fig. 5.8a, Fig. 5.8b, and Fig. 5.8c, show the temperature distribution on the specimen's surface at the time when the laser was still turned on. From the 4th frame, i.e. after 50 ms of starting the stimulation, the laser spot

was turned off and the heat started to dissipate through the test material. It is easily clear that the full extent of the crack becomes easier to perceive with elapsed time, where the crack will block the heat flow and change its diffusion rate causing a 'D' shape thermal contours producing on the surface temperature distribution; which means there exists a crack.

It is worth to mention, the temperature rise scales in Fig. 5.8a are in IR camera 'digital level' units and in Fig. 5.8b, and Fig. 5.8c are in units of degrees Celsius. So, the conversion factor is around 300. Based on thermograms images set of Fig. 5.8; it is clearly illustrated there is a good reasonably agreement between the sets of experimental and simulated thermal images which can validate this simulation that has been done via FEM ANSYS.



**a.** non-defective specimen          **b.** defective specimen
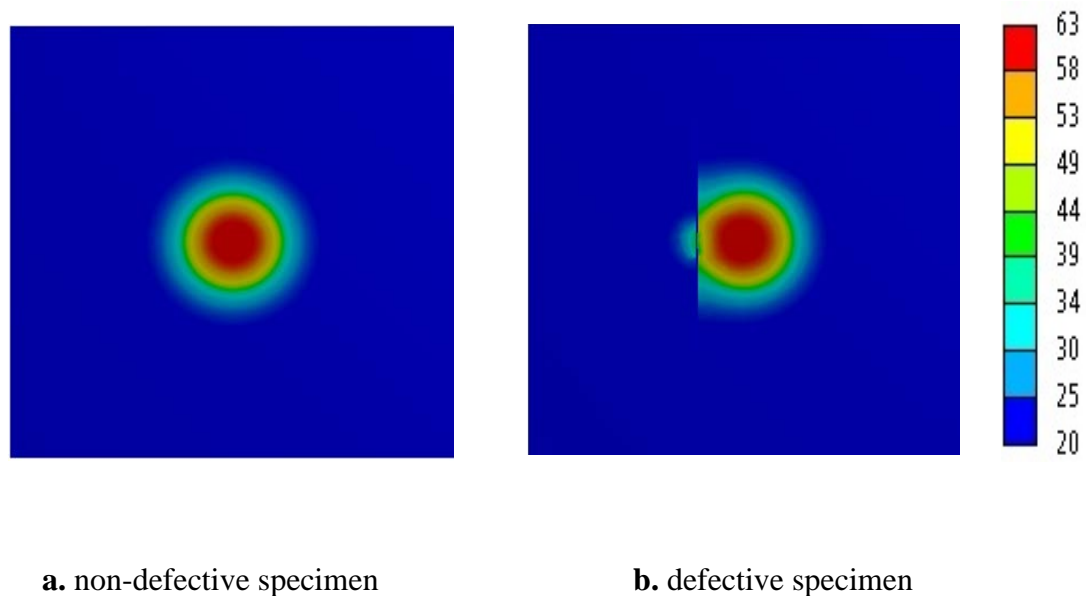
Figure 5.7 Test specimen's surface temperature distribution [$^{o}$C]
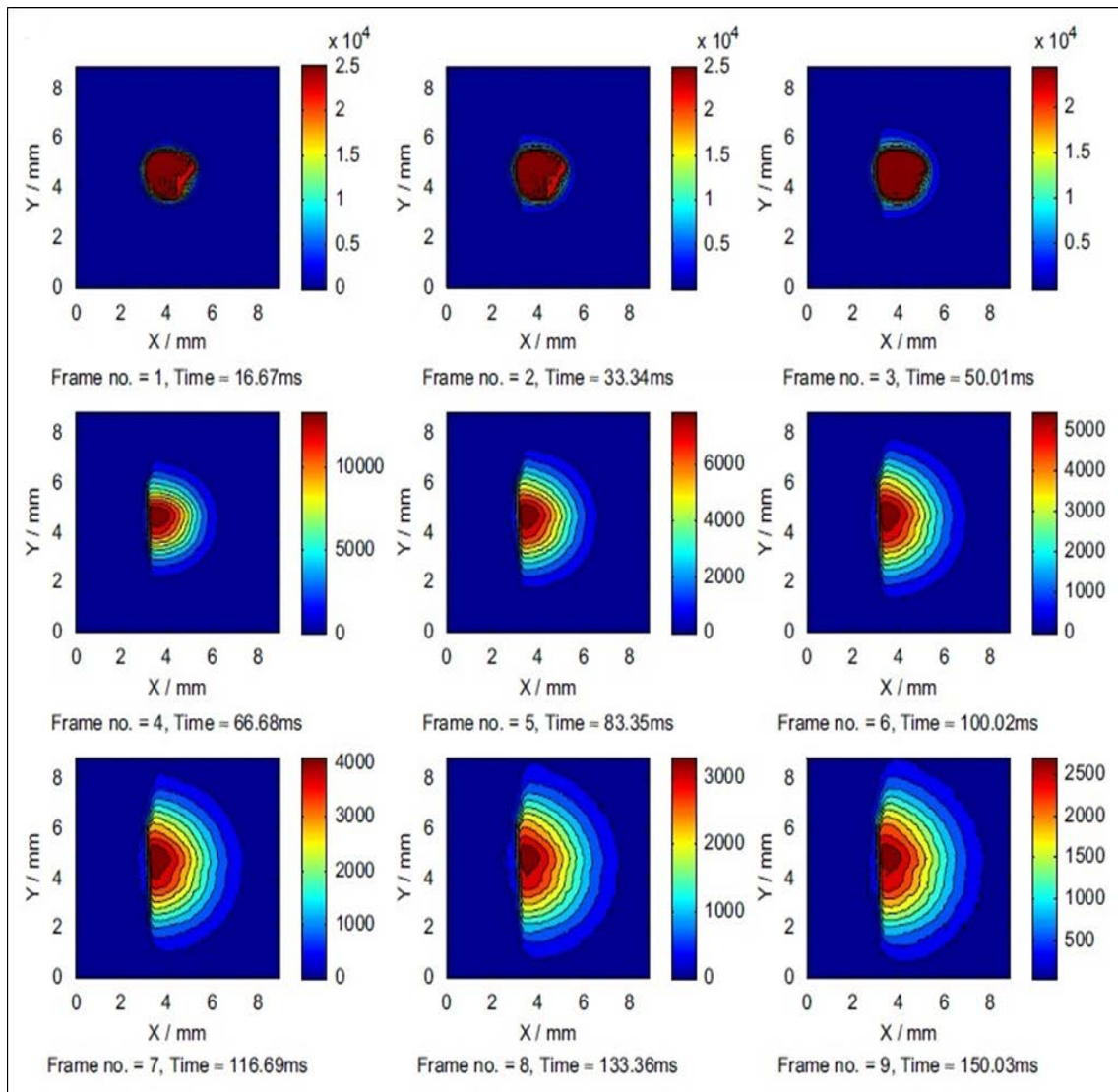
a. Test specimen's surface temperature distribution, experimental [150]

Figure 5.8 Shows the Resulting experimental thermal contour images and the corresponding by FEM and ANSYS [$^{o}$C]
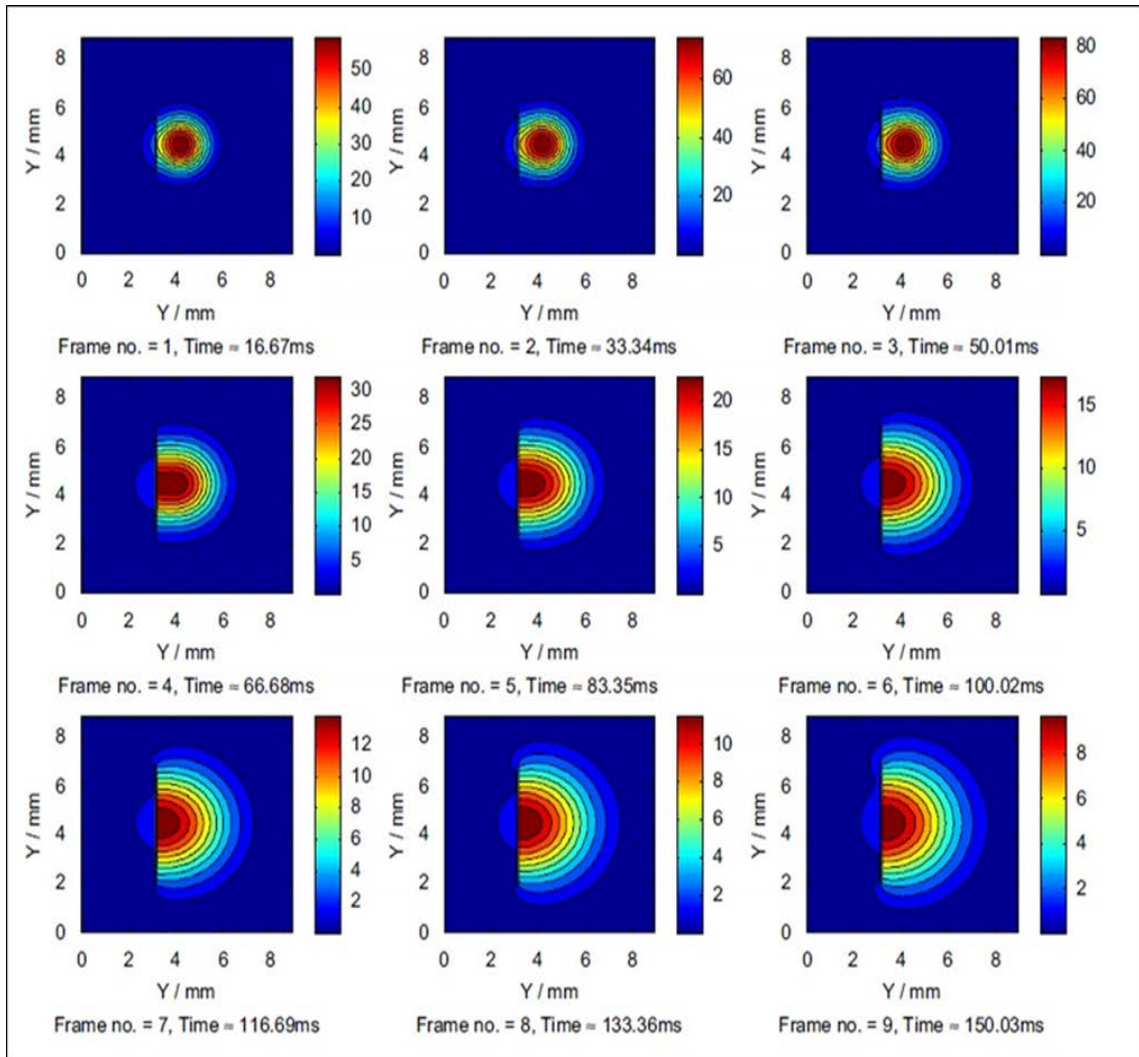
b. Corresponding simulated thermal contour images obtained by FEM [150]

Figure 5.8 (continued)
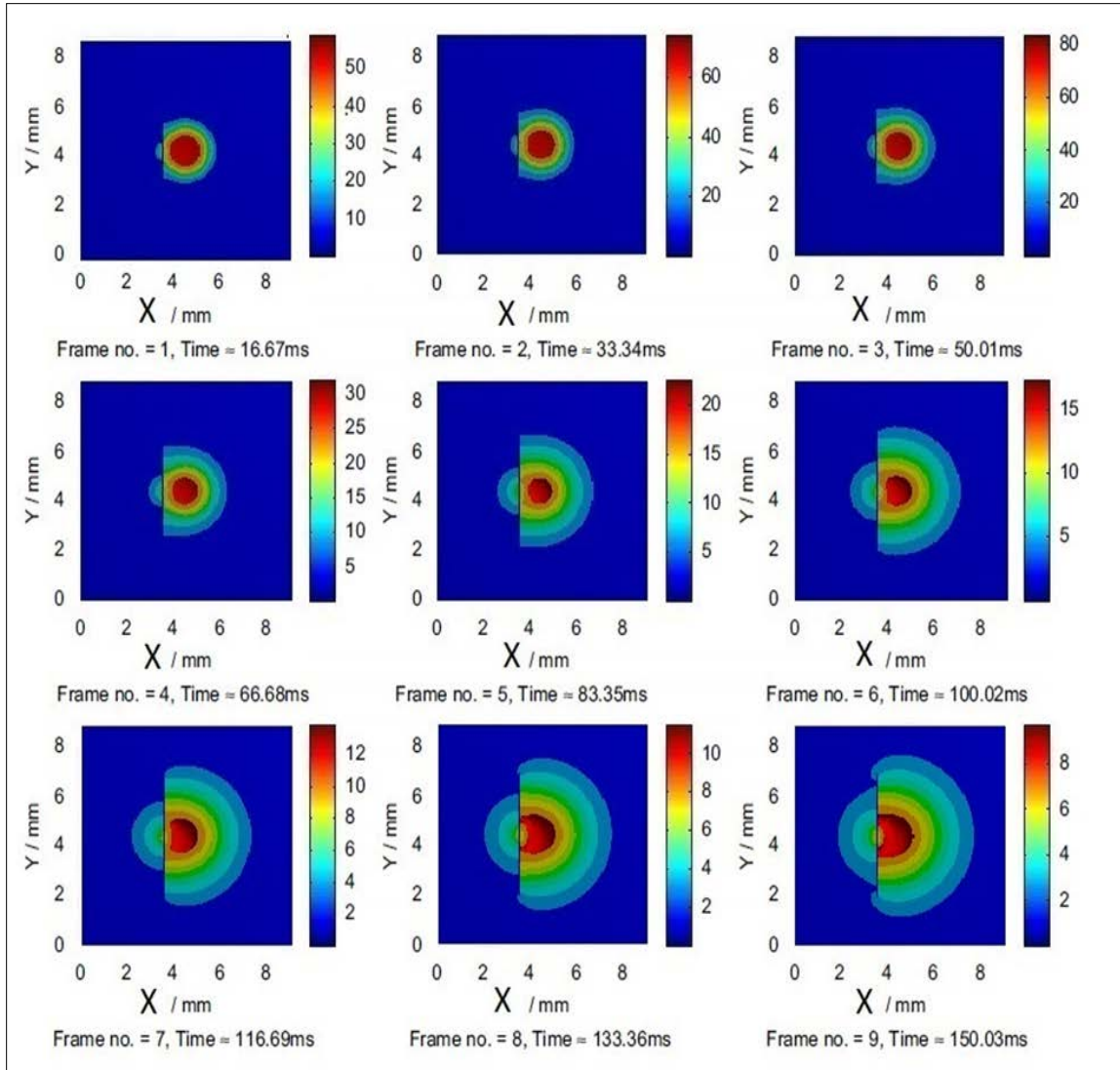
c. Corresponding simulated thermal contour images obtained by ANSYS

Figure 5.8 (continued)

Moreover; Fig. 5.9 and Fig. 5.10 show both of the ampligram and phasegram images as 2D and 3D respectively; where they were created by MATLAB (Appendix B.3) after importing the associated temperature time history from ANSYS. It is clearly visible on both images there is irregularity of temperature distribution above the excitation point caused by the crack presence. Hence, this refers to the fact of a subsurface fault presence (crack).



**a.** 2D Ampligram [$^{o}$C]                    **b.** 2D Phasegram [rad]
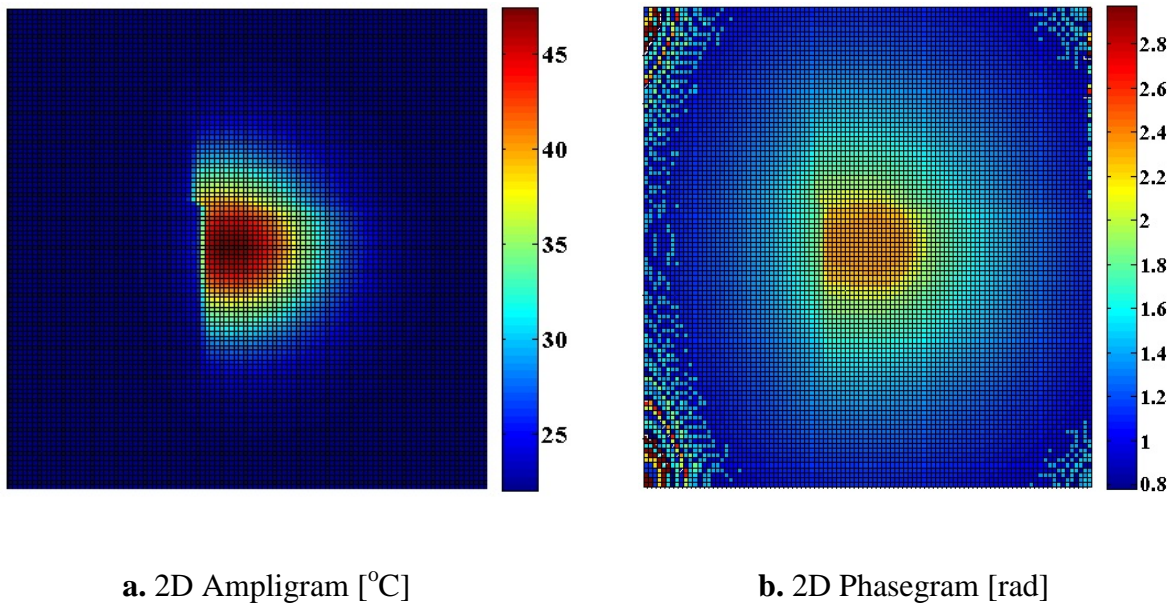
Figure 5.9 Two dimensions Amplitude and Phase images obtained by MATLAB

(Appendix B.3)

**a.** 3D Ampligram [$^o$C]
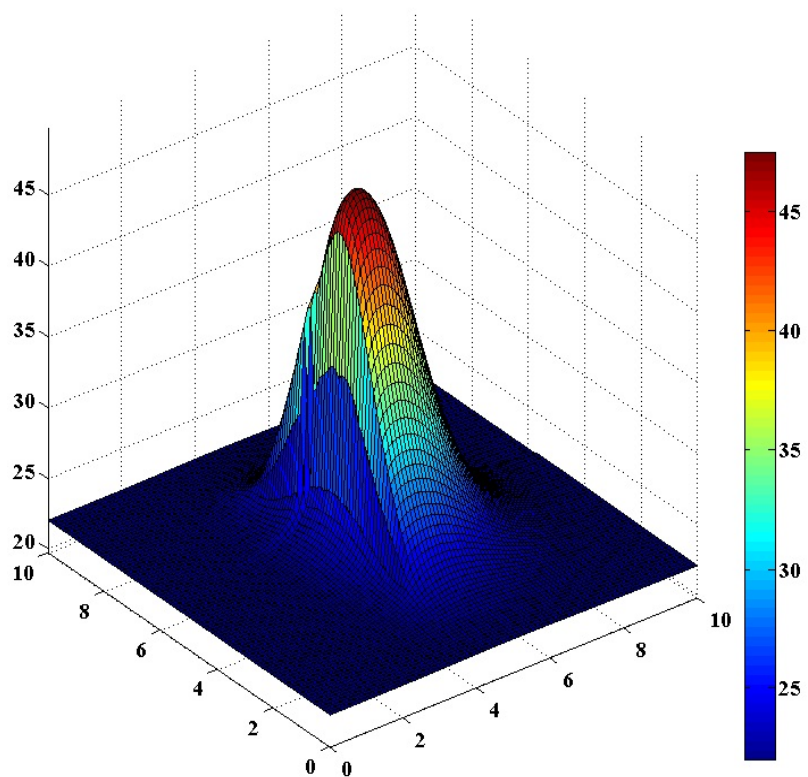
**b.** 3D Phasegram [rad]
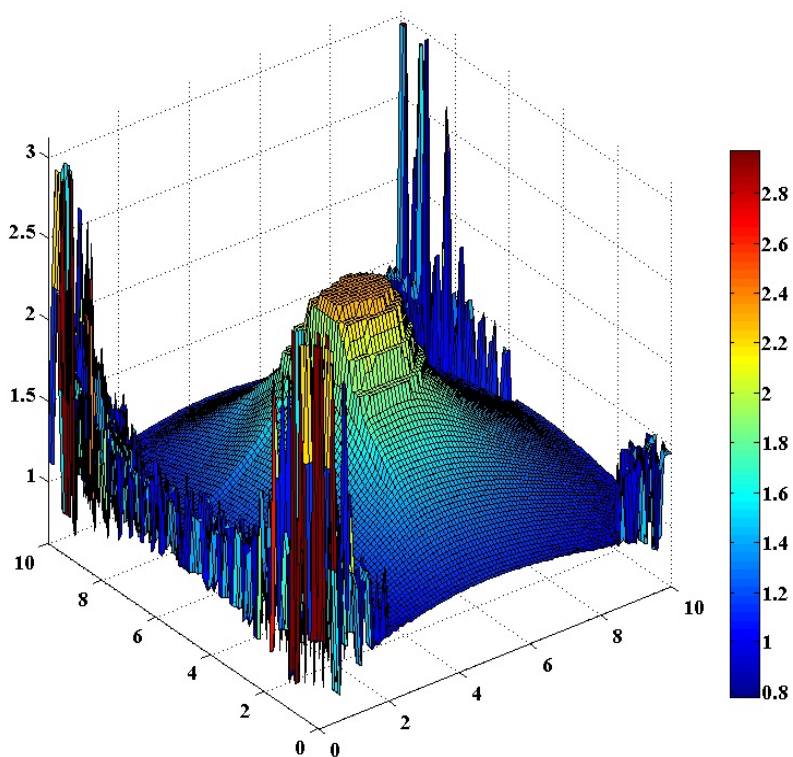
Figure 5.10 Three dimensions Amplitude and Phase images creating by MATLAB

(Appendix B.3)

### 5.6 ANALYTICAL AND NUMERICAL MODELING (ANSYS)

**5.6.1 3D Analytical Modeling-Point Heating.** There are no 3D analytical results for the distribution of a heat flow in a material containing narrow vertical cracks. However, results are available for the temperature rise caused by a laser source in a homogeneous, isotropic and semi-infinite material, such as metal. The 3D heat conduction in such a material can be expressed as [153,155]:

$$\frac{\partial^2 T}{\partial x^2} + \frac{\partial^2 T}{\partial y^2} + \frac{\partial^2 T}{\partial z^2} - \frac{1}{\alpha} \cdot \frac{\partial T}{\partial t} = -\frac{q'''}{k} \tag{30}$$

Where T [K] is the temperature rise, *x, y,* and *z* are the Cartesian coordinates, and $q'''$ [W/m$^3$] is the heat produced per unit volume per unit time.

Also, the instantaneous temperature rise from a point source [153] is:

$$T(r,t) = \frac{Q}{8\rho c_p (\pi \alpha t)^{3/2}} \, exp\left(-\frac{r^2}{4\alpha t}\right) \tag{31}$$

Where, Q [J] is the total energy of the heat source, and r [m] is the radius in a polar coordinate (pole is the point source center).

A continuous heat source has the same effect as a sequence of a very large number of small instantaneous sources of equal size. Thus, for a point source with continuous heating and when Q is constant, the integrated temperature result in the time domain is [155]:

$$T(r,t) = \frac{Q}{8\rho c_p (\pi \alpha t)^{3/2}} \int_0^t \frac{exp(-r^2/4\alpha t')}{t'^{3/2}} = \frac{q}{4\pi k r} \, erfc(\frac{r}{2(\alpha t)^{1/2}}) \tag{32}$$

Where $q$ [watt] is the source power.

However, the 'cooling' effect after the laser spot is switched off is not considered in equation (32). After convoluting the laser pulse (a square "top-hat" shape in the time domain, Gaussian shape in the spatial domain) with the instantaneous temperature rise, for a Gaussian shape round spot source with continuous heating, the integrated temperature result in the time domain is [153,156]:

$$T(r,z,t) = \frac{I_{max} \, r_a^2 \, \sqrt{\alpha}}{k\sqrt{\pi}} \int_0^t \frac{P(t-t')exp\left(-z^2/4\alpha t' - r^2/(4\alpha t' + r_a^2)\right)}{t'^{1/2}(4\alpha t' + r_a^2)} dt' \qquad (33)$$

Where ($r$, $z$) are cylindrical coordinates with the origin on the surface at the center of the irradiated spot, $I_{max}$ [watt] is the maximum power density of the laser pulse, and p$(t)$ is the normalized temporal profile of the laser pulse at the time $t$, and $r_a$ is the laser beam radius.

**5.6.2 3D Finite Difference Modeling.** For 3D finite difference modelling, the heat boundary condition of the surface with laser spot irradiation in Cartesian coordinates is:

$$-k\frac{\partial T(x,y,z=0,t)}{\partial z} = \frac{P}{\pi a^2} \, exp[-(x^2 + y^2)/a^2] \qquad (34)$$

For the other five boundaries, we assume they are insulated. For example, at the boundary when $x$=0, we have:

$$\frac{\partial T(x=0, y, z, t)}{\partial x} = 0 \tag{35}$$

The heat boundary condition of the surface with laser line irradiation in Cartesian coordinates is:

$$-k\frac{\partial T(x, y, z=0, t)}{\partial z} = \frac{P}{a\sqrt{\pi}} \, exp(-y^2/a^2) \tag{36}$$

The effects of cracks may be simulated by 'Ghost Points' in a numerical modelling grid that are generated by balancing thermal fluxes flowing into a crack and through a crack, with those flowing out of the crack according to Fourier's Law. They guarantee correct thermal gradients in the bulk material either side of the crack.

**5.6.3 Ghost Point Heat Diffusion Model.** The concept of the ghost point [157-160]; or a fictitious point, in a 1-D finite difference heat transfer model is shown in Figure 5.11. In this case, the crack is embedded between the current grid point (i) and its left grid point (i-1). The width of the crack ($\delta$) may be far smaller than the grid spacing (d). The distance of the crack to the left grid point is ($\sigma$). Usually, the crack is full of air and its conductivity ($k_a$) is much lower than the conductivity of the metal block ($k_s$). Thus the thermal gradient across the crack will be larger than in the other parts of the metal block [157].
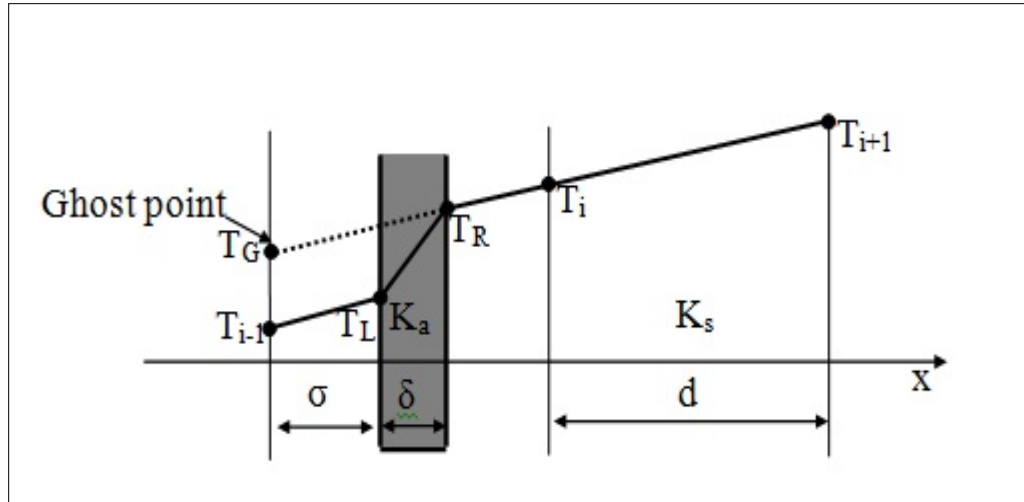
Figure 5.11 1-D 'ghost point' finite difference heat diffusion model. Heat flux is balanced when it flows into, through and out of the crack [157]

The heat flux balance in the x-direction when it flows from the grid point (i-1) into the crack, through the crack and then flows out of the crack to the grid point (i), as it is shown in this equation [151]:

$$k_s \frac{T_L - T_{i-1}}{\sigma} = k_a \frac{T_R - T_L}{\delta} = k_s \frac{T_i - T_R}{d - \sigma - \delta} = \text{g} \tag{37}$$

where *Ti-1*, *TL*, *TR*, *Ti*, and *Ti+1* are respectively the temperature rise at the grid point (*i-1*), the left boundary of the crack, the right boundary of the crack and the grid points of (*i*) and (*i+1*), and *g* is the heat flux.

By defining a ghost point to equal the temperature increase effect because of the crack, the isotropic heat transfer model can still be applied; however, the temperature rise at the grid point (*i-1*) should be replaced by the value of the ghost point ($T_G$). The next equation (Eq.28) shows the calculation of the temperature rise at the ghost point [151]:

$$k_s \frac{T_i - T_G}{d} = \text{g} \tag{38}$$

After substituting Eq. (37) into Eq. (38), we can represent $T_G$ by $T_i$ and $T_{i-1}$; then:

$$T_G = \frac{\xi}{\xi + d}\, T_i + \frac{d}{\xi + d}\, T_{i-1} \tag{39}$$

Where $\xi$ is related to $k_s$, $k_a$ and $\delta$ as it is shown in this relation:

$$\xi = \left(\frac{k_s}{k_a} - 1\right) \cdot \delta \tag{40}$$

The 3-D heat diffusion equation with no internal heat generation is shown in this equation:

$$k \nabla^2 T = \frac{\partial T}{\partial t} \tag{41}$$

Or the 1-D heat diffusion equation with no internal heat generation is shown in this equation:

$$k \frac{\partial^2 T}{\partial x^2} = \frac{\partial T}{\partial t} \tag{42}$$

By Substituting Eq. (39) into Eq. (41), and representing Eq. (41) by using finite difference elements, it will have these relations:

$$T_{i,j,m}^{n+1} = \frac{k \cdot \Delta t}{d^2} \cdot (T_{i+1,j,m}^n - a_c T_{i,j,m}^n + b_g T_{i-1,j,m}^n + N) + T_{i,j,m}^n \tag{43}$$

$$N = T_{i,j+1,m}^n + T_{i,j-1,m}^n + T_{i,j,m+1}^n + T_{i,j,m-1}^n \tag{44}$$

Where $\Delta t$ is the time step, $T_{i,j,m}^n$ is the temperature rise of the grid point '$i$, $j$, $m$' at time $n$ and $T_{i,j,m}^{n+1}$ is the temperature rise at the next time step. The values of $a_c$ and $b_g$ are:

$$a_c = \frac{5\xi + 6d}{\xi + d} \qquad (45)$$

$$b_g = \frac{d}{\xi + d} \qquad (46)$$

If the heat diffusion model is 1-D, then the value of $a_c$ becomes:

$$a_c = \frac{\xi + 2d}{\xi + d} \qquad (47)$$

If the heat diffusion model is 2-D, then the value of $a_c$ becomes:

$$a_c = \frac{3\xi + 4d}{\xi + d} \qquad (48)$$

If the crack is embedded between the current grid point '$i, j, m$' and the point '$i+1, j, m$', then the grid point '$i+1, j, m$' becomes the 'ghost point' and the temperature rise at this point should multiply the coefficient $b_g$ like the ghost point '$i-1, j, m$' in Eq. (43) [151]. Moreover; the temperature gradient across the crack can also be derived from Eq. (37) as follows [157]:

$$\frac{T_R - T_L}{\delta} = \frac{T_i - T_{i-1}}{\frac{k_a}{k_s(d - \delta)} + \delta} \qquad (49)$$

By using the ghost point's method to balance the heat flux, the heat transfer model avoids the need of the very fine mesh spacing that is necessary to deal with real cracks that often have openings of only a few micrometers [157-160].

## 5.7 ANALYTICAL AND NUMERICAL MODELING COMPARISON

This section discusses the analytical modeling [150], the corresponding numerical modeling by 3D ghost point finite difference modelling results [150] and FEM ANSYS results, based on the temperature rise caused by laser-spot source for different depths. Figure 5.12 shows three graphs Fig. 5.12a, Fig. 5.12b, and Fig. 5.12c which represents the temperature rise within steel after an incident Square laser pulse based on 3D analytical modelling results [150], 3D ghost point finite difference modelling results [150], and ANSYS modeling results respectively.

The laser pulse was a top-hat (square shape) of 50 ms in the time domain. The radius of the spot was taken to be 1mm (1/e fall and ra=1 mm). Laser output power was 20W, thus, $I_{max} \approx 20/(\pi a2) \approx 6.37 \times 106 W/m2$. In these simulations, the boundary conditions for the inspected specimen were assumed to be insulation; i.e. adiabatic. Therefore; the reflectivity of the sample surface was not considered in either model; i.e. all the 20W of energy was assumed to be absorbed by metal samples for each of the modeling methods; 3D analytical modeling; 3D ghost point finite difference modelling, and the ANSYS modeling. Each graph corresponds to temperatures rises of the laser spot center at different depths in the metal block. Each graph contains five curves with different colors; and each color refers to a specific depth. It is very clear from these graphs, almost there is not any difference between the corresponding curves else the curves at depth of 0.1 mm, where there is a small difference which is about 1%. This may be due to the fact that there are several factors which can cause these differences; such as boundary conditions of the 3D numerical model, 3D analytical modelling and the

accuracy of the 3D numerical model and FEM ANSYS; such as time step space step and different numerical methods [156,161].

The explicit finite difference method [150] was employed with 0.1mm grid spacing and 0.1 ms time steps. The simulation programs were formulated in MATLAB and run on a conventional PC [150].  Where the time step, that was used to provide this FEM ANSYS model, was 1 ms because the curves were not a smooth enough when took a time step more than 1ms. Figure 5.8c has created based on the ANSYS's results which has restored on MS Excel file as a data sheet then processed to provide these curves. Ultimately, by take a look on those graphs, then it can find out they have the same behavior. Hence, there is good agreement between the analytical and the modeling results and this validate the ANSYS modeling.
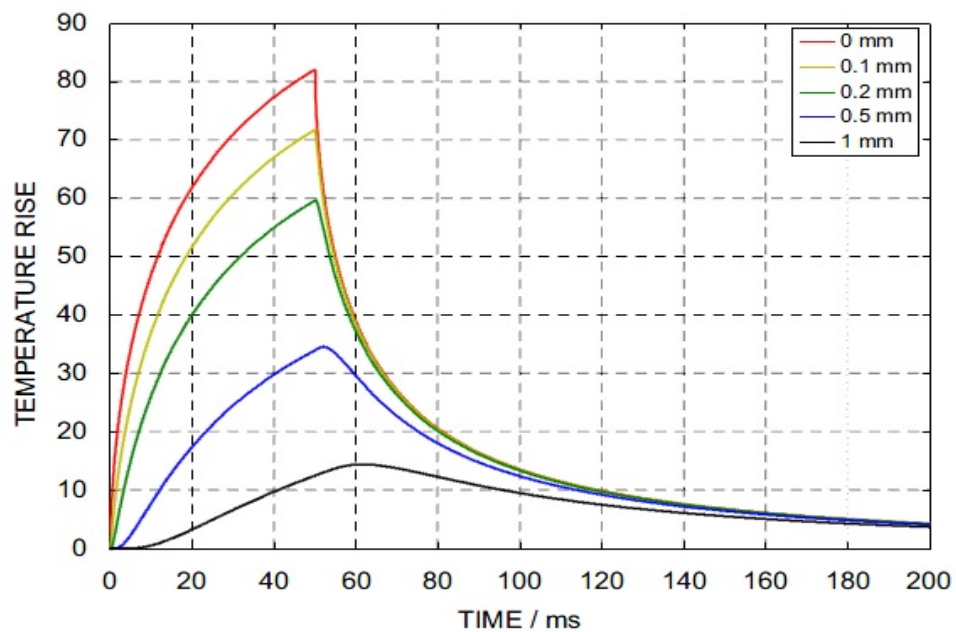
a. 3D analytical modelling results [150]
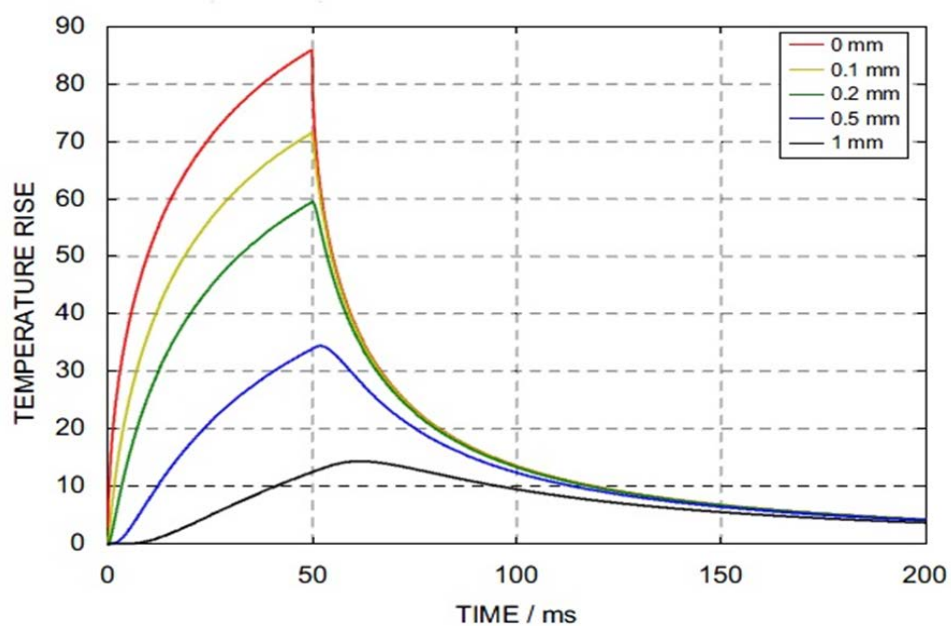


b. 3D ghost point finite difference modelling results [150]

Figure 5.12 Temperature Rise within Steel after an incident Square laser pulse
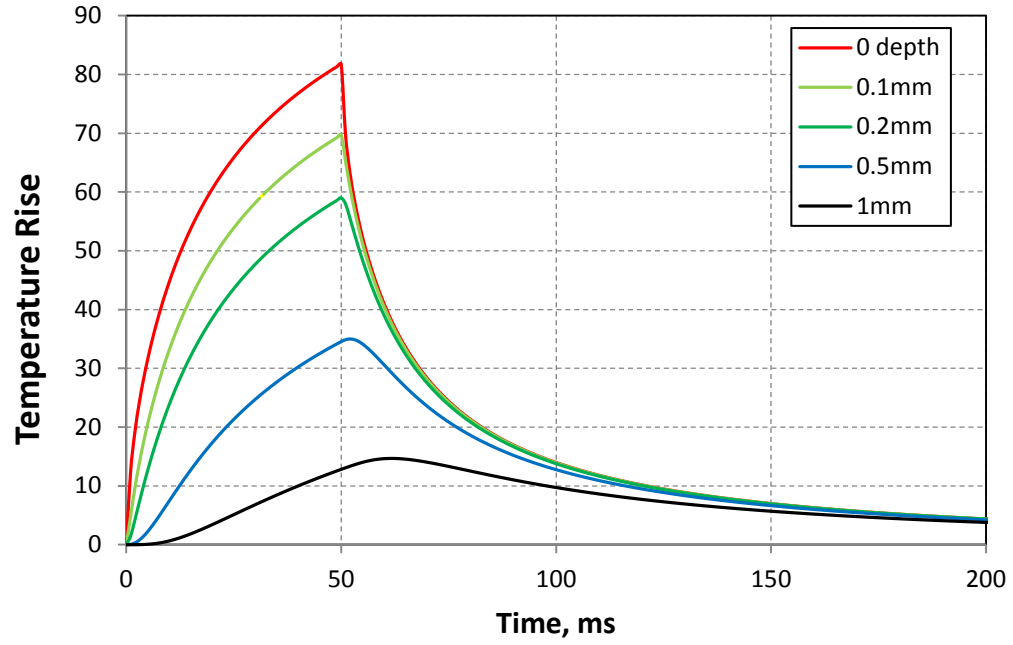
c. Numerical FEM ANSYS modeling results

Figure 5.12 (continued)

## 5.8 CONCLUSION

The results presented in this work indicate that the pulsed laser spot thermography LST technique has a good sensitivity and sensibility of crack detection, especially micro-cracks which are perpendicular to its surface, competitive with the classical IRT techniques (PT/LT). The LST technique has the benefits of being a non-contacting and requiring no surface processes or preparation. Although, it is well known that to be more accurate, the inspected specimen's surfaces should be clean and free of any scratch, deep scrabble or indentations that would disturb heat flow in a similar manner to a crack. However, it is observed that this technique is still far slower than a PT technique and its areas of application will probably be the inspection test of localized defect-prone zones on relatively small components.

# 6. LASER DIGITAL DEVICE THERMOGRAPHY

## 6.1 INTRODUCTION

In this section, an investigation of Laser Digital Micromirror Thermography (LDMT) as a means of detecting and imaging cracks is presented; especially micrometer cracks which are perpendicular to its surface. This technique is based on using a digital mirror device (DMD) which has ability to produce multi laser beams; i.e. multi hot spot onto the specimen's surface being examined which can generate a heat flow will propagate radially by diffusion through the specimen. In one word, this technique was derived from LST technique.

The previous thermography technique of laser spot thermography (LST) has been presented that it has the ability to deal properly with cracks with openings in the micrometer range; especially cracks perpendicular to its surface. However there is a challenge with following this technique (LST) about reaching the suitable local place to apply the laser spot to be able to reveal the defect. The suitable location to apply the laser spot, which can reveal the defect; it has to be at crack's vicinity, where if the laser spot is applied into the crack's proximity then the crack can be easily identified from the contour itself. So it is not possible to detect the defect, if the spot laser applies into place far away relative to the defect's location. In this case, it should apply the laser spot at another place and repeat this process until revealing the defect, i.e. until reaching the defect's proximity. Hence for an object with a large surface area, it is required to have a long observation time until reaching the crack or its proximity then detecting the crack. However, this limitation can be surmounted by applying multi spot in the same time then

saving the time. But it is too expensive to use many laser sources to provide those multi hot spots.

This thesis presents new thermography technique that can overcome these challenges which can call it Laser Digital Micromirror Device Thermography (LDMDT or simply LDMT). LDMT technique stands as an active infrared thermography approach which is based on using a powerful laser beam and a digital micro-mirror device (DMD) which can provide multi-hot spots in same time on the specimen's surface being inspected and saving the inspecting observation time in comparison with LST. Thus; LDMT is a very attractive and powerful to be used instead of LST to detect the micrometer cracks which are perpendicular to its surface; especially the specimens with large surface area. A DMD chip has on its surface several hundred thousand microscopic mirrors which are arranged in a rectangular matrix, where its mirrors can reflect a digital image onto any surface; i.e. providing multi-spots on the specimen's surface being inspected by using only single incoming laser source, as it is clear in Figure 6.1 and Figure 6.3 [162-163].

Basically, the DMD chip is a micro-mirrors array. Each Micromirror is 16 μm square and there's a gap of 1 μm between them, making it a 17 μm pitch. It reacts with a processor that allows each mirror to move into two directions that could refer to on or off state. With this matrix and the fact that micro-mirrors reflect light, the system is able, when illuminated, to reflect the light (laser) onto any surface (test specimen's surface), see Figure 6.3 [164].
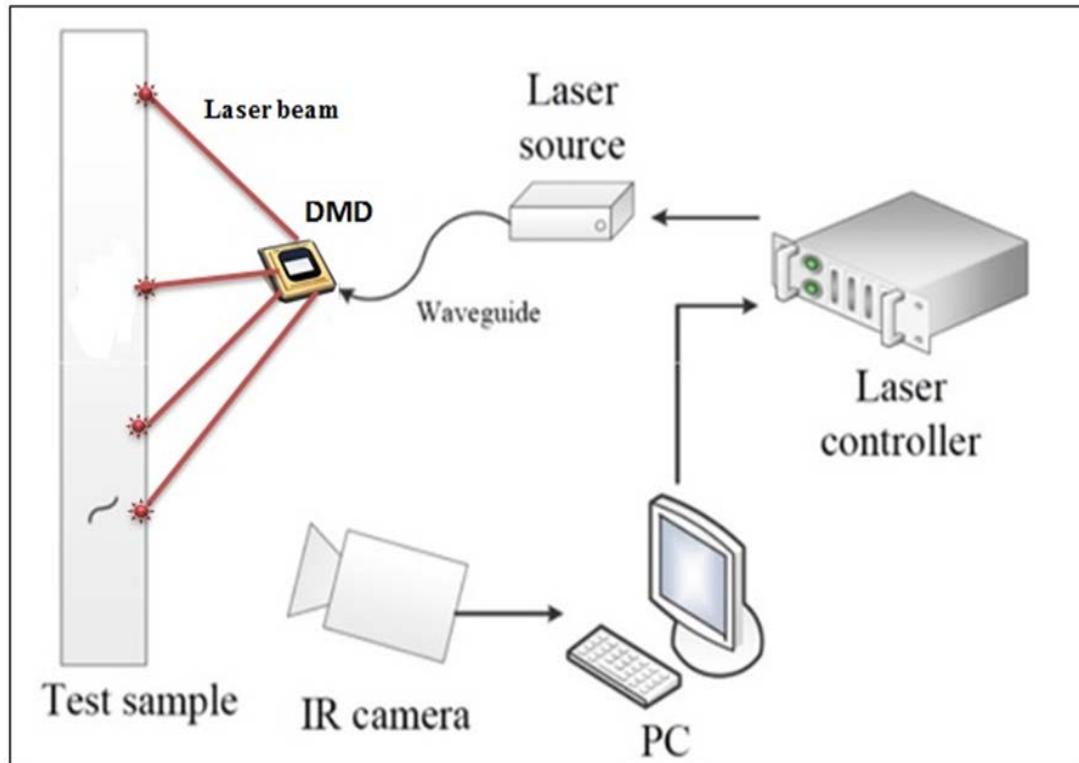
Figure 6.1 Laser DMD thermography test setup

## 6.2 DIGITAL MIRROR DEVICE (DMD)

In 1987 Dr. Larry Hornbeck and Dr. William E. "Ed" Nelson of Texas Instruments has invented and developed one of the earliest nano-technology devices, represented by the Digital Micro Mirror Device or DMD. DMD is an optical semiconductor which represents the core/heart of DLP projector technology (Digital Laser Projector). The story of the DMD project began as the deformable mirror device in 1977, using micromechanical and analog light modulators. The first analog DMD product

was the TI DMD2000 airline ticket printer that used a DMD instead of a laser scanner [162,163].

The DMD chip is probably the world's most advanced light switch. It contains a rectangular array of up to 8 million hinge-mounted microscopic mirrors; each of these micro-mirrors measures less than one-fifth the width of a human hair [164].

The DMD is a unique combination of opto-mechanical and electro-mechanical elements. The story starts with understanding how one pixel works and building on that to encompass the entire array of pixels that comprise a DMD. The DMD pixel is an opto-mechanical element in that these two positions estimate the direction that light is deflected. In particular, the DMD is a spatial light modulator. By convention, the positive (+) state is tilted toward the illumination; i.e. it is referred to as the on state. Similarly, the negative (–) state is tilted away from the illumination; i.e. it is referred to as the off state [163].

Simply, the DMD is an array of microscopically small of square mirrors (some half a million or more in a space no larger than a finger nail) each of which has ability to be turned on and off thousands of times per second. In which, each mirror or micro-mirror corresponds to a single pixel in the projected or displayed image. In other words; a DMD chip contains on its surface about millions or several hundred thousand microscopic mirrors which are arranged in a rectangular array; i.e. array of individual pixels, which are corresponded to the pixels in the image to be displayed [163,165,166].

The DMD is a square chip, based on computer RAM (Random Access Memory). The chip has an array of microscopic mirrors, one on each memory location. The array

dimensions being determined by the resolution of the particular DMD, i.e. the number of mirrors set the resolution in the image to be displayed, based on that each single mirror in the DMD chip equals one pixel in the image to be displayed. The RAM on the chip is told to turn on or off or to show black or white on the screen. In the DLP projection, the mirrors can be individually rotated ±10-12°, to an on or off state. In the on state, light from the projector bulb is reflected into the lens making the pixel appear bright on the screen. Similarly; in the off state, the light is directed elsewhere (usually onto a heat sink), making the pixel appear dark. The RAM chip can be changed thousands of times per second allowing the mirror to oscillate and create different light levels or greys [163,165,166].
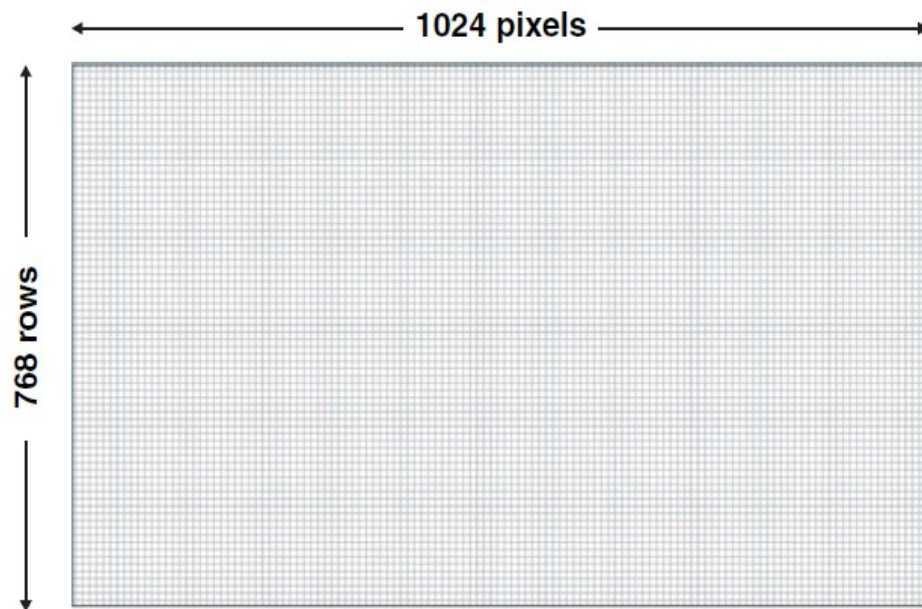


Figure 6.2 DMD Array (consists of 768 rows of 1024 pixels long. 0 = off, 1 = on) [163]

**a.** DMD chip
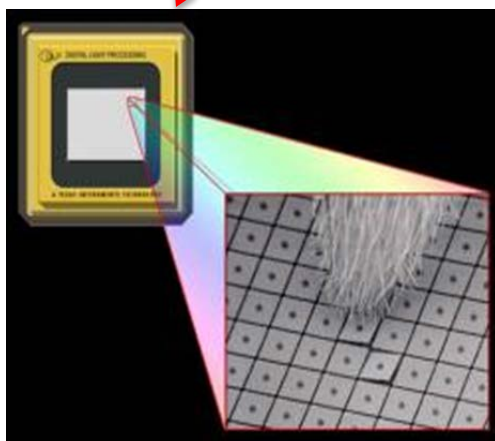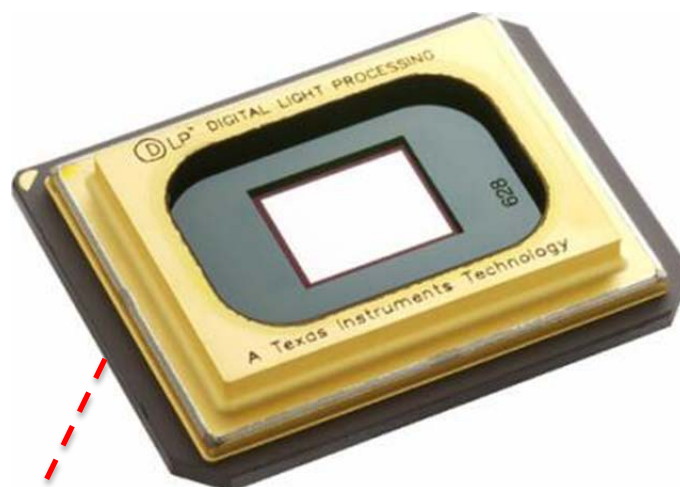


**b.** Reflection
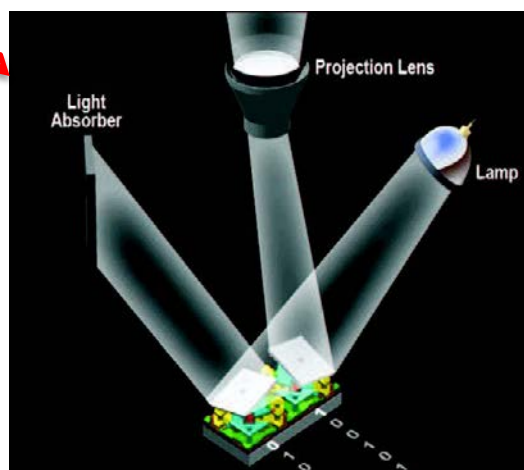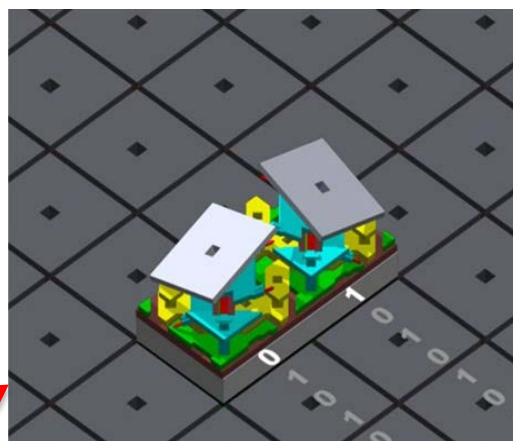
**c.** Pixels in On and Off State

Figure 6.3 DMD technologies [163]

## 6.3 BASIC CONCEPT AND THEORY FOR LDMT

Laser digital Micromirror device thermography stands as an active non-destructive inspection thermographic approach. LDMT is based on an external thermal excitation mode generated by a high power laser source. LDMT technique is a safe, non-contact, non-destructive test, and fast in comparison with LST technique. LDMT presents a detection IRT method of open surface cracks; with openings in the micrometer range. The detection of open surface cracks is an important task to prevent structural failure. Especially with regard to the widespread use of low ductility, high performance steel in lightweight construction, this is a subject of increasing interest. Basically, LDMT can be used in applications and fields that LST technique is used with. The observation and measurement is based on the analysis of thermal contrasts in surface temperature distribution in close neighborhood area of the stimulating laser spots. In previous section (5); it has used LST technique by applied the laser to point on the test specimen's surface at the defect's proximity area, then providing a heat spot and reveal the subsurface defect easily since the defect's location is already known. But in reality, the local location of the subsurface crack is unknown. So it is required to repeat the processes of LST many times by providing a heat spot upon the test specimen's surface at each time until reaching the defect's position or its proximity that is maybe after covering most the specimen's surface. Hence; LST technique takes a long time to detect the subsurface cracks.

This work introduces an advanced thermography method to characterize cracks starting at the surface; especially cracks perpendicular to its surface. In general this technique is based on the LST's operating principles. By using local thermal excitation it is possible to image anisotropies; faults, in the lateral diffusivity by recording the

temporal temperature data with an infrared camera. The resulting temperature distribution at the surface is recorded with an infrared camera, allowing estimating the heat flow into the object. Therefore; LDMT is possible to accomplish a fast, contact-free and reliable crack characterization in comparison with LST.

In general, the operation principle of LDMT is almost similar to this one in case of LST.  Basically; the phenomena as follow; pulsed laser source is used for producing a high power focused pulsed laser spot on the sample near to a surface breaking crack to generate a highly localized heating spot in which heat propagates radially by diffusion. That is by aiming the laser beam of the excitation source into DMD device. Where, it can control the DMD device by a computer and estimate where and how many heat spots are needed to be produced on the specimen's surface being inspected. A crack developed perpendicular to the surface that is close to the heated spot will delay the lateral heat flow and this disturbance can be easily observed by an IR camera, which will reveal the state or fact of defect's presence. The disturbance of the lateral heat flow caused by the crack leads to an unsymmetrical thermal footprint of the laser. Due to the fact that this crack acts as a barrier then changes the thermal diffusion rate.

As it has mentioned in previous section (5) that there are several parameters that affect the thermal images or heat distribution pattern include: host material, crack opening, length depth and geometry; laser power and pulse duration; spot imaging time and spot distance from the crack.

The thermographic images of laser heated spots are perturbed by nearby cracks, providing NDE techniques for crack detection. In compared with the LST, detect defects

with LDMT results in a substantial reduction in inspection time. In other words, the observing time of the LDMT thermography technique is shorter than that of the laser spot thermography technique; whilst producing crack images of similar quality.

## 6.4 GEOMETRY AND MESHING

The geometry was studied numerically by using ANSYS tools and run it on a regular computer machine and without needing a professional computer machine. This modeling has been done via non-commercial ANSYS 14 through a transient thermal as an analysis system. The test specimen has designed by Auto-Cad based, and then imported it to the design modeler of geometry of ANSYS. For calibrating the analysis procedure, test specimen sized (10 x 10 x 5 mm³) made of stainless steel plate with a fatigue crack has developed perpendicularly to the surface. The defect represents a gap filled within air. The thickness of the plate is 5 mm. The physics thermal properties of the inspected object are shown in table 6.1. A mesh with (467,187) nodes and (306,324) elements created in a sufficient accuracy features; as it is shown in Figure 6.4. The element size was not chosen uniformly, but with high smoothing, fast transition, and fine span angle center. The test specimen has stimulated from one side; the non-defective surface side, by a laser spot with 1 mm diameter.
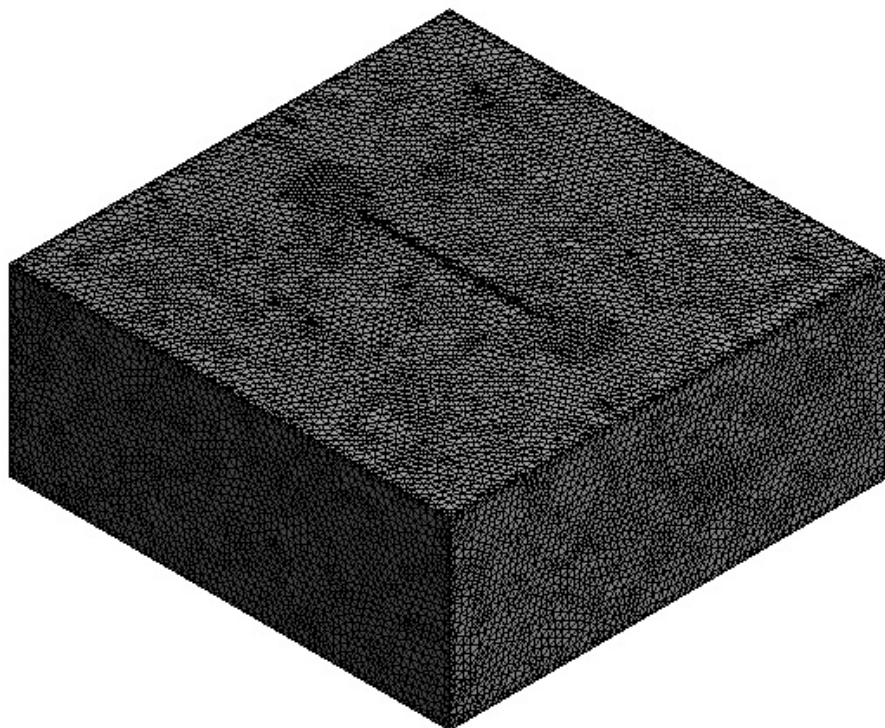
Figure 6.4 Shows meshing of test specimen obtained via ANSYS 14

Table 6.1 Thermal properties of materials used in LDMT and LST simulations.

| Materials | Thermal Conductivity $k$ [W/m.K] | Specific Heat $C_p$ [J/kg.K] | Density $\rho$ [kg/m³] | Thermal Diffusivity $\alpha$ [m²/s] $\alpha = k/(\rho.C_p)$ |
|---|---|---|---|---|
| Structural steel | 60.5 | 434 | 7850 | 1.7 E-05 |
| Air | 0.025 | 1000 | 1.205 | 2 E-05 |

## 6.5 LST AND LDMT SIMULATIONS

Figure 6.5 shows the modeled surface temperature images, temprature distribution of the test specimen's surface (nondefective side), of a laser beam incident on a stractural steel metal block obtained from this model. These thermal counters image has obtained when the test object was excited by a laser pulse. The laser excitation is applied with power of 22 Watt spot heating of 0.5 mm radius at several locality postions away from the crack which is perpendicular to its surafce. The pulse width duration is 50 ms . The width of crack (opening) is set to 50 µm, the length is 5 mm, and the depth is about 4 mm.

Figure 6.5 shows thermograms images that obtained by applying LST for some of them and LDMT for others one, for the same spcimen model. In one hand, the laser spot center, in LST simulation, was seted-up relative to the crack's center as follow;  4 mm, 2.5 mm, 2.5 mm, 4 mm,  and 0.5 mm, as it is clearly shown in shown in each of Figures 6.5a, 6.5b, 6.5c, 6.5d, and 6.5e. On the other hand, for LDMT simulation, it has applied three heat spots on the test specimen's surface in one-time at different locations to stimulate the object as follow; 3 mm on left side of crack, 1 mm, and 3 mm on right side of crack, as it is clearly shown in shown in Figure 6.5f.

As it is mentioned previously in part 5.7 of section 5, it is clearly obvious in the set of images of (a, b, c, and d) in Fig. 6.5  which looks likes that the specimen is nondefective; especially with comparison to the thermoragm image of the nondefective speciemn in Fig. 5.7a. But wherever the sopt heat being close to the crack as then the pcrack presence will lead to form a reverse 'D' shape rather than a round shape in

inspected specimen without crack as it is clearly shown in Fig. 5.7a; as shown in image Fig. 6.5e and one of the three spots of Fig. 6.5f, because of the heat blockage by the crack.  Hence; it can detect the crack.

Figure 6.5 shows that using LST technique, it is not suitable to detect the subsurface defect, especially cracks perpendicular to its surface, by applying the heat spot far away from the crack proximity, as it is shown in Figures 6.5a, 6.5b, 6.5c, and 6.5d. So it is required to apply the heat spot to another position until reaching the defect proximity and revealing it, as it is shown in Fig. 6.5e. But it is appropriate to apply multi heat spots in same time, to save the time and make the inspection in fast way, where some of these spot may be in proximity area of subsurface defect; hence it can reveal the defect as it is shown in Figure 6.5f.

Moreover; Figure 6.6 shows the temperature distribution on the test specimen's surface. First two images (frames), Fig. 6.6a, and Fig. 6.6b, show the temperature distribution on the specimen's surface at the time when the laser was still turned on. The third image, Fig. 6.6c, was at time of 50.01 ms, i.e. after 50 ms of starting the stimulation, the laser spot was turned off and the heat started to dissipate through the examined speciemn. If the pulse is long, heat will start to dissipate in the material whilst the laser is still on. This phenomenon is more obvious in metal samples.

a.  LST, L=4mm

b.  LST, L=2.5mm

c.  LST, L=2.5mm

d.  LST, L=4mm

e.  LST, L=0.5mm

f.  LDMT, 3 spots
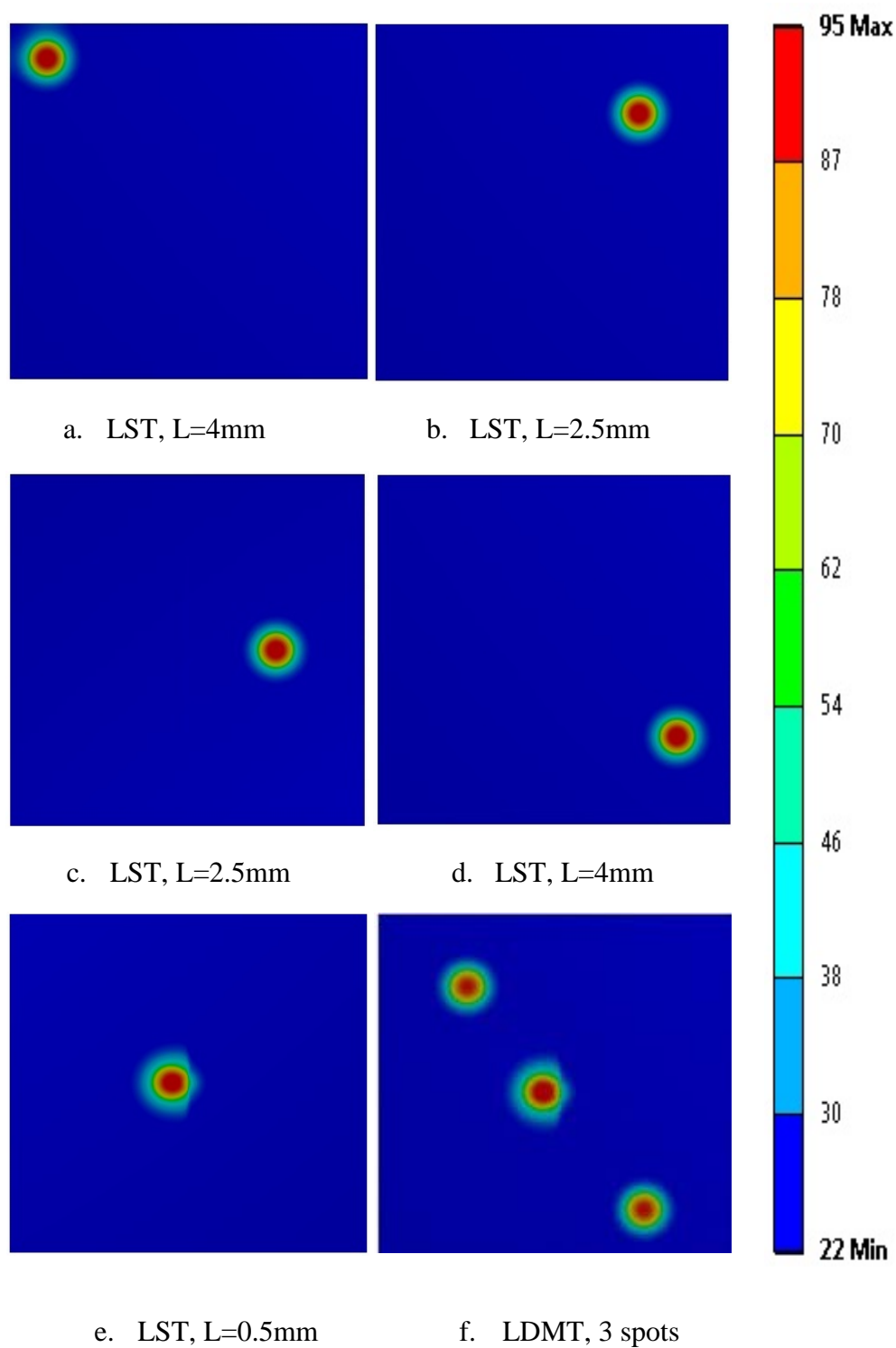
Figure 6.5 LST and LDMT techniques with pulsed spot at different distances away from

the crack center (L) [$^{o}$C]

Figure 6.6 clearly illustrates the sets of thermal images that are obtained by using LST technique simulation and simulated thermal images that are obtained by using LDMT technique. Hence, this is a good reasonably agreement to use the thesis's proposal technique, i.e. LDMT, which it is faster (save time) than LST technique.
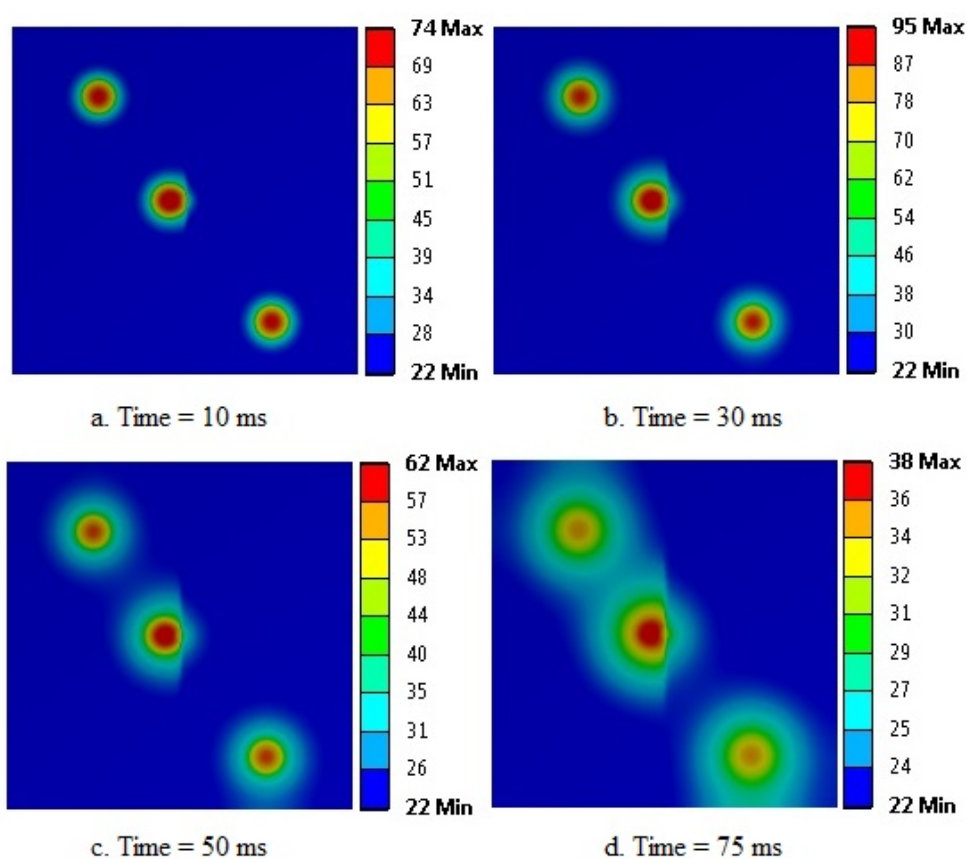


Figure 6.6 Temperatures distribution of test specimen's surface by using LDMT

technique with three pulsed spot at different times [$^{o}$C]

# 7. CONCLUSION

Infrared Thermography is an attractive and powerful nondestructive testing and evaluating inspection technique that provides a safe remote (non-contact) inspection of components and structures without changing the integrity and properties of the examined specimens and without causing any damage, through a mapping of thermal patterns on the surface of the objects of interest. Defect detection fundamental in active thermography is based on the fact that the variations in temperature that exists between the reference area and a defective region based on its emitted infrared radiations, which can be used for defect detection and quantification purposes.

In conclusion, for the in-plane defects which are parallel to its surface; such as coating adhesion failures, delamination or impact damage in carbon fiber composites, then it can use pulsed thermography technique (PT) or lock-in thermography (LT).

In one hand, data acquisition in pulsed thermography is quick, simple, and allows the inspection of extended surfaces. However, non-uniformities of applied heating, emissivity variations, surface geometry and reflections from the environment have a great impact on thermal data obtained by PT.

Lock-in thermography, on the other hand, allows the reconstruction of phase images that are less affected by the problems mentioned above. Furthermore, depth quantification by lock-in thermography is performed simply through the diffusion length equation; i.e. Eq. (20). In spite of that, long acquisition times constitute the principal drawback of lock-in thermography, since LT requires a single experiment test for every

inspected depth for every inspected depth. Furthermore; in LT technique, permanent regime has to be reached. Hence; these makes LT a slow technique in comparison with PT, however LT allows achieving a high qualitative results.

Moreover for the defects which are perpendicular to its surface, especially the micrometer cracks; such as fatigue cracks, then laser spot thermography (LST) technique has ability for detecting and imaging these types of surface breaking cracks with openings as small as a few micrometers; but data acquisition in LST is slow; i.e. observation time in this technique is long. However; laser digital micromirror thermography (LDMT) has ability to detect these types of perpendicular defects in quicker way than in LST method.

The numerical modeling simulations of infrared thermography techniques, that have been simulated based on FEM ANSYS in this thesis, have shown a reasonable agreement in comparison to their corresponding experiments and authorized doing infrared thermography nondestructive techniques via FEM ANSYS. Hence; this demonstrates the truth that FEM ANSYS represents a powerful tool to be used as an IRT. In other words, doing infrared thermography inspections via FEM ANSYS is a successfully authorized to do more advanced researches and improvements about IRT techniques and study the limitations that affect the result's resolutions instead of doing it laboratory; hence it helps to save time and money as well.

# REFRENCES

1. Shingō, S., A study of the Toyota production system from an industrial engineering viewpoint. 1989: Productivity Press.

2. Xiao N H 2004 New Technologies and Technical Standards for Modern Non-Destructive Testing Technology and Application (China: Beijing Silver Sound Audiovisual Press)

3. Mc Cann D M and Forde M C 2001 Review of NDT methods in the assessment of concrete and masonry structures NDT&E Int. 34 71–84.

4. Shen G T 2006 Review of non-destructive testing in China Insight 48 398–40.

5. Quantitative nondestructive testing using Infrared Thermography, Arun Manohar.

6. A. Sophian, G.Y. Tian, D. Taylor, and J. Rudlin. A feature extraction technique based on principal component analysis for pulsed eddy current ndt. NDT & E International, 36(1):37–41, 2003.

7. J. Blitz and G. Simpson. Ultrasonic methods of Nondestructive Testing, volume 2. Springer, 1995.

8. R.K. Miller and P. McIntire. Nondestructive testing handbook. vol. 5: Acoustic emission testing. American Society for Nondestructive Testing, 1987,,page 603, 1987.

9. G. Wang and T.W. Liao. Automatic identification of different types of welding defects in radiographic images. Ndt & E International, 35(8):519–528, 2002.

10. YY Hung. Shearography: a new optical method for strain measurement and nondestructive testing. Optical Engineering, 21(3):213391–213391, 1982.

11. P.J. Shull. Nondestructive evaluation: theory, techniques, and applications, volume 142. CRC, 2002.

12. J. Blitz. Electrical and magnetic methods of non-destructive testing, volume 3. Springer, 1997.

13. X. Maldague, editor. Infrared Methodology and Technology, volume 7. Gordon and Breach Science Publishers, 1994.

14. Characterization of Cracks by Laser Excited Thermography, J. Schlichting, G.N. Kervalishvili, Ch. Maierhofer, and M. Kreutzbruck

15. Sfarra S, Bendada A, Paoletti A, Paoletti D, Ambrosini D, Ibarra-Castanedo C and Maldague X 2010 Square pulse thermography (SPT) and digital speckle photography (DSP): nondestructive techniques (NDT) applied to the defects detection in aerospace materials Proc. 2nd Int. Symp. on NDT in Aerospace (Hamburg, Germany, 22–24 November 2010) pp 1–8

16. X.P.V. Maldague, Theory and Practice of Infrared Technology for Nondestructive Testing, Wiley, New York (2001)

17. Quantitative subsurface defect evaluation by pulsed phase thermography: depth retrieval with the phase, Clemente Ibarra Castanedo, 2005.

18. C. Meola and G.M. Carlomagno. Recent advances in the use of infrared thermography. Measurement Science and Technology, 15(9):R27, 2004.

19. Challenge for the future, NIPPON AVIONICS CO.,LTD http://www.infrared.avio.co.jp/en/products/ir-thermo/what-thermo.html

20. Infrared Thermography for Temperature Measurement and Non-Destructive Testing, Rub´en Usamentiaga, Pablo Venegas, Jon Guerediaga, Laura Vega , Julio Molleda and Francisco G. Bulnes

21. Inverse Heat Conduction Approach for Infrared Non-destructive Testing of Single and Multi-Layer Materials, Ehsan Borazjani, Ottawa, Canada, 2012

22. Detection of subsurface skin lesion using frequency modulated thermal wave imaging: a numerical study, Arka Bhowmik, Ramjee Repaka, Subhash C. Mishra, Ravibabu Mulaveesala, San Diego, California, USA, ASME 2013

23. Infrared thermography as a non-destructive tool for materials characterization and assessment, N.P. Avdelidis, T-H. Gan, C. Ibarra-Castanedo, X.P.V. Maldague, 2011.

24. J.L. Miller: Principles of Infrared Technology: A Practical Guide to the State of the Art. (John Wiley Sons, New York NY 2001)

25. http://www.bullard.com/V3/products/thermal_imaging/history_of_thermal_imaging.php, accessed on Sep., 2014

26. Maldague X. P. V., Streckert H. H and Trimm M. W. "Introduction to infrared and thermal testing: Part 1. Nondestructive testing," in Nondestructive Handbook, Infrared and Thermal Testing, Volume 3, X. Maldague technical ed., P. O. Moore ed., 3$^{rd}$ edition, Columbus, Ohio, ASNT Press, 2001, 718 p.

27. Experimental Comparison of Lock-in and Pulsed Thermography for the Nondestructive Evaluation of Aerospace Materials, W. Ben Larbi, C. Ibarra-Castanedo, M. Klein , A. Bendada, and X. Maldague

28. Inspection of aerospace materials by pulsed thermography, lock-in thermography and vibrothermography: A comparative study, Clemente Ibarra-Castanedo, Marc Genest, Stéphane Guibert, Jean-Marc Piau, Xavier P. V. Maldague and Abdelhakim Bendada.

29. P. O. Moore ed., X. Maldague technical ed., NDT Handbook on Infrared technology, ASNT Handbook Series, ASNT Press (American Society for NonDestructive Testing) Press, 732 p, 2001.

30. A Heat Transfer textbook, 3rd ed., JOHN H. LIENHARD IV and JOHN H. LIENHARD V, accessed on Aug 2003

31. Heat transfer textbook, $3^{rd}$ Ed., chapter 4, John H. Lienhard IV and John H. Lienhard V, 2008.

32. The Thermal Properties of Materials, J. Ziman. 1967 by Scientific American, Inc.

33. Lock-in Thermography textbook, Basics and Use for Evaluating Electronic Devices and Materials, Second Edition, O. Breitenstein, W. Warta, M. Langenkamp, May 2010.

34. Active infrared thermography techniques for the nondestructive testing of materials, Clemente Ibarra-Castanedo, Marc Genest, Jean-Marc Piau, Stéphane Guibert, Abdelhakim Bendada and Xavier P. V. Maldague

35. S.K. Lau, D.P. Almond, J.M. Milne: 'A Quantitative Analysis of Pulsed Video Thermography'. NDT&E International, 24 (4), 195, (1991)

36. Quantitative subsurface defect evaluation by pulsed phase thermography: depth retrieval with the phase, Clemente Ibarra Castanedo, 2005.

37. www.thermalwave.com

38. W.B. Larbi, C. Ibarra-Castanedo, M. Klein, A. Bendada, and X. Maldague. Experimental comparison of lock-in and pulsed thermography for the nondestructive evaluation of aerospace materials. In $6^{th}$ International Workshop, Advances in Signal Processing for Non Destructive Evaluation of Materials (IWASPNDE), Ontario, Canada. Citeseer, 2009

39. Giorleo G. and Meola C. "Comparison between pulsed and modulated thermography in glass-epoxy laminates", NDT&E International, 35:287–292, 2002.

40. Crack Imaging By Pulsed Laser Spot Thermography, T. Li1, D. P. Almond1, D. A. S. Rees1, B. Weekes2,a UK Research Centre in NDE (RCNDE), Department of Mechanical Engineering University of Bath, Claverton Down, Bath, BA2 7AY, UK, b UK Research Centre in NDE (RCNDE), Imperial College, London, SW7 2AZ, UK

41. Flying Laser Spot Thermography for the Fast Detection of Surface Breaking Cracks, Joachim Schlichting 1,2, Mathias Ziegler 1, Christiane Maierhofer 1, and Marc Kreutzbruck

42. 3D FEM SIMULATIONS OF LASER THERMOGRAPHY, Mohammed Basheer Chalil, Parag Ravindran, and Krishnan Balasubramaniam.

43. Meola, C. Origin and Theory of Infrared Thermography. In Infrared Thermography: Recent Advances and Future Trends; Meola, C., Ed.; Bentham Science: New York, NY, USA, 2012.

44. Modest, M.F. Radiative Heat Transfer; Academic Press: Waltham, MA, USA, 2013.

45. Canadian institute for NDE (cinde) 2004, "what is ndt? [Online] : <http://www.cinde.ca/ ndt.shtml>, accessed on July, 2014

46. The American Society for Nondestructive Testing (ASNT), https://www.asnt.org /MajorSiteSections/NDT-Resource Center/Introduction %20to%20Nondestructive %20Testing, accessed on Aug, 2014

47. Detecting defects in a complex wiring system, The AMMTIAC Quarterly, Volume 1, Number 2, 2006.

48. Non-destructive testing for plant life assessment, International Atomic Energy Agency ,IAEA, VIENNA, 2005

49. Nonderstructive Evaluation, Handbook, Charles J. Hellier, Chapter 9 Thermal

    Infrared testing.

50. Benefit analysis of nondestructive testing for roadway management, William L. Herbert, Ryan P. Jennette

51. AMERICAN INSTITUTE OF PHYSICS (AIP) 2004, Review of progress in quantitative nondestructive evaluation, Proc. AIP - American Institute of Physics [online] :< http://www.aip.org/> accessed on Aug, 2014.

52. Detecting defects in a complex wiring system, The AMMTIAC Quarterly, Volume 1, Number 2, 2006.

53. A. Manohar and F. Lanza di Scalea. Determination of defect depth and size using virtual heat sources in pulsed infrared thermography. Experimental Mechanics, pages 1–11, 2012. 10.1007/s11340-012-9670-9.

54. An IR Lock-in Thermography Nondestructive Test System Based on the Image Sequence Processing, Junyan LIU , Jingmin DAI , Yang WANG , Hui LIU  and Zijun WANG

55. Introduction to Infrared Thermography, Jeff Beard, 2007

56. Infrared vision applications for the nondestructive testing of materials, 5th Pan American Conference for NDT, Clemente IBARRA-CASTANEDO, Abdelhakim BENDADA, Xavier P.V. MALDAGUE 2-6 October 2011, Cancun, Mexico.

57. Frauenthal, A.H., Ten Year's Progress in Inspection. Manufacturing Industries,

1928.

58. Nonderstructive Evaluation, Handbook, Charles J. Hellier, Chapter 9 Thermal Infrared testing.

59. Thermography: Current Status And Advances In Livestock Animals And In Veterinary Medicine, Handbook, Fabio Luzi, Malcolm Mitchell, Leonardo Nanni Costa, Veronica Redaelli, Brescia, marzo 2013.

60. Zissis, G.J.; Wolfe, W.L. The Infrared Handbook. Technical report, DTIC document, 1978.

61. Gaussorgues, G. Infrared Thermography; Springer: Berlin/Heidelberg, Germany, 1994.

62. Gade, R.; Moeslund, T.B. Thermal cameras and applications: A survey. Mach. Vision Appl.2014, 25, 245–262

63. E.M. Sparrow, R.D. Cess, Radiation heat transfer. Hemisphere Pub. Corp., 1978

64. INCROPERA F. P. AND DE WITT D. P. 1990, Fundamentals of Heat and Mass Transfer, 3rd edition, John Wiley & Sons, USA.

65. Infrared Thermography, http://www.foresighthomeinspections.com/ accessed on July, 2014.

66. The Earth's Atmosphere, its physics and dynamics, Kshudiram Saha

67. Radiation in Vedic physics, John Frederic Sweeney

68. D. P. Dewitt Gend. D. Nutter, "Theory and Practice of Radiation Therrnometry", 1988, John Wiley & Sons Inc.

69. Vollmer, M.; Mollmann, K.P. Infrared Thermal Imaging: Fundamentals, Research and Applications; Wiley: Weinheim, Germany, 2011.

70. Accurate Measurements of and Corrections for Nonlinearities in Radiometers, C. L. Sanders

71. HIS GlobalSpec, Optical Components and Optics, Wavelength Range, http://www.globalspec.com/learnmore/optics_optical_components/optical_compo nents/achromats, accessed on Aug 2014

72. Maldague, "Introduction to NDT by Active Infrared Thermography", Materials Evaluation, Volume 60, Issue 9, 2002, Pages 1-22.

73. Quantitative nondestructive testing using Infrared Thermography, Arun Manohar.

74. Active Infrared Thermography in Non-destructive Testing, M. Hain, J. Bartl, V. Jacko

75. TISSOT J. L. 2004, "IR Detection with Uncooled Sensors", Infrared Phys. Technol., 46:147-153, 2004.

76. Mark's technology news, Black And Decker TLD100 Thermal Leak Detector Finds Power-Draining Drafts, http://www.markstechnologynews.com/2010/01/ black-and-decker-tld100-thermal-leak-detector-finds-power-draining-drafts.html, accessed on Aug. 2014.

77. Flash lamp, http://www.dx.com/p/sp-690ii-c-speedlite-speedlight-flash-lamp-for canon-dslr-black-4-x-aa-151380#.VA6VUihU2M4, accessed on Aug. 28, 2014

78. Halogen lamp, http://www.victorpopov.com/pages/41/%D1%82%D0%B5%D1% 85%D0%BD%D0%B8%D0%BA%D0%B0, accessed on Aug. 28, 2014

79. Zweschper, T.; Dillenz, A.; Riegert, G.; Scherling, D.; Busse, G. Ultrasound excited thermography using frequency modulated elastic waves. Insight-Non-Destructive Test. Cond. Monit. 2003, 45, 178–182.

80. Reynolds W N 1986 Thermographic methods applied to industrial materials Can. J. Phys. 641150-1154

81. Thermography as a tool for damage assessment, M. Krishnapillai , R. Jones , I.H. Marshall , M. Bannister , N. Rajic

82. Thermal imaging theory, VERONICA REDAELLI1, SIMONE CAGLIO, University of Milan, VESPA Department, Italy

83. F C Sham, Nelson Chen and Liu Long, "Surface crack detection by flash thermography on concrete surface", Insight, Volume 50, No. 5, May 2008, Pages 240-243

84. Monica A. Starnes, Nicholas J. Carino, and Eduardo A. Kausel, "Preliminary Thermography Studies for Quality Control of Concrete Structures Strengthened with Fiber-Reinforced Polymer Composites", Journal Of Materials in Civil Engineering, May/June 2003, Pages 266-273

85. D. Wu, Th. Zweschper, A. Salerno, and G. Busse, "Lock-in Thermography for Nondestructive Evaluation of Aerospace Structures", Revue Générale de Thermique, Volume 37, Issue 8, September 1998, Pages 693-703

86. C. Wallbrink, S. A. Wade and R. Jones, "The effect of size on the quantitative estimation of defect depth in steel structures using lock-in thermography", Journal of applied physics, Volume 101, 2007, Pages 104907(1-8)

87. Introduction to NDT by Active Infrared Thermography, X. Maldague

88. PARKER W. J., JENKINS R. J., BUTLER C. P. AND ABBOTT G. L. 1961, "Flash Method of Determining Thermal Diffusivity, Heat Capacity, and Thermal Conductivity," *J. Appl. Phys.*, **32**(9):1679-1684.

89. HUDSON R. D. 1969, "Infrared System Engineering", John Wiley & Sons Inc., USA.

90. Future electronics, "infrared detectors", http://www.futureelectronics.com /en/optoelectronics/infrared-detector.aspx, accessed on Aug. 2014.

91. Mark's technology news, Black And Decker TLD100 Thermal Leak Detector Finds Power-Draining Drafts, http://www.markstechnologynews.com/2010/01/ black-and-decker-tld100-thermal-leak-detector-finds-power-draining-drafts.html, accessed on Aug. 2014.

92. FLIR Systems, thermal imaging, www.flir.com, accessed on Aug, 2014

93. http://www.thedimensionzone.com/paranormal/the_technology_thermal_imaging _devices.htm, accessed on Sept. 2014

94. Super-Resolution Thermal Image Reconstruction, Krzysztof Malczewski, Ryszard Stasinski

95. NDT in Composite Materials with Flash, Transient, and Lockin Thermography, Markus Tarin and Ralph Rotolante MoviTHERM, Inc.

96. M.P. Rigney, E. A. Franke, "Machine vision applications of low-cost thermal infrared camera" in Thermosense XXII, RB Dinwiddie and DH Lemieux. eds., Proc. Soc. of Photo-Opt. Instrumentation Eng. (SPIE), 4020: 15-26, 2000.

97. D. P. DeWitt, G. D. Nutter, Theory and Practice of Radiation Thermometry, John Wiley, New York, 1138 p. 1988.

98. Thermography Camera Flir i3/ i5 / i7, http://www.industrial-needs.com/technical-data/thermography-camera-flir-i3-i5-i7.htm. accessed on Aug, 2014

99. http://www.ansys.com

100. H. Kaplan, Practical Applications of Infrared Thermal Sensing and Imaging Equipment, Second Edition, Proc. Soc. of Photo-Opt. Instrumentation Eng. (SPIE), TT34, 160, 1999.

101. Oliferuk W. (2008), Termografia podczerwieni w nieniszczacych badaniach materiałów i urzadzen, Biuro Gamma, Warszawa.

102. Milne, J.; Reynolds, W. The non-destructive evaluation of composites and other materials by thermal pulse video thermography. In Proceedings of the 1984 Cambridge Symposium. International Society for Optics and Photonics, Cambridge, UK, 23 October 1985; pp. 119–122.

103. Daponte, P.; Maceri, F.; Olivito, R. Frequency-domain analysis of ultrasonic pulses for the measure of damage growth in structural materials. In Proceedings of the Ultrasonics Symposium, IEEE 1990, Honolulu, HI, USA, 4–7 December 1990; pp. 1113–1118.

104. Martin, R.E.; Gyekenyesi, A.L.; Shepard, S.M. Interpreting the results of pulsed thermography data. Mater. Eval. 2003, 61, 611–616.

105. Carslaw H. S. and Jaeger J. C. Conduction of Heat in Solids, 2nd edition, Clarendon Press, Oxford, 1986.

106. Physical Properties of Foods textbook , Serpil Sahin, Servet Gülüm Sumnu

107. Bracewell R. The Fourier Transform and its Applications, McGraw-Hill, USA, 1965.

108. The integral error functions for each element of x, http://www.mathworks.com/matlabcentral/fileexchange/15646-environmental-modeling/content/ierfc.m, accessed on Aug. 2014.

109. Algorithms for efficient and quantitative nondestructive testing by pulsed thermography, S. Lugin and U. Netzelmann, NDT&E International, 40:220-228, 2007

110. Maldague X. P. and Marinetti S. "Pulse Phase Infrared Thermography," J. Appl. Phys. 79(5):2694-2698, 1996

111. P.K. Kuo, T. Ahmed, H. Jin, and R.L. Thomas, Phase-Locked Image Acquisition in Thermography, SPIE 1004, 41-45 (1988)

112. Thermal Failure Analysis by IR Lock-in Thermography, O. Breitenstein, C. Schmidt, F. Altmann, D. Karg

113. Thermographic NDT System, Anna Vladova Andonova and Dimitar Georgiev Todorov

114. Nordal P. E. and Kanstand S. O. "Photothermal radiometry," Physica Scripta, 20:659-662, 1979.

115. Simultaneous measurement of thermal diffusivity and optical absorption coefficient using photothermal radiometry. I. Homogeneous solids, Raquel Fuente, Estibaliz Apin˜aniz, Arantza Mendioroz, and Agustı´n Salazar

116. Evaluation of defects in composite plates under convective environments using lock-in thermography, W Bai and B S Wong, 2000

117. Wong B S, Tui C G and Bai W M 1999 Insight 41 504

118. CARLOMAGNO G. M. AND MEOLA C. 2002, "Comparison between thermographic techniques for frescoes NDT," NDT&E Int., 35(8):559-565.

119. BRACEWELL R. 1965, the Fourier Transform and its Applications, McGraw Hill, USA.

120. G. Busse, "Nondestructive evaluation of polymer materials," NDT&E Int'l, 27, : 253-262 (1994)

121. Fourier, J. B. J. 1822, "Théorie analytique de la chaleur", Paris, Firmin Didot.

122. Keston D. 1998, "Joseph Fourier - Politician & Scientist," [online]:<http://www.todayinsci.com/F/Fourier_JBJ/FourierPoliticianScientistBio.htm>accessed on April 26, 2004.

123. O'CONNOR J. J. and Robertson E. F. 2005, "The MacTutor History of Mathematics archive: Jean Baptiste Joseph Fourier," [online]:

<http://wwwgroups.dcs.st-and.ac.uk/~history/Mathematicians/Fourier.html>
accessed on April 26, 2004

124. LAU S. K., ALMOND D. P. AND PATEL P. M. 1991, "Transient Thermal Wave Techniques for the Evaluation of Surface Coatings," J. Phys. D: Appl. Phys., 24:428-436

125. FAVRO L. D. AND HAN X. 1998, "Thermal Wave Materials Characterization and Thermal Wave Imaging," in Birnbaum G., Auld B. A. (eds.): Sensing for Materials Characterization, Processing and Manufacturing, ASNT TONES, 1:399-415.

126. Busse G. "Techniques of infrared thermography: Part 4. Lockin thermography," in Nondestructive Handbook, Infrared and Thermal Testing, Volume 3, X. Maldague technical ed., P. O. Moore ed., 3rd edition, Columbus, Ohio, ASNT Press, 2001, 718 p.

127. Handbook of Technical Diagnostics: Fundamentals and Application to Structures and Systems, Horst Czichos, January 11, 2013

128. ROSENCWAIG A. AND BUSSE G. 1980, "High-Resolution Photoacoustic Thermal-Wave Microscopy", Appl. Phys. Lett., 36(9):725–727

129. Wu D. and Busse G. "Lock-in Thermography for NonDestructive Evaluation of Materials," Rev. Gén. Therm., 37:693-703, 1998

130. HAN X., FAVRO L. D., KUO P. K. AND THOMAS R. L. 1996, "Early-Time Pulse-Echo Thermal Wave Imaging," in D. O. Thompson and D. E. Chimenti (ed.): Review of Progress in Quantitative Nondestructive Evaluation, 15:519-524

131. Busse G., Wu D. and Karpen W. "Thermal Wave Imaging with Phase Sensitive Modulated Thermography," J. Appl. Phys., 71(8):3962-3965, 1992

132. Non-destructive evaluation of composites materials by pulsed-phase thermography: depth inversion, Fernando López Rodríguez, Vicente de Paulo Nicolau, Hugo Oshiro, Daniel Tancredi

133. BUSSE G. and ROSENCWAIG A. 1980, "Subsurface Imaging with Photoacoustics," Appl. Phys. Lett., 36(10):815-816

134. BUSSE G. 1979, "Optoacoustic Phase Angle Measurement for Probing a Metal", Appl. Phys. Lett., 35:759–760

135. BUSSE G. 1982, "Optoacoustic and Photothermal Material Inspection Techniques", Appl. Optics., 21(1):107–110

136. THOMAS R. L., POUCH J. J., WONG Y. H., FAVRO L. D. AND KUO P. K. 1980, "Subsurface Flaw Detection in Metals by Photoacustic Microscopy", J. Appl. Phys., 51(2): 1152–1156

137. KRAPEZ J. C. AND CIELO P. 1991, "Thermographic Nondestructive Evaluation: Data Inversion Procedures. I: 1D Analysis," Res. Nondestr. Eval., 3(2):81-100

138. Krapez J. C. "Compared performances of four algorithms used for modulation thermography", Proc. 4th Conference on Quantitative InfraRed Thermography - QIRT, D. Balageas, G. Busse, C. Carlomagno (eds.), Eurotherm Seminar 60, Lodz, Pologne, September 7-10, 1998, 148-153

139. Active thermography signal processing techniques for defect detection and characterization on composite materials, C. Ibarra-Castanedo, N. P. Avdelidis, M. Grenier, X. Maldague and A. Bendada

140. KREYSZIG E. 1993, Advanced Engineering Mathematics, 7th ed., John Wiley and Sons, Inc.

141. BRIGHMAN E. O. 1974, the Fast Fourier Transform, Prentice-Hall, Inc., Englewood Cliffs, N. J

142. CASTLEMAN K. R. 1996, Digital Image Processing, Prentice-Hall, Upper Saddle River, N. J

143. COOLEY J.W. and TUKEY J.W. 1965, "An Algorithm for the Machine Calculation of Complex Fourier Series," Mathematics of Computation, 19(90):297-301

144. MALDAGUE X. and COUTURIER, J-P. 1997, "Review of Pulse Phase Infrared Thermography," Proc. 4th International Workshop on Advanced Infrared Technology and Applications (AITA), Firenze, Italy, September 15-16, 53(1):271-286

145. AUTOMATIC ALGORITHM FOR QUANTITATIVE PULSED PHASE THERMOGRAPHY CALCULATIONS, C. Ibarra-Castanedo, D. González and X. Maldague

146. Estimation of defect depth in steel plate using, lock-in IR thermography, Monika ZIMNOCH, Wiera OLIFERUK, Michał MAJ

147. Lau S K, Almond D P, and Milne J M 1991 A quantitative analysis of pulsed video thermography NDT&E Int. 24 195-202

148. Shepard S M, Lhota J R, and Ahmed T 2007 Flash thermography contrast model based on IR camera noise characteristics Nondestructive Testing and Evaluation 22 113-126

149. Laser spot thermography of welded joints, Jakub Roemer, Łukasz Pieczonka, Tadeusz UHL

150. LiT, etal.Crack imaging by scanning pulsed laser spot thermography. NDT& EInt (2010), doi:10.1016/ j.ndteint.2010.08.006

151. Crack imaging by scanning pulsed laser spot thermography, Teng Li, Darryl P. Almond, D.Andrew S. Rees

152. Crack imaging by pulsed laser spot thermography, T. Li, D. P. Almond, D. A. S. Rees, B. Weekes

153. Li T, Almond D P, Rees D A S, Weekes B, and Pickering S G 2010 Review of Progress in QNDE29Aed D. O. Thompson and D. E. Chimenti (New York: Melville) p 435-442

154. Rantala J, Hartikainen J and Jaarinen J 1990 Photothermal determination of vertical crack lengths in silicon nitride Applied Physics A: Materials Science & Processing 50(5) 465-471

155. Carslaw H S and Jaeger J C 1959, *Conduction of Heat in Solids* (London: Oxford University)

156. Almond D P and Patel P M 1996, Photothermal Science and Techniques (London: Chapman& Hall)

157. Li, T., Almond, D. P. and Rees, D. A. S. (2011) Crack imaging by scanning laser-line thermography and laser-spot thermography. Measurement Science & Technology, 22 (3). ISSN 0957-0233

158. Rashed A, Almond D P , Rees D A S, Burrows S, and Dixon S 2007 Crack detection by laser spot imaging thermography Review of Progress in QNDE, 26, ed D. O. Thompson and D. E. Chimenti (New York: Plenum Press) p 500-506

159. Burrows S E, Rashed A, Almond D P, and Dixon S 2007 Combined laser spot imaging thermography and ultrasonic measurements for crack detection Nondestructive Testing and Evaluation, 22(2–3), p. 217–227

160. Rantala J and Hartikainen J 1991 Numerical estimation of the spatial resolution of thermal NDT techniques based on flash heating Research in Nondestructive Evaluation 3(3) 125-139

161. John F. Ready J F 1971, Effects of high-power laser radiation(New York: Academic Press)

162. www.texasbusiness.com

163. TEXAS INSTRUMENTS, Introduction to Digital Micro mirror Device (DMD) Technology

164. Reliability of the Digital Micromirror Device, Begon Martin, Ciapala Richard and Deaki Zoltan, 2007

165. L.A. Yoder, "An introduction to the digital light processing (DLP) technology", DLP Technology (22.02.2005)

166. M.R. Douglass, "DMD reliability: a MEMS success story", SPIE Proceedings Vol. 4980 (2003)

167. Method of detectors offset correction in thermovision camera with uncooled microbolometric focal plane array, Grzegorz Bieszczad, Tomasz Orżanowski, Tomasz Sosnowski, Mariusz Kastek

**APPENDIX**

**A. ANSYS MECHANICAL HEAT TRANSFER**

The Workbench project schematic is a graphical representation of the workflow defining a system or group of systems. From the toolbox a selection can be dragged and dropped onto the schematic (or double clicked). In general, the steps as follow;

1. It can access ANSYS and launching its "Mechanical Workbench" from the "Windows start menu"

2. Open Workbench and specify the unit system: Metric (kg, m, s, ℃, A, N, V)

3. Choose to "Display Values in Project Units"

4. Open the Workbench Project Schematic and choose a "Transient Thermal" analysis system from the toolbox

5. Double click the Engineering Data cell to add/edit the materials

6. Highlight (single click) the Geometry branch to create and modifies geometry as preprocessor for analysis models;

    i. Double click the "Geometry" cell and design the geometry inside the geometry "Design Modeler DM" or

    ii. RBM (right click) the Geometry cell and import the geometry model if it is already available and or done by another program such as Auto-Cad

to assure this step was done in right way, it will appear a right sign.

7. Double click the "Model" cell to open the geometry in Mechanical project application window

8. Expand the Geometry branch and assign the material to its specific part by choosing the materials of each part of geometry model by select this part

from the geometry branch and then select its special material from the window of "Graphics Properties" at branch of "materials"

9. Activate body selection to highlight whole the part that want to be meshed, or activate specific face selection from the tools bar. Then highlight the Mesh branch and expand the "Sizing" section in the details. Note, the default mesh is quite coarse for this model;

   i. Generate mesh based on its default specifications by RBM > Generate mesh,

   ii. If the default mesh is not good enough to achieve the desired mesh then it is required to control the element size control through the tools window of "Details of Mesh"

10. In case of needing to export the temperature surface distribution to generate the "Ampligram" and "Phasegram" images as in LT and LST. Then it is required to mesh the front surface of the specimen (stimulated side which is the non-defective side) in way to generate rectangular elements. To do that;

    i. RBM on mesh cell> then will get a list, stand on the "Insert" and will get another sub-list> choose "Mapping Face Meshing"

    It can control the sizing of these rectangular elements through the tools window of "Details of Mesh"

11. The initial/ambient temperature can be edited through the "Initial Temperature" branch

12. Step control, number of steps, and time steps can be controlled/edited through the "Analysis  Settings" branch; which can be used to control the heat pulse long as in PT,LST, and LDMT

13. Scope the required "Heat Flux" or "Heat Flow" load onto part's surface can be applied by;

i.      Activate face selection by choose the surface that is required to be stimulated (heated up)

ii.     Then RBM on this activated surface > Insert > Heat Flow/ Heat Flux

14. Estimation the amount/value of the applied heat load through;

i.      Highlight the "Heat Flow/Heat Flux" cell branch of "Thermal Transient" list will lead to appear a window of "Heat Flow/Heat Flux" details

ii.     From this window, highlight the "Magnitude" cell and click on the arrow which is placed on the right side of the in-front rectangular of the "Magnitude" cell

iii.    Then will appear a list which contain some optional choices

iv.     Choose "Constant" if the applied heat load is constant as in case of PT, LST, and LDMT, then estimate the heat load value by entering its amount as digits in the magnitude field

➢   Controlling the heat pulse long (duration) can be controlled/edited form the table of "Tabular Data" which is shown on the right bottom corner of main window of "Transient Thermal of Mechanical Workbench"

      v.   Choose "Function" if the applied heat load is changed periodically as in case of LT, then estimate the heat load amount by entering the periodic thermal function in the magnitude field

➢ Be careful about how to enter the variables of the heat load function. For instance; for a sinusoidal heat wave with power of (10000). Thus; the function of the periodic thermal wave can be expressed as;

    ❖ 10000-10000*cos (360*time); i.e. do not use *t* as a time but use time as it is clearly shown in previous relation.

15. RBM on "Solution" branch in main list of project > "Insert" > "Thermal" > "Temperature"

16. Solve > RMB and "Evaluate All Results", which will show the result for whole body

➢ To estimate the temperature distribution for a particular surface; such as the front surface of the specimen (stimulated side which is the non-defective side); then

➢ After doing step 15, then single click on the "Temperature" branch of "Solution" branch of the main project list (on the left upper corner)

➢ Then form the window of details of "Temperature" > "Scope" > click on "Geometry" filed then estimate the surface by activate  face selection

➢ Repeat step 16, which will give data results about this specific surface

> ➤ RBM on "Temperature" branch > "Export" , which will export the date time history (surface temperature distribution) of this surface as an Excel sheet file

> ➤ The generated date sheet will be used for MATLAB CODE to help producing the required "Ampligram" and "Phasegram" images

❖ As Mechanical Workbench tools have ability to generate these results; then using ANSYS Parametric Design Language (APDL) tools in ANSYS Mechanical APDL can do that as well.

**APPENDIX**

**B. MATLAB CODES**

These MATLAB codes that have used to generate the ampligram and phasegram images that shows in this thesis. Data that used in those codes were generated via FEM ANSYS in form of excel sheet data.

## B.1 MATLAB CODE FOR LT TECHNIQUE

This code made by *Hayder Abdulnabi Thajeel*

```
clear,clc

W=xlsread('LT');

function [A]=amplitude(F);
n = length(F);
for i = 1 : n;
   A(1,i)=sqrt(real(F(1,i)^2) + abs(imag(F(1,i)^2)));
end

function [phi]=angles(d);
phi=atan(imag(d(:))/real(d(:)));

 % for plate dimensions of xt*yt which is 170*195 in this test

yt=0:0.1:195; % y axis which is corresponding to length of one of the surface edges
ny=length(yt);

xt=0:0.1:170; % x axis which is corresponding to length of second edge of the surface edges
nx=length(xt);

ky = 0;
kx = 0;
hx = 0;
hy = 0;

disp('   x            y    '); % for build new metrics
disp('--------------------------------')

ht = 0;
t=[]; % time vector
xe=0:0.1:170;
ye=0:0.1:195;

[X,Y]= meshgrid(ye,xe);
amp=[];
phii=[];
```

```matlab
for y  = 1 : 0.1 : 196; % due to mat-lab start from 1 NOT 0
  yt2 = y - 1; % re-addressing to start from 0
  ky = ky + 1; % for lopping to jump to next pixel

  ko(ky) = ky-1;
  yo(ky) = yt2;

for x  = 1 : 0.1 : 171
  xt2 = x - 1;
  kx  = kx + 1;

ht=ht+1

t(ht,:)=W(ht,:);

d(ht,:)=fft(t(ht,:));
%h=fftshift(d);

a=amplitude(d(ht,:));
[aa bb]=max(t(ht,:));
amp(ht) = a(1);
amp22(ht) = aa;
b=angle(d(ht,:));
phii(ht) = b(1);
phii22(ht) = b(bb);

ko2(kx) = kx-1;
xo(kx) = xt2;

%disp([ht xo(kx) yo(ky)]); % fill the output data in its real position that corresponding to its address in input
excel sheet

%figure, plot(amp(ht))
end
end

% disp([ht' xo' yo'])

ampl=reshape(amp,nx,ny); ampl22=reshape(amp22,nx,ny); % re-addressing from 35*40 to real dimension
170*195 (plate dimension)

phie=reshape(phii,nx,ny); phie22=reshape(phii22,nx,ny);

set(gcf, 'Color', [1,1,1]);
figure; surf(Y,X,ampl22),title('Real Amplitude');

set(gcf, 'Color', [1,1,1]);
figure; surf(Y,X,phie22),title('Real Phase');

set(gcf, 'Color', [1,1,1]);
figure; surf(Y,X,abs(phie22)),title('Real Phase');
```

## B.2 MATLAB CODE FOR LT TECHNIQUE FOR MST LOGO MODEL

This code made by *Hayder Abdulnabi Thajeel*

```
clear,clc

W=xlsread('MST');

function [A]=amplitude(F);
n = length(F);
for i = 1 : n;
   A(1,i)=sqrt(real(F(1,i)^2) + abs(imag(F(1,i)^2)));
end

function [phi]=angles(d);
phi=atan(imag(d(:))/real(d(:)));

yt=0:0.1:50.8;
ny=length(yt);

xt=0:0.1:50.8;
nx=length(xt);

ky = 0;
kx = 0;
hx = 0;
hy = 0;

disp('   x          y    ')
disp('------------------------------')

ht = 0;
t=[];
xe=0:0.1:50.8;
ye=0:0.1:50.8;

[X,Y]= meshgrid(ye,xe);
amp=[];
phii=[];

for y  = 1 : 0.1 : 51.8
   yt2 = y - 1;
   ky = ky + 1;
   ko(ky) = ky-1;
   yo(ky) = yt2;


for x  = 1 : 0.1 : 51.8
```

```
   xt2 = x - 1;
   kx  = kx + 1;

ht=ht+1
t(ht,:)=W(ht,:);

d(ht,:)=fft(t(ht,:));
%h=fftshift(d);

a=amplitude(d(ht,:));
[aa bb]=max(t(ht,:));
amp(ht) = a(1);
amp22(ht) = aa;
b=angle(d(ht,:));
phii(ht) = b(1);
phii22(ht) = b(bb);

ko2(kx) = kx-1;
xo(kx) = xt2;

%disp([ht xo(kx) yo(ky)])

%figure, plot(amp(ht))

end
end

% disp([ht' xo' yo'])

ampl=reshape(amp,nx,ny); ampl22=reshape(amp22,nx,ny);
phie=reshape(phii,nx,ny); phie22=reshape(phii22,nx,ny);

set(gcf, 'Color', [1,1,1]);
figure; surf(Y,X,ampl22),title('Real Amplitude');

set(gcf, 'Color', [1,1,1]);
figure; surf(Y,X,phie22),title('Real Phase');

set(gcf, 'Color', [1,1,1]);
figure; surf(Y,X,abs(phie22)),title('Real Phase');
```

## B.3 MATLAB CODE FOR LST TECHNIQUE

This code made by *Hayder Abdulnabi Thajeel*

```
clear,clc

W=xlsread('MST');

function [A]=amplitude(F);
n = length(F);
for i = 1 : n;
   A(1,i)=sqrt(real(F(1,i)^2) + abs(imag(F(1,i)^2)));
end

function [phi]=angles(d);
phi=atan(imag(d(:))/real(d(:)));

yt=0:0.1:10;
ny=length(yt);

xt=0:0.1:10;
nx=length(xt);

ky = 0;
kx = 0;
hx = 0;
hy = 0;

disp('    x               y     ')
disp('-------------------------------')

ht = 0;
t=[];
xe=0:0.1:10;
ye=0:0.1:10;

[X,Y]= meshgrid(ye,xe);
amp=[];
phii=[];

for y  = 1 : 0.1 : 11
   yt2 = y - 1;
   ky = ky + 1;
   ko(ky) = ky-1;
   yo(ky) = yt2;


for x  = 1 : 0.1 : 11
```

```
   xt2 = x - 1;
   kx  = kx + 1;


ht=ht+1
t(ht,:)=W(ht,:);

d(ht,:)=fft(t(ht,:));
%h=fftshift(d);

a=amplitude(d(ht,:));
[aa bb]=max(t(ht,:));
amp(ht) = a(1);
amp22(ht) = aa;
b=angle(d(ht,:));
phii(ht) = b(1);
phii22(ht) = b(bb);

ko2(kx) = kx-1;
xo(kx) = xt2;

%disp([ht xo(kx) yo(ky)])

%figure, plot(amp(ht))

end

end

% disp([ht' xo' yo'])

ampl=reshape(amp,nx,ny); ampl22=reshape(amp22,nx,ny);
phie=reshape(phii,nx,ny); phie22=reshape(phii22,nx,ny);

set(gcf, 'Color', [1,1,1]);
figure; surf(Y,X,ampl22),title('Real Amplitude');

set(gcf, 'Color', [1,1,1]);
figure; surf(Y,X,phie22),title('Real Phase');

set(gcf, 'Color', [1,1,1]);
figure; surf(Y,X,abs(phie22)),title('Real Phase');
```

# VITA

Hayder Abdulnabi Thajeel was born in the city of Baghdad, Iraq. He obtained his Bachelor's Degree of Science in Mechanical Engineering from University of Baghdad in Baghdad, Iraq in May 2004, with the $4^{th}$ class honor.

He successfully received his Master's Degree of Science in Mechanical Engineering from department of Mechanical and Aerospace Engineering of Missouri University of Science and Technology (Missouri S&T, formerly the University of Missouri - Rolla) in December 2014.